Conceptual and Modeling Approaches to Investigate Coastal Road Vulnerability to High Water Tables and Flooding

by

Bruno Jose de Oliveira Sousa

A dissertation submitted to the Graduate Faculty of
Auburn University
in partial fulfillment of the
requirements for the degree of
Doctor of Philosophy

Auburn, Alabama
August 9, 2025

Keywords: coastal hydrology, groundwater level, sea-level rise, distributed hydrologic modeling, infrastructure vulnerability

Approved by

Dr. Jose G. Vasconcelos, Chair, Professor, Civil and Environmental Engineering
Dr. Frances C. O'Donnell, Associate Professor, Civil and Environmental Engineering
Dr. Xing Fang, Professor, Civil and Environmental Engineering
Dr. Luke J. Marzen, Professor, Geosciences
University Reader: Dr. Anna Linhoss, Associate Professor, Biosystems Engineering

Abstract

Low-lying coastal areas face increasing risks from elevated groundwater levels and sur flooding due to sea-level rise (SLR), extreme p itation, and storm surges. The objective of this research is to develop and apply a transferable framework to assess the vulnerability of coastal road infrastructure to shallow groundwater tables and flooding, using Alabama State Route 180 (AL-180) as a case study. The methodology integrates a data-driven empirical model and a physics-based distributed hydrologic model to evaluate sub-daily interactions between precipitation, tidal fluctuations, and groundwater dynamics. The empirical model estimates groundwater level (GWL) time series using simplified inputs such as rainfall, tidal elevation, surface elevation, and distance from tidal bodies. It was validated with field data from monitoring wells along AL-180. Performance metrics include Nash–Sutcliffe Efficiency (NSE) values of up to 0.73 and root mean squared errors (RMSE) as low as 0.06 m. This model was implemented along longer segments of the road using a Geographic Information System (GIS) platform at 100-meter intervals and used in conjunction with spatiotemporal analysis tools to detect long-term trends and identify vulnerable segments. Additionally, the Gridded Surface Subsurface Hydrologic Analysis (GSSHA) model was calibrated and validated in a coastal setting to simulate surface and groundwater processes during moderate and extreme events. Results show that combined surface-subsurface interactions have a significant impact on flood extent and pavement saturation, particularly during extreme rainfall events. Together, the modeling approaches identified road segments with high saturation persistence, informing locations for infrastructure maintenance and adaptation. This framework supports transportation agencies in developing resilient road systems and can be applied to other coastal corridors with minimal data requirements.

Acknowledgements

I would like to thank my committee chair and advisor, Dr. Jose G. Vasconcelos, for his guidance, mentorship, patience, and unwavering support throughout my time at Auburn. I also wish to thank my committee members, Dr. Frances C. O'Donnell, Dr. Xing Fang, Dr. Luke J. Marzen, and the university reader, Dr. Ana Linhoss. I appreciate the ideas, field support, and friendship of my fellow graduate students, Victor Geller, Michael Bragg, Luiz Morgado, Ashmita Poudel, Excie Guillot, as well as the alumni Gianlucca Nicolaico and Luis Fernando Castaneda Galvis. Additionally, I would like to thank the administrative staff of the Department of Civil and Environmental Engineering for their assistance in navigating the academic system.

I would like to thank my parents, Carlos Alberto de Sousa and Jacilene de Oliveira Sousa, for instilling in me the value of education; this was crucial in keeping me motivated. I am grateful to my sisters, Lisiane and Carla, and my brother, Carlos, for ensuring I could count on them at every stage of the process. Additionally, I would like to thank all the friends I made in Auburn for their support throughout this journey and for providing me with relaxing moments.

Lastly, I want to thank the Effects of Sea Level Rise (ESLR) program from the National Oceanic and Atmospheric Administration (NOAA), National Centers for Coastal Ocean Science (Grant no. NA21NOS4780146) for funding this research in partnership with the Federal Highway Administration (FHWA) and the Alabama Department of Transportation (ALDOT).

Table of Contents

List of Tables

List of Figures

List of Abbreviations

BL	Boat Launch
CONED	Coastal National Elevation Database
DEM	Digital Elevation Model
DOT	Department of Transportation
GSSHA	Gridded Surface Subsurface Hydrological Analysis
GWL	Groundwater Level
GWL_m	Modeled Groundwater Level (time dependent)
IPCC	Intergovernmental Panel on Climate Change
MESONET	Mesoscale Network.
NAIP	National Agriculture Imagery Program
NAVD88	North America Vertical Datum of 1988
NC	Navy Cove
NLCD	National Landcover Database
NNBF	Nature and Nature-Based Features
NSE	Nash–Sutcliffe Efficiency
P	Precipitation
PN	The Pines
R	Rise component of the Groundwater Level
RMSE	Root Mean Squared Error
SLR	Sea Level Rise
SSURGO	Soil Survey Geographic Database
USGS	United States Geological Survey

GWL_R Groundwater Level relative to GWL_{st}

GWL_{st} Stable Groundwater Level

GWL_T Tidal component of the Groundwater Level

Chapter 1. Introduction

Climate change is intensifying the impacts of both extreme events and gradual processes on coastal infrastructure. Projections indicate that sea levels may rise between 0.23 and 0.53 meters by 2050, while extreme precipitation events are expected to become more frequent and intense (Easterling et al., 2017; Garner et al., 2021; Sweet et al., 2022). In low-lying coastal regions, these factors can combine to create chronic saturation conditions, reduce drainage effectiveness, and increase the exposure of transportation infrastructure to prolonged hydrologic stress (Cox et al. 2019; Peña et al. 2023).

One of the critical challenges in coastal engineering is quantifying the vulnerability of pavements to shallow groundwater levels (GWL) and repeated saturation. Prolonged subgrade moisture can accelerate structural degradation, leading to deformation, rutting, and premature pavement failure (Titus-Glover et al., 2019; Chen & Wang, 2023a). These impacts are often persistent, as the recovery of the mechanical capacity of pavement layers may take weeks or even months after groundwater levels subside.

Addressing this challenge requires an integrated understanding of the interaction between rainfall, tides, and shallow groundwater dynamics. However, many hydrologic modeling tools commonly applied to inland settings are not well adapted to the complexity of coastal systems, particularly in regions with minimal channelized flow and dominant subsurface–surface interactions. In this context, distributed models and data-driven approaches provide pathways for representing the spatial variability and temporal dynamics of groundwater levels.

This dissertation proposes two modeling frameworks to assess saturation risk along Alabama State Route 180 (AL-180), an evacuation corridor in Fort Morgan Peninsula in Alabama. The first component develops and implements a data-driven empirical model to predict sub-daily groundwater level fluctuations based on site-specific conditions. The second component utilizes a physics-based, distributed hydrologic model to simulate surface and subsurface processes at high spatial and temporal resolutions. Together, these models aim to identify road segments most vulnerable to groundwater-related impacts and to inform maintenance and adaptation strategies for coastal transportation infrastructure. The research is organized into chapters that correspond to each phase of the methodology, including model development, validation, spatial application, and scenario-based analysis. By combining physical and empirical modeling approaches, this work

helps close methodological gaps in coastal hydrology and supports decision-making for resilient infrastructure planning.

1.1. Contextualization

Coastal regions present unique challenges for hydrologic and groundwater modeling due to the interaction between rainfall, tides, and shallow groundwater in low-gradient, high-water-table, and high hydraulic conductivity environments (Rotzoll & Fletcher, 2013; Werner et al., 2013). Figure 1 illustrates how sea level can influence groundwater tables in coastal areas. Additionally, high uncertainty in subsurface properties, dynamic boundary conditions, and limited monitoring infrastructure hinder the reliable application of conventional models in these areas. These limitations have resulted in several knowledge gaps, including the difficulty of representing surface runoff, flooding, and groundwater dynamics in coastal areas using hydrological models, and the need to predict infrastructure vulnerability using easily measurable site characteristics.

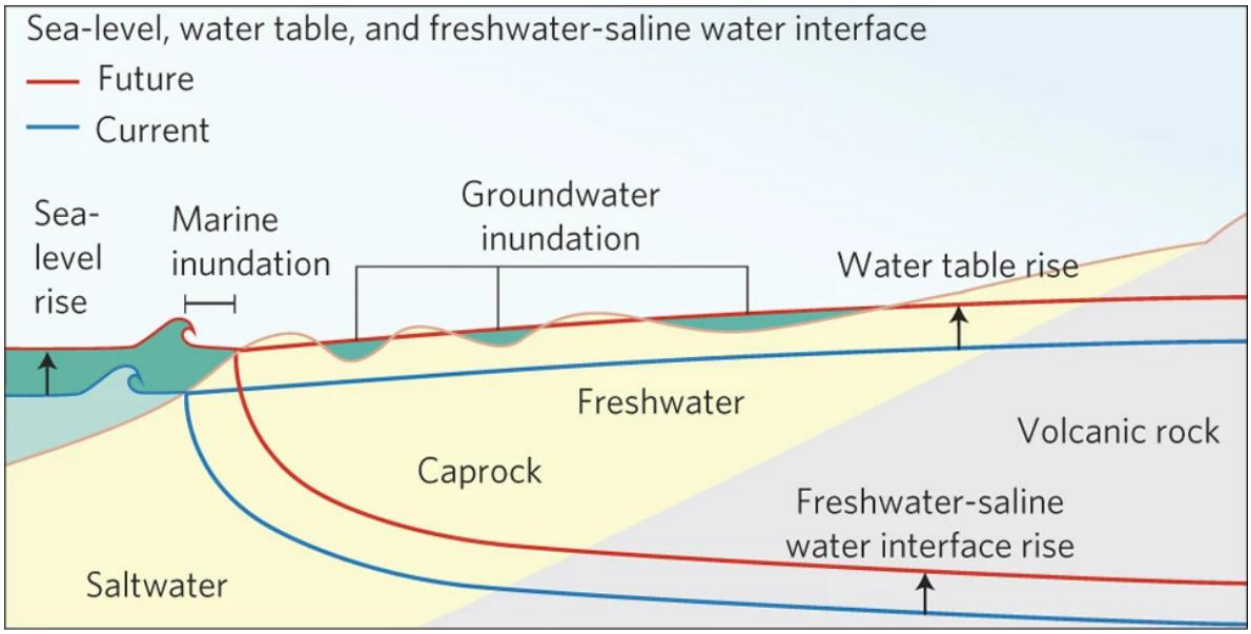

Figure 1 – Schematics of the water table rise caused by a higher sea level (Rotzoll & Fletcher, 2013).

1.1.1. Groundwater Dynamics in Coastal Environments

In coastal regions with shallow water tables, groundwater levels (GWL) respond rapidly to meteorological and oceanographic drivers such as precipitation, tidal fluctuations, and sea level rise (de Oliveira Sousa et al. 2023). These responses are particularly significant in low-relief landscapes with sandy soils and high hydraulic conductivity, where vertical exchanges dominate and subsurface water can persist near the surface for extended periods (Ferguson & Gleeson, 2012; Rotzoll & Fletcher, 2012). Elevated GWL reduces infiltration capacity and increases surface saturation, undermining the structural performance of pavements by decreasing their load-bearing capacity (Cox et al., 2019; Peña et al., 2023). This persistent subgrade moisture is difficult to mitigate and can lead to fatigue cracking, rutting, and surface failures (Titus-Glover et al., 2019; Chen & Wang, 2023b). Furthermore, recovery after flooding is delayed because the subgrade remains weakened even after visible water recedes (King & Taylor, 2023).

1.1.2. Data-Driven Models for Groundwater Prediction

Data-driven models have gained traction for their ability to derive empirical relationships from observed hydrometeorological data. These models, ranging from multiple linear regression to machine learning methods such as neural networks and decision trees, are particularly useful in systems where data availability is high but computational or calibration constraints limit the use of physics-based models (Solomatine & Ostfeld, 2008; Sun et al., 2022; Haaf et al., 2023).

In coastal settings, data-driven models can be used to estimate GWL responses to tidal fluctuations and rainfall, particularly when soil and hydrologic conditions are relatively homogeneous and dominated by vertical fluxes (Ali et al., 2024; Xie & Zhang, 2024). However, many of these applications focus on monthly or daily time steps and broad spatial scales, limiting their utility for infrastructure-specific applications that require sub-daily resolution and localized predictions. Furthermore, the predictive reliability of such models depends heavily on the representativeness of training data, making careful site-specific calibration essential. These models can help overcome the limitations of traditional inland models by capturing unique coastal dynamics such as rapid tidal responses and shallow aquifer behavior.

1.1.3. Distributed Hydrologic Modeling and GSSHA

To quantify the interactions between surface water and groundwater, hydrologic models must resolve spatial heterogeneity and simulate coupled surface–subsurface flow. Lumped and semi-distributed models, while widely used in inland catchments, average soil and land cover properties, and often neglect lateral and vertical flow interactions (Scharffenberg, 2016; Rossman, 2015). These limitations are particularly critical in coastal environments, where groundwater levels fluctuate on fine temporal scales and topographic gradients are minimal (Panday & Huyakorn, 2004).

The Gridded Surface Subsurface Hydrologic Analysis (GSSHA) model addresses many of these limitations. Developed by the U.S. Army Corps of Engineers, GSSHA is a physically based, fully distributed model capable of simulating 2D overland flow, 1D channel routing, vertical infiltration, shallow groundwater flow, evapotranspiration, and surface retention (Downer & Ogden, 2004). Its use of a gridded computational domain (Figure 2) enables high-resolution spatial representation of variability, making it suitable for local-scale coastal systems where water movement is highly localized.

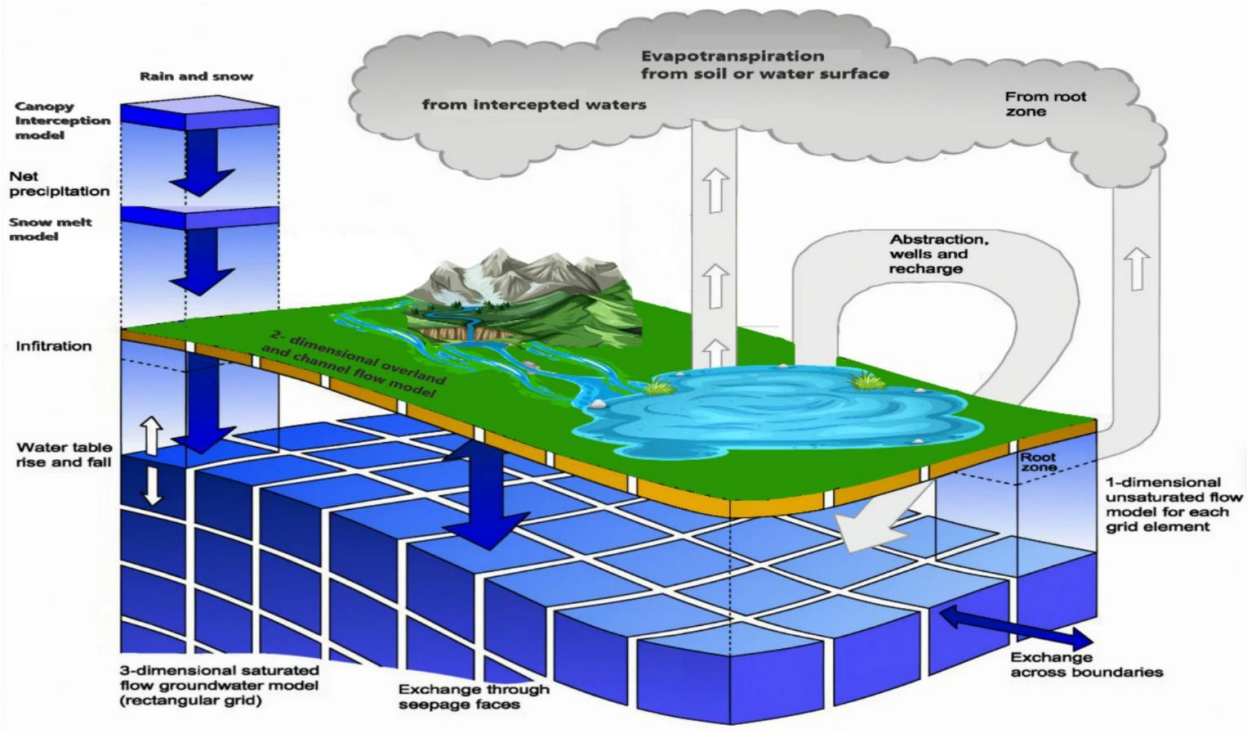

Figure 2 – Schematics of a gridded computational domain (Khurshid et al., 2025).

Although GSSHA has been applied in urban stormwater planning (Downer et al., 2011), watershed-scale flood prediction (Serrano et al., 2021), and even urban coastal contexts (Yang et al., 2022), its performance in low-urbanization coastal corridors remains underexplored. Understanding its behavior under such conditions is crucial to determining whether traditional hydrologic tools can adequately represent hydrologic processes that impact pavement infrastructure.

1.1.4. Traditional Groundwater Modeling

Groundwater models such as MODFLOW and its variants remain the most widely used numerical tools to simulate saturated flow in aquifers (Langevin et al., 2017; Navarro-Farfán et al., 2024). These models are based on the finite-difference solution of the groundwater flow equation and rely on well-defined boundary and initial conditions. Despite their robustness, traditional models are limited in coastal areas by: (1) their coarse temporal resolution (daily or monthly); (2) difficulties in representing transient tidal influences; and (3) data requirements that are rarely met in low-infrastructure regions (Bosserelle et al., 2023; Shaikh & Eldho, 2021). For this reason, data-driven and hybrid methods are increasingly an option for rapid assessment and vulnerability analysis of infrastructure in shallow aquifer settings.

1.1.5. Integrated Modeling for Infrastructure Risk Assessment

While physics-based models, such as GSSHA, capture spatially explicit interactions and hydrologic processes, empirical models offer computational efficiency and practical deployment for rapid scenario testing and decision support. This dissertation applies both modeling approaches to investigate the hydrologic behavior of Alabama State Route 180 (AL-180), a coastal corridor subject to shallow groundwater conditions. The empirical model is developed to predict GWL responses at segments of AL-180 that are located within 200 m of Mobile Bay. In contrast, the GSSHA model is applied in a selected catchment to evaluate high-resolution surface and subsurface conditions.

Based on this discussion, the main knowledge gaps that this dissertation aims to address are:

- The lack of sub-daily groundwater level prediction tools incorporating both tidal and rainfall drivers.
- The absence of transferable empirical models applicable across coastal linear infrastructure networks.
- The need to create frameworks to use hydrologic models in non-traditional low-lying coastal areas for infrastructure vulnerability mapping.

1.2. Objectives

1.2.1. General

This research aims to assess the vulnerability of coastal transportation infrastructure to shallow groundwater levels, with particular focus on sub-daily saturation dynamics driven by rainfall and tidal fluctuations. It integrates a physics-based distributed hydrologic model and a data-driven groundwater prediction framework to develop methodologies for evaluating pavement saturation risks along Alabama State Route 180 (AL-180). The broad objective is to inform technical and political strategies to improve the long-term resilience of coastal infrastructure to withstand increasing hydrologic stressors, including sea level rise (SLR), extreme rainfall, and elevated groundwater tables.

1.2.2. Specific

- Investigate if we can predict groundwater level variation based on measurable site characteristics.
    - Formulate a simplified empirical model using key predictors such as distance to tidal or large water bodies (Mobile Bay and Little Lagoon), surface elevation, tidal variation, and precipitation time series.
    - Verify if the framework is accurate compared to sub-daily GWL data collected along AL-180 under varying meteorological and tidal conditions.

    - Extend the empirical framework to other segments of AL-180 using a Geographic Information System (GIS)-based implementation at 100-meter intervals.
    - Evaluate if the pavement will be vulnerable to chronic high water tables.
- Evaluate whether a physically based distributed hydrologic model (GSSHA) can represent surface runoff, flooding, and groundwater dynamics in a non-traditional coastal setting when it was designed for use in traditional watersheds.
    - Identify which parameters are most important for model calibration in comparison with groundwater level observations.
    - Apply the model to quantify the vulnerability of coastal transportation infrastructure due to saturated water tables, including extreme coastal events

Chapter 2. Conceptual data-driven approach for analyzing the vulnerability of coastal roadways to groundwater level changes

This chapter is a version of an article of the same title by Bruno J. de Oliveira Sousa; Bret M. Webb; Daniel B. Wright; T. Prabhakar Clement; Jose G. Vasconcelos that has been published in the Journal of Environmental Management.

de Oliveira Sousa, B. J., Webb, B. M., Wright, D. B., Clement, T. P., & Vasconcelos, J. G. (2025). Conceptual data-driven approach for analyzing the vulnerability of coastal roadways to groundwater level changes. Journal of Environmental Management, 390, 1–12. https://doi.org/10.1016/j.jenvman.2025.126295

2.1. Introduction

Moisture infiltrating into an asphalt or concrete layer can damage pavements by increasing compressive strain on the subgrade. This can lead to surface depressions and striping that will form in localized holes (Chen and Wang 2023a; Titus-Glover et al. 2019). Our field site is the Fort Morgan peninsula coastal roadway AL-180 that connects Gulf Shores to Fort Morgan in Baldwin County, Alabama. It serves as an important transportation and evacuation route and has been impacted by rising water levels. In addition, according to information gathered from local communities, there are locations with flooding and standing water along the road during and after a rainfall event. These problems may affect evacuation during an extreme event such as a hurricane. In addition, despite being sandy and featuring high hydraulic conductivity, the soil along the peninsula is saturated for extended periods (Soil Survey Staff 2022).

Flooding and pavement saturation in AL-180 may be related to increased soil moisture and reduced infiltration due to elevated water table levels due to its proximity to Mobile Bay (MB; Housego et al. 2021; Rahimi et al. 2020). For example, Das et al. (2021) found that storm surges can cause near-instantaneous shallow groundwater level (GWL) responses in coastal areas. Precipitation can also cause coastal flooding since it can rapidly increase in the shallow GWL in high hydraulic conductivity soils with elevated water tables (Sukop et al. 2018). In addition, low hydraulic gradients between the peninsula and the bay can delay GWL recession after rainfall

(Xiao et al. 2024). Currently, there is a lack of systematic approaches to evaluate the risks of these groundwater-related impacts on roadways.

Groundwater flow dynamics is traditionally modeled by applying different types of analytical and numerical models (Curtis et al., 2018). MODFLOW is a good example of a numerical model that uses spatial discretization and is mostly used to simulate the impacts of wells, rivers, or other hydrologic changes in large aquifers (Langevin et al., 2017). One of its advantages is to simulate heterogeneous and anisotropic aquifers under variable recharge and extraction conditions in a three-dimensional environment (Navarro-Farfán et al., 2024). Other models, such as Gridded Surface Subsurface Hydrological Analysis (GSSHA) and MIKE-SHE (DHI, 2025; Downer & Ogden, 2006), present a simplified combination of surface and groundwater interactions. They both couple overland, channel, and subsurface flow, and can also perform water quality calculations. This allows for calculating interactions, such as channel discharge, generated both from excess infiltration and from soil saturation, in addition to lateral groundwater flow (Downer & Ogden, 2004; Saha & Quinn, 2020)Therefore, physically based models are still essential for groundwater modeling because they can simulate lateral recharge and account for soil heterogeneity. However, their data and computational demands often limit their application for rapid planning assessment.

Most studies that include groundwater in coastal areas focus either on surface flooding effects or on predicting long-term groundwater level variations and their impacts (Chang et al. 2016). Yu et al. (2022) evaluated the total storage using a detailed coupled surface–subsurface hydrological model. In contrast, Hayek (2019) created a simplified approach to solve for groundwater table elevation by applying the Boussinesq equation to model water level as a function of space and time. This equation calculates water level in unconfined aquifer systems in terms of discharge or recharge, depending on initial and boundary conditions, hydraulic conductivity, and specific yield (Hayek 2019; Tang et al. 2016). Nonetheless, all these approaches require detailed information about the study areas. These include geometry, soil characteristics, land cover information, geological units, etc., which are not always available(Bartlett and Porporato 2018; Park and Parker 2008; Shaikh and Eldho 2021). Therefore, due to limitations in data availability and computational resources, investigations have often employed models that use data with relatively coarse time and spatial resolutions to evaluate groundwater dynamics, typically neglecting sub-daily interactions (Bosserelle et al. 2023; Hussain et al. 2022).

In recent years, data-driven models have been used to study groundwater systems mostly at large scales over longer periods of time to investigate the behavior of large-scale aquifers. Most of these studies use regression and/or machine learning techniques to predict GWL time series based on observed data. Doglioni and Simeone (2017) investigated the effect of monthly precipitation on the variation of the groundwater table by applying evolutionary polynomial regression. Haaf et al. (2023) compared various approaches and found that extreme gradient boosting has more predictive power than multiple linear regression when considering neighboring groundwater well data. Xie and Zhang (2024) developed a method to extract the spatiotemporal dependence of variables to improve GWL predictions for a 3D coastal area. Their results are satisfactory in predicting GWLs in terms of daily precipitation, but neglect sub-daily groundwater variations, which are relevant in many coastal environments. Sun et al. (2022) tested different neural network models to predict groundwater depths at monthly and daily scales and found good calibration results with Nash-Sutcliff efficiency of up to 0.9. However, their prediction errors were in the range of 0.5 to 1.5 meters, which is impractical in highly conductive soil where the water table variation has the same magnitude as these errors. Therefore, it is understandable that the reliability of data-driven models, both empirical and machine learning, depends on the spatial and temporal representativeness of training data (Ali et al., 2024; Khan et al., 2023). Therefore, it justifies creating a generalizable model as a means to inform engineering problems.

Considering the complexity of groundwater dynamics of each coastal roadway setting (e.g., soil conditions, precipitation characteristics, tidal characteristics, sea level rise projections), a data-driven approach represents a practical approach to describing subsurface pavement saturation in response to precipitation, tides, and sea level rise. Therefore, in this study, we propose a straightforward data-driven approach to simulate sub-daily estimates of groundwater response to understand the impacts of shallow groundwater level variations on coastal roadways. The proposed data-driven model is intended to provide engineering estimates to manage pavement maintenance problems in coastal areas.

The proposed approach introduces key simplifications afforded by the selected study site in that there are no assumed lateral groundwater flows, soil characteristics are uniform, and high soil hydraulic conductivity. As a result, it is hypothesized that the local GWL variations are dependent only on the distance from a large tidal water body (Mobile Bay, in this case), tidal levels, rainfall depths, and a simplified representation of groundwater abstractions. The absence

of lakes, rivers, and other major water bodies supports the assumption that vertical fluxes (infiltration and evapotranspiration) are the primary drivers of short-term groundwater fluctuations. The proposed approach's applicability is limited by these assumptions, which are nevertheless aligned with other simplified conceptual frameworks to represent groundwater (Burek et al., 2020; Rossman, 2015). In order to test this methodology, this empirical model was compared to GWL datasets collected along a coastal road AL-180 in Alabama. Moreover, it was used to evaluate future groundwater scenarios to investigate the impacts of climate change effects, namely sea level rise, on GWL fluctuations.

2.2. Data Collection

To allow for the calibration of the models (verifying if they represent reality and adjusting the variables according to field data). The following sensors were installed along AL180 (see Figure 3):

- Two level loggers model HOBO Water Level U20 Data Logger: one for the intermittent drainage channel on the outlet of the subbasin formed in Point 1 (Boat Launch); the second one to measure the water level at one side of the road in the western part of the peninsula, where an Alabama DOT employee reported inundation problems; one at the Mobile Bay side of the culvert close to the public boat launch and Kiva Dunes Resort to capture change in water depth.
- Six HOBO level logger model U20L to capture shallow groundwater elevation were installed with the support of the Alabama DOT (which constructed monitoring wells) in the following locations (one on each side of the pavement, 6 in total): Navy Cove (located in the western part of the peninsula); close to the public boat launch and Kiva Dunes Resort; and at the field location called The Pines (Figure 3). One HOBO level logger model U20L
- One level logger model HOBO Water Level U20L Data Logger to measure atmospheric pressure to be used to correct the pressure measured by the sensors in the water and get water level data.
- Two rain gauges model HOBO Rain Gauge RG3-M Data Logger, one close to Point 1 (Boat Launch) and the other in the western part of the peninsula to start collecting

precipitation data used in the future to calibrate the models together with the water level data.

  - There is also one weather station (Latitude: 30.2387°N, Longitude: 87.8540°W) from the South Alabama Mesonet network that is being used to get precipitation data.

- Four conductivity loggers model HOBO U24 were installed at the Navy Cove, the public boat launch, and The Pines to better understand the relationship between the salinity (calculated through the conductivity measurements) of the shallow groundwater and the water levels at Mobile Bay and the Gulf of Mexico (see Table 1 and Figure 3).

Table 1 - Summary of monitoring variables by location

	Groundwater monitoring	Conductivity Monitoring
Navy Cove North	**X**	
Navy Cove South	X	X
Boat Launch North	X	
Boat Launch South	X	X
Pines North	X	
Pines South	X	X

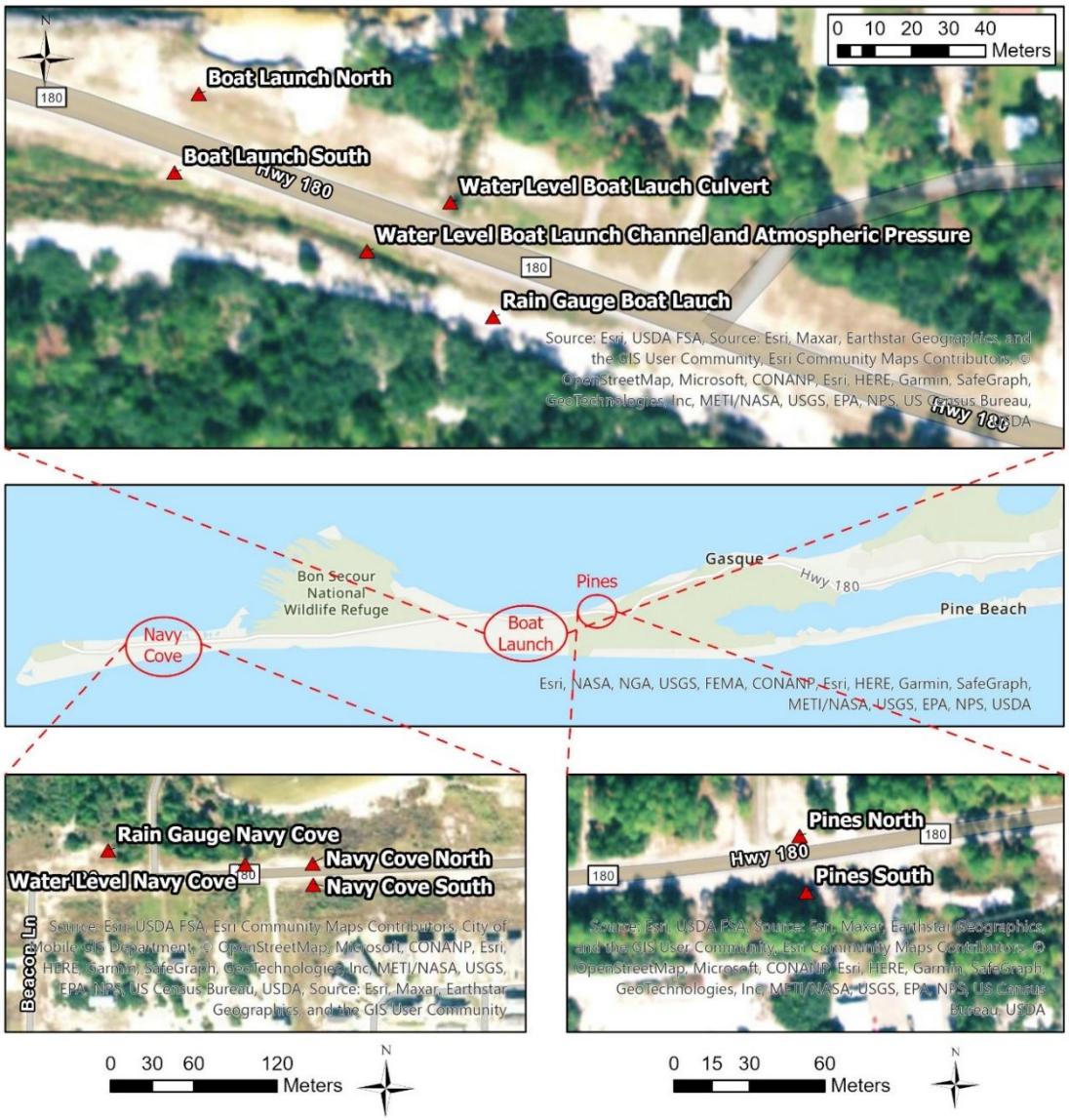

Figure 3 - Monitoring locations.

Figure 4a shows a well setup at the Pines location, a little further away from the pavement than the other wells. Figure 4b illustrates the atmospheric pressure sensor hanging from a tree and a sensor/datalogger being removed from the PVC encasing in the intermittent drainage channel located at the Boat Launch location. Figure 4c, on the other hand, is of the westernmost location in the peninsula, Navy Cove. It measured the water level downstream of a culvert. Figure 4d returns to the Boat launch location to show how the two wells were positioned at each location opposite each other, covering both sides of AL-180. Sensors in locations that had intermittent water levels had to be encased in PVC to avoid overheating. This was done after the channel and

atmospheric pressure sensor in Figure 4b presented problems because they remained dry for long periods of time. The groundwater sensors were installed using cords, and the distances shown in Figure 4 were collected to make it possible to calculate the water levels from the NAVD88 vertical datum. “L” is the length of the cord on which the sensors are attached up to the sensor location in the logger, “H” is the length of 2-inch PVC pipes above ground (Figure 5), and the ground elevation was collected using an RTK GPS device.

Figure 4 – a: Well set up at the Pines location, a little further away from the pavement; b: atmospheric pressure sensor hanging from a tree and a sensor/datalogger being removed from the PVC encasing in the intermittent drainage channel located at the Boat Launch location; c: Navy Cove water level downstream of a culvert; d: two wells were positioned opposite each other at the Boat Lauch location.

Regular site visits involved sensor installation, data retrieval, checking if the sensors were functioning properly, and visual inspection of road segments after rainfall events. In total, 14 trips were taken to Fort Morgan, with three of those trips also including the installation and maintenance of sensors in Dauphin Island. This data collection effort ensured a robust dataset for empirical

modeling and offered insights into the spatial and temporal dynamics of groundwater near the road. The inclusion of this fieldwork was essential to produce, calibrate, and validate the simplified predictor and ensure its grounding in real-world conditions. In addition, this data was used in the calibration and validation of the distributed hydrologic model to ensure it was a good representation of reality.

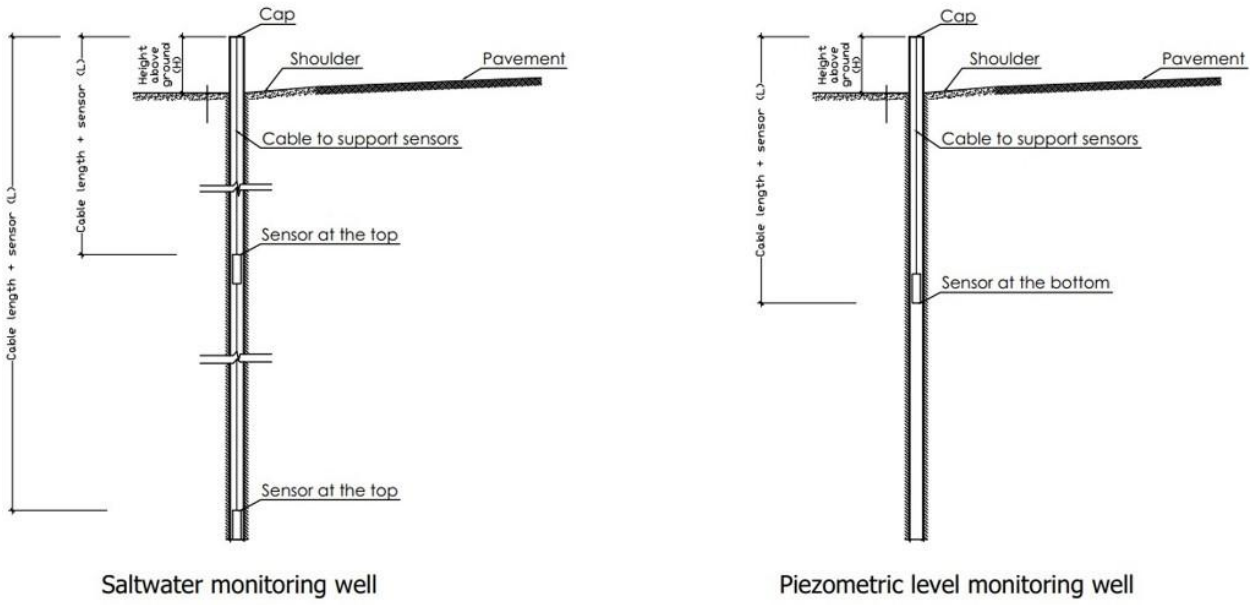

Figure 5 - Groundwater wells disposition.

2.3. Methods

The field site selected for this study is located along Alabama State Route 180 (AL-180) in Fort Morgan Peninsula (Figure 6). The groundwater monitoring wells installed at this site are also shown. AL-180 is a single-lane roadway with shoulders on both sides, but with few drainage features such as ditches or culverts, since the sandy beaches along the road are expected to have a large infiltration capacity. This was confirmed by the predominant fine sand soil, supporting high infiltration rates. However, part of the system is well drained (26%) while the remainder (about 74%) is poorly drained because of high water table conditions, as illustrated in Figure 6 (soil classification A/D on the east and west of the peninsula, meaning they have a high infiltration rate but also high water tables; (Soil Survey Staff 2022). Saturated hydraulic conductivity (K), while high, can vary on the order of 10-100 m/day (Chang et al. 2016).

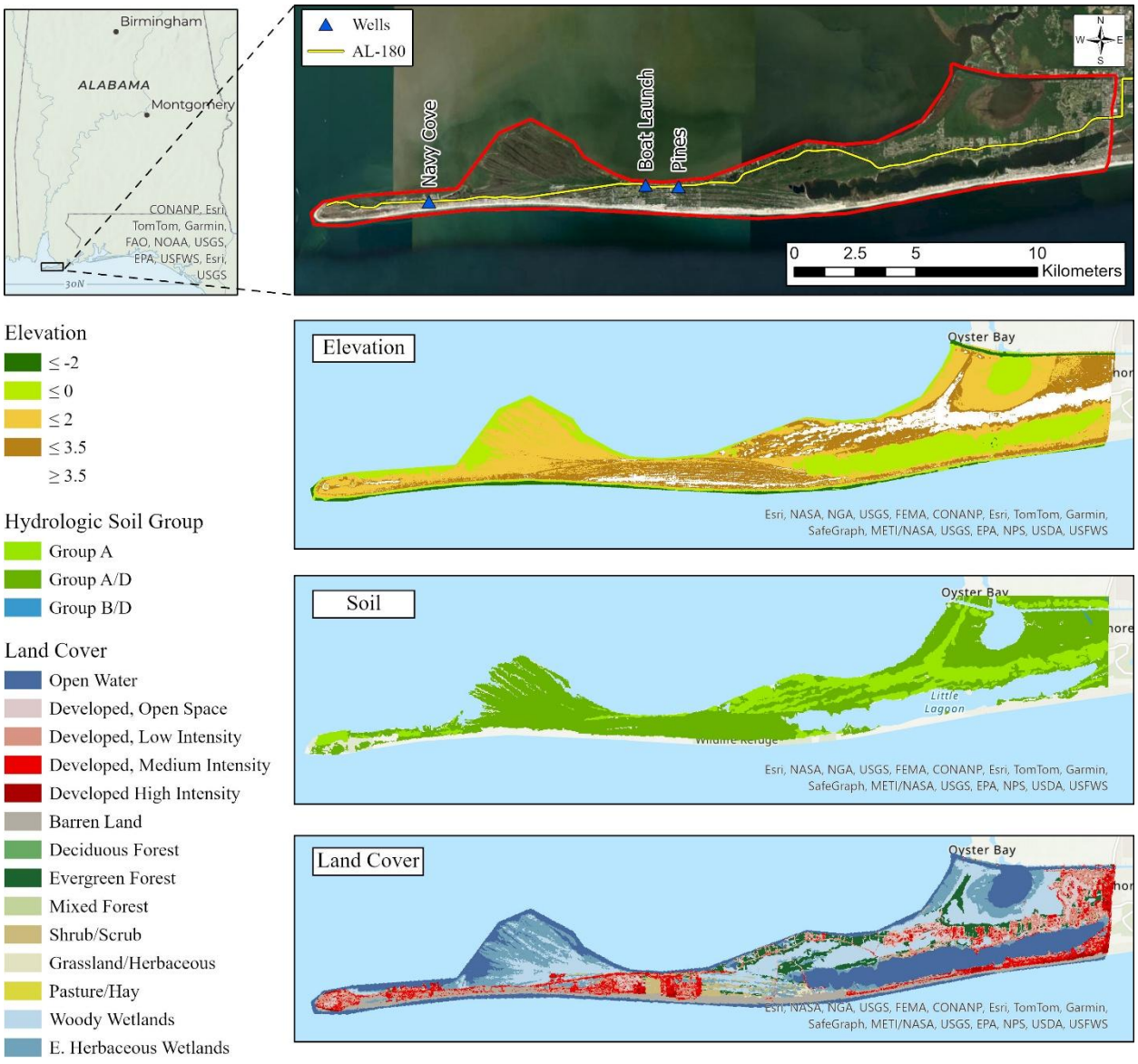

Figure 6 - Location, elevation, hydrological soil group, and land cover for Alabama State Route 180 (AL-180) in Fort Morgan Peninsula. Soil classification A means the soil has a high infiltration rate but also high water tables and, therefore, is poorly drained.

Three groundwater monitoring wells were installed next to the roadway shoulders. These are referred to as the Pines (PN), Boat Launch (BL), and Navy Cove (NC; see Figure 3). The data from PN and BL were used for model development and calibration. The data obtained in NC was used for model validation and testing. As in other data-driven frameworks (Koley, 2023), the predictive capacity is sensitive to the quality of the calibration dataset. While our model relies on limited groundwater well data, these locations were selected to represent varying degrees of

saturation. In addition to GWL measurements, we also collected rainfall and tidal data from available sources (Dauphin Island Sea Lab 2024; Kimball and Terwey 2024; NOAA 2024).

There are no perennial streams near the study area, and the major nearby water bodies are Mobile Bay (MB) to the north and the Gulf of Mexico to the south. The mean annual precipitation in the region is 1,581 mm (62.3 inches; NOAA, 2022), and the climate is classified as Humid Subtropical Climate (Beck et al. 2018). The main land cover classes are woody and emergent wetlands (44%), low-intensity developed land (13.1%), medium-intensity development (11.2%), barren land (11.4 %), and evergreen forest (8%).

While there are no drainage structures near PN or NC sites, there is a drainage ditch near the BL site located to the south of the roadway, which influences the local groundwater levels. This ditch is part of a drainage system connecting upstream to Kiva Dunes Public Golf Course, and its drainage ditch water depth near the BL site was also monitored. The surface water reservoirs in the golf course allow gradual drainage of surface runoff following rainfall events. The intermittent flow conditions and standing water in the ditch contribute to keeping the GWL at the BL site high even after surface infiltration is complete.

2.3.1. Tidal Elevations and Rainfall Data

Tidal data was obtained from the National Oceanic and Atmospheric Administration (NOAA) Tides and Currents database from the Dauphin Island Station, located across the Fort Morgan Peninsula (not shown in Fig. 1). Tidal data is collected every six minutes but was averaged to a 15-minute temporal resolution to match the groundwater level data collected in this study. The maximum tidal level in the data set between November 2022 and October 2023 was 0.8 m, and the minimum level was -0.5 m, relative to the NAVD88 vertical datum. The average GWL was assumed to be rising at the same rate as SLR in future scenarios (Sukop et al. 2018), and the tidal variation (i.e., amplitude) was assumed to be the same as the present variation.

Rainfall data were collected from the South Alabama MESONET program at Gasque station, located approximately 1.8, 3.1, and 12.1 km from the Pines, Boat Launch, and Navy Cove locations, respectively. An Excel VBA code was created to identify separate rainfall events, assuming rain events are separated by 6 hours (Huff 1967). Also, rainfall events less than 2 mm

were removed because they did not cause any noticeable changes in the measured GWLs. The remaining events were used to investigate the correlation between rainfall depth and GWL response.

2.3.2. Water level and pressure measurements

To enable comparison between ground elevation, tidal, and GWL data, all elevations reported in this study use the NAVD88 datum. The ground levels at the selected sites were measured using an RTK GPS receiver, and the elevations were 2.12 m at the Pines (PN), 2.19 m at Boat Launch (BL), and 1.21 m at Navy Cove (NC) sites, respectively. The distances between the three GW monitoring sites to MB were 136, 47, and 45 m for PN, BL, and NC, respectively. Five HOBO U20L water level loggers were deployed, measuring absolute pressures up to 207 kPa with a precision of 1 cm every 15 minutes. The loggers were distributed as follows:

- Three loggers were placed in 6 m deep, 2-inch diameter PVC-encased wells drilled on the south shoulders of AL-180 at the three groundwater monitoring sites shown in Figure 3.
- One HOBO level logger was placed at the ditch near the BL site.
- One HOBO level logger was used for monitoring atmospheric pressure near site BL.

2.3.3. Proposed GWL predictor model

In the proposed methodology, the time-dependent GWLs, referred to as $GWL_m(t)$, are computed as a function of four components. The first component is a steady level, which models the baseline static GWL, referred to as GWL_{st}. This steady baseline component was estimated for each location based on data collected for an extended period without rainfall (e.g., 3 weeks or more) when groundwater recession reached a stable baseline level with negligible changes. The value of GWL_{st} was observed to increase with the distance (d) from the MB; i.e., the steady-state groundwater gradient slopes downward toward the MB. The other three components that contributed to $GWL_m(t)$ are time-dependent:

- Tidal contribution to the GWL, or $GWL_T(t)$: This effect was also determined using data collected for longer periods without rainfall. This was computed by comparing 24-hour GWL amplitudes at the monitoring sites with the corresponding MB tidal amplitude. In

addition, the fact that GWL_T decreases in magnitude with distance d from the coastline has been documented by previous studies (Casasso et al., 2015; Li et al., 2002).

- Episodic GWL rise is the precipitation-induced recharge component R. Due to the high hydraulic conductivity of local soils, rainfall has a rapid effect on GWLs. Due to the absence of large additional water bodies along AL-180, such as lakes or rivers, no lateral GW recharge was assumed in the GWL predictor model. Hence, the proposed formulation assumes that the only factor influencing the rise in GWL is recharge due to the rainfall. An immediate GW rise response after rainfall events in coastal areas has also been observed by Casasso et al. (2015) and Sukop et al. (2018). The only exception was the BL location, where the drainage ditch water level was added to the model results after calibration.
- Recession following rainfall events, designated as D. It is assumed that GWL drops following rain events due to GW one-dimensional flow (lateral flow in this narrow strip island can be ignored) toward MB or due to evapotranspiration. These two processes are combined into the term D. The lower limit for the recession effect is assumed to be constrained by the local GWL_{st}; thus, it is assumed that the recession cannot drop the GWL below the observed base level GWL_{st}.

The methodology assumes that: 1) the main source of groundwater rise is recharge from rainfall; 2) the study area has high conductivity soils, yielding rapid GWL response; and 3) there are no other factors that can influence GWL, such as nearby streams and lakes. The combination of the three time-varying components results in the GWL rise term $GWL_R(t)$, which is updated over time using the equation presented below:

$$GWL_R(t + \Delta t) = GWL_R(t) + f(d, GWL_T(t), R, D) \quad (1)$$

where the terms of the function f are explained in the subsequent sections. $GWL_R(t)$ corresponds to the local GWL measured above the static value GWL_{st}. As shown in Figure 7, the predicted value for the local groundwater level is the summation of $GWL_R(t)$ and GWL_{st}:

$$GWL_R(t) = GWL_m(t) - GWL_{st} \quad (2)$$

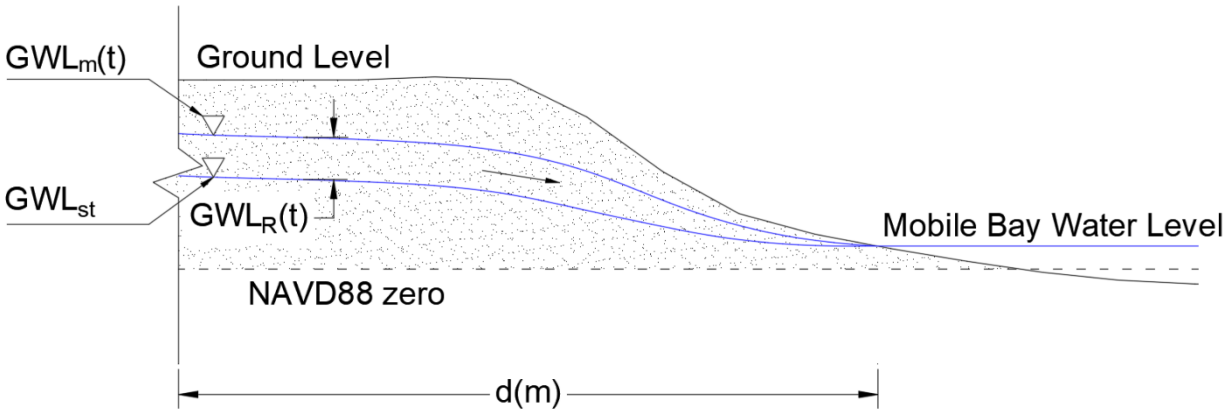

Figure 7 - Schematic profile illustrating the variables presented. Stable Groundwater

If the methodology assumptions apply for a coastal site, the terms that appear in equations 1 and 2 need to be calibrated to reflect the site-specific response to tide fluctuations, rainfall recharge, and recession. The following discussion details the terms of the function presented in Equation 2 to update GWL_m.

2.3.3.1. Stable GWL and Tidal Influence

The linear relationship between MB's short (sub-daily) and long-term tidal levels and the GWL was determined at our study locations independently of rain events. The distance between the GW well and MB was the independent variable (d) in both cases. The first dependent component, GWL_{st}, was obtained through curve fitting (Figure 8) in terms of the distance between the monitoring location and MB, defined as d (expressed in m):

$$GWL_{st} = 0.0041d + 0.0514 \quad (3)$$

Also, a nonlinear relationship was developed between the observed GW daily amplitude linked with the tide fluctuations in MB and the distance from it in extended periods without rainfall. The effects of the tidal fluctuation from the Gulf of Mexico side (i.e., the southern border of Fort Morgan peninsula) were not considered since the installed GW wells are at least seven times closer to MB than the Gulf of Mexico (e.g., 47 m vs. 340 m). An Excel VBA code was created to identify peaks and troughs from the GW data and tide data for periods without rainfall and with that identify daily GW level amplitudes. Subsequently, an expression for the tide contribution to GWL, or $GWL_T(t)$, was identified and in terms of the distance d:

$$GWL_T(t) = 0.260e^{-0.026 \cdot d} H_{tide}(t) \quad (4)$$

Where: $H_{tide}(t)$ = MB tide elevation with reference to NAVD88 vertical datum.

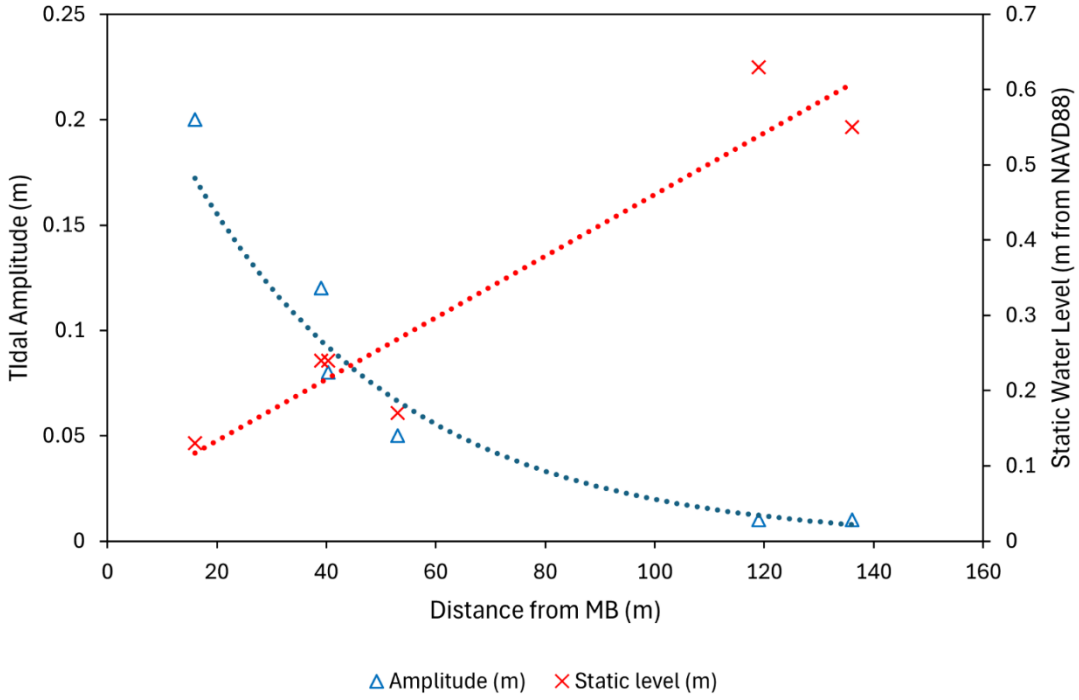

Figure 8 - Stable Groundwater Level (GWL) and Tidal fluctuation measured in wells as a function of distance (d).

2.3.3.2. Local GW Recharge

The well water level rise was studied after each rainfall event, utilizing the rain event separation process mentioned in Section 2.1. This process consisted of identifying GWL levels before and after each precipitation event. The episodic nature of recharge and the gradual recession between events align with the groundwater storage dynamics presented by Gleeson et al. (2014), in which water storage changes are calculated in aggregated time steps. The relationship between the rise in GWL and D is presented in Figure 9. A linear trendline was adjusted between D and the observed GWL rise, shown in Eq. 5:

$$R = 4.0 \cdot P \quad (5)$$

Where: R = GWL rise (m) and P = precipitation depth (m). In deriving Eq. 5, a few rain events recorded at the MESONET station were omitted, since they did not result in observable changes

in GWL. These were assumed to be either incorrectly reported rainfall depths or that rain did not fall near the GW wells.

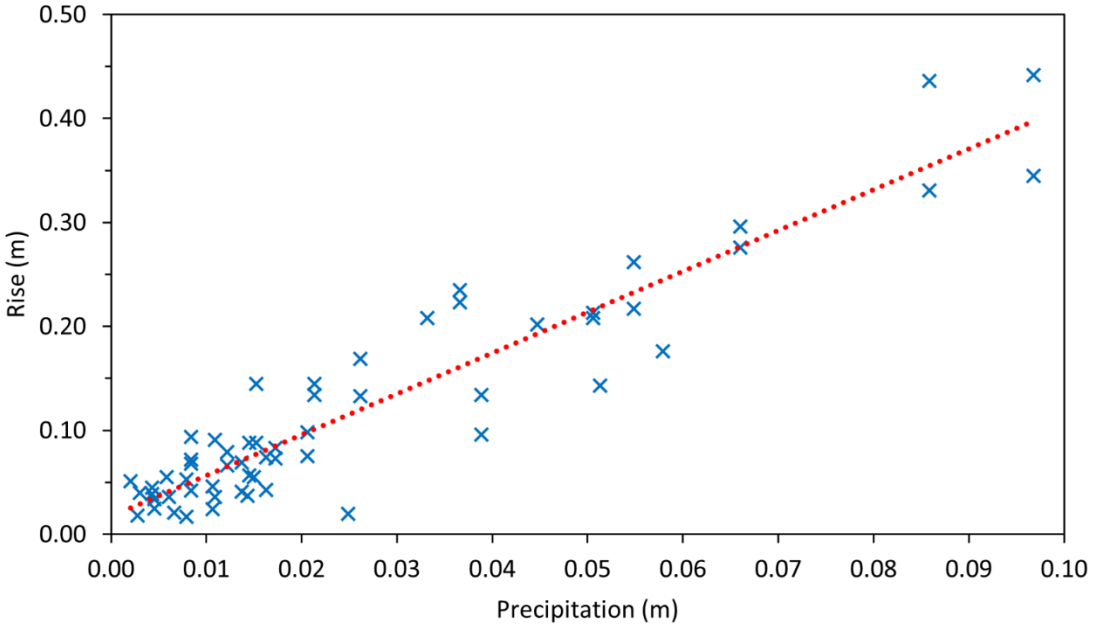

Figure 9 - Groundwater response to rainfall as a linear relationship.

Since rain events are episodic, GWL_R and GWL_m were updated after each rain event was over through equation 6, and the calculation time step Δt was set to the rainfall duration:

$$GWL_R(t+\Delta t) = GWL_R(t) + GWL_{tide}(t) + R$$
$$GWL_m(t+\Delta t) = GWL_{st} + GWL_R(t) + GWL_{tide}(t) + R \quad (6)$$

2.3.3.3. Recession Estimates

Between rain events, GWL at the monitored sites decreased due to GW flows toward MB and evapotranspiration effects, which depend on the soil's hydraulic conductivity and potential evapotranspiration. The changes in GWL due to recession occur gradually, as opposed to episodic and fast GWL rises due to rainfall. Recession effects on GWL were computed every 15 minutes using two separate approaches by updating the changes on the GWL above the steady value (i.e., GWL_R).

The method to compute the recession D assumed that the GWL_R recession is first order (Petricci et al. 2023) and hence can be modeled using the equation $\frac{d}{dt}GWL_R = K_d \cdot GWL_R$. For instance, the approach to simulate recession as a first-order decay is consistent with the linear reservoir application used in global-scale models such as CWatM (Burek et al., 2020). Coefficient K_d (in m day^{-1}) was calibrated to best represent the local GWL behavior, selected as -0.060 m/day for all selected monitoring sites. Based on this second approach, and using a 1st order Forward Euler approximation for the numerical solution of the ODE, the recession term became:

$$D = K_d \cdot GWL_R(\mathrm{t}) \cdot \Delta t = -0.060 \cdot GWL_R(\mathrm{t}) \cdot \Delta t \tag{7}$$

Through equations 6 or 7, the effect of recession on GWL_R and GWL_m is expressed through equation 8:

$$\begin{aligned} GWL_R(t + \Delta t) &= GWL_R(t) + GWL_T(t) + D \\ GWL_m(t + \Delta t) &= GWL_{st} + GWL_R(t) + GWL_T(t) + D \end{aligned} \tag{8}$$

2.3.3.4. Updating the predicted GWL value

The computational steps used in this study are summarized in the flowchart presented in Figure 10. The calculations employed 15-min time steps, updating GWL_R through Eq. 8, except when rain events occurred. When rain events occurred, the time step Δt matched the rainfall duration, and the value for $GWL_R$was updated through Eq. 6. However, if the GWL_R became equal to zero, the methodology forces it to remain at zero until another rainfall event is reached. Once the desired time of the simulation is reached, the calculation of GWL_R is completed (see Appendix A for the implementation in MS Excel VBA).

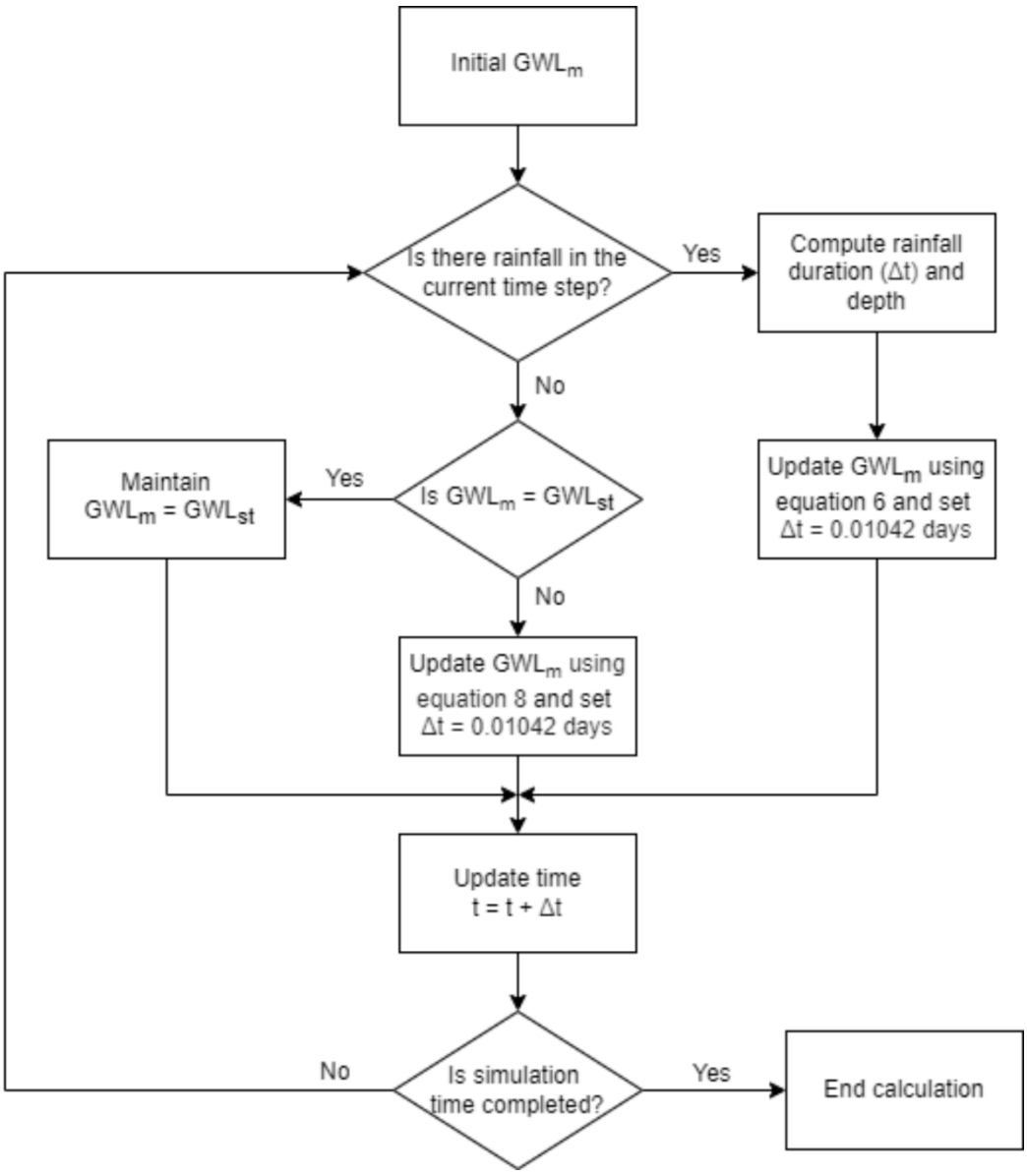

Figure 10 - Flowchart illustrating all the calculation steps used for simulating the Groundwater Levels (GWLs).

2.3.3.5. Validation

The R and D terms in equations 6 and 9 were calibrated using GWL measurements taken at the PN and BL sites. Later, they were validated using data from the NC site. The proposed methodology was applied to generate $GWL_m(t)$ predictions at the NC site and compared to local GWL measurements. Due to its location 9 km west of BL, rainfall data was generated based on both MESONET and the Dauphin Island rainfall stations, weighing according to the inverse

distance to the location. In addition, due to their widespread use for evaluating hydrologic models (Althoff and Rodrigues 2021), Root Mean Squared Error (RMSE) and Nash–Sutcliffe Efficiency (NSE) were used to evaluate the model's predictive efficiency at all three locations. Motovilov et al. (1999) suggests that NSE values greater than 0.75 are considered good, while NSE values between 0.36 and 0.75 are considered satisfactory. In addition, two Shared Socioeconomic Pathways (SSPs) from the Intergovernmental Panel on Climate Change (IPCC) 6th Assessment Report (AR6), SSP3-7.0 and SSP5-8.5, were applied to assess climate scenarios in terms of Sea Level Rise (SLR) (Garner et al., 2021; Intergovernmental Panel on Climate Change (IPCC), 2023; Kopp et al., 2023). These scenarios were incorporated into the validated model to evaluate the potential impacts of SLR on the groundwater table and, consequently, on pavement conditions along AL-180.

2.4. Results and Discussion

2.4.1. Observations on GWL dynamics

To illustrate GW dynamics at the three sites, Figure 11 shows GWL measurements in a period encompassing three rainfall events for all three study sites. The sections of AL-180 closer to MB (i.e., near BL and NC) present a similar tidal response in the GWL in terms of daily fluctuations and amplitudes. Both locations show a delay of around 90 minutes between the tidal peak and peak values observed in wells by the road. Most variation in the GWLs is caused by recharge due to rainfall and the associated recession it creates. This indicates the importance of both recharge and recession. As shown in Figure 11, GWLs rose immediately after rainfall and were followed by a recession period that lasted until the next rain event. Considering the second rain event, for instance, the same rainfall depth (70 mm) caused a R value of 30 cm, 28 cm, and 36 cm at NC, BL, and PN, respectively. The ratio of rainfall to the GWL rise R As shown in Figure 11, the ratio was in the range of four or more, which is roughly similar to Peña et al. (2022), who found ratios for large rainfall events in the range of five times in a watershed in north Miami.

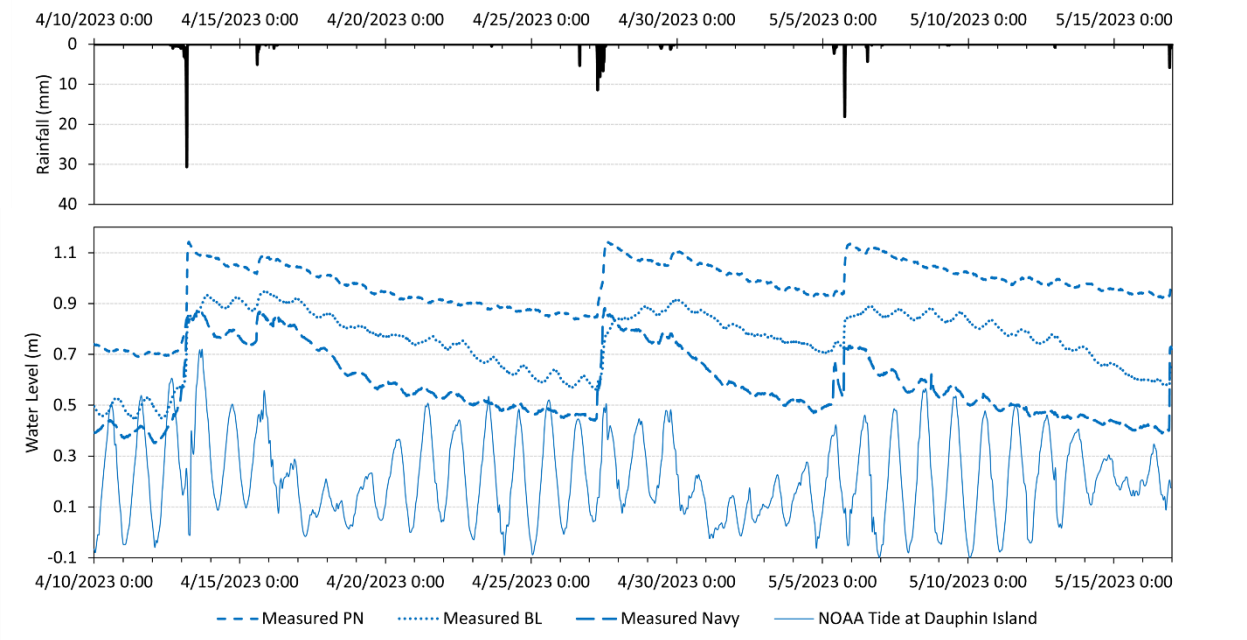

Figure 11 - Flowchart illustrating all the calculation steps used for simulating the Groundwater Levels (GWLs).

Variations in tide amplitude measured in the wells are attributed to the distance to MB. At the PN site, there is a smaller amplitude tidal effect on the local GWL due to the longer distance between the site and MB. Habel et al. (2019) applied a physically based model to represent GWL in coastal areas in Honolulu, HW. Whereas that study acknowledged the effects of tidal signal attenuation, their work did not implement such attenuation in their predictions. Housego et al. (2021) observed attenuation of the tidal signal in GWLs in coastal North Carolina.

2.4.2. Model Results

Figure 12 compares measured GWL and the results from the proposed methodology for PN and BL locations, showing satisfactory agreement following a similar pattern to the observed values over a simulation period of almost one year. It can be observed that the greater proximity of BL to MB led to greater tidal influences on GWL_m. In addition, the formulation presented for tidal influence agrees very closely with the observed data in the wells. The discrepancy between the measured GWL and GWL_m at BL is attributed to the periods in which there was standing water in the ditch near the well, as is further explained below.

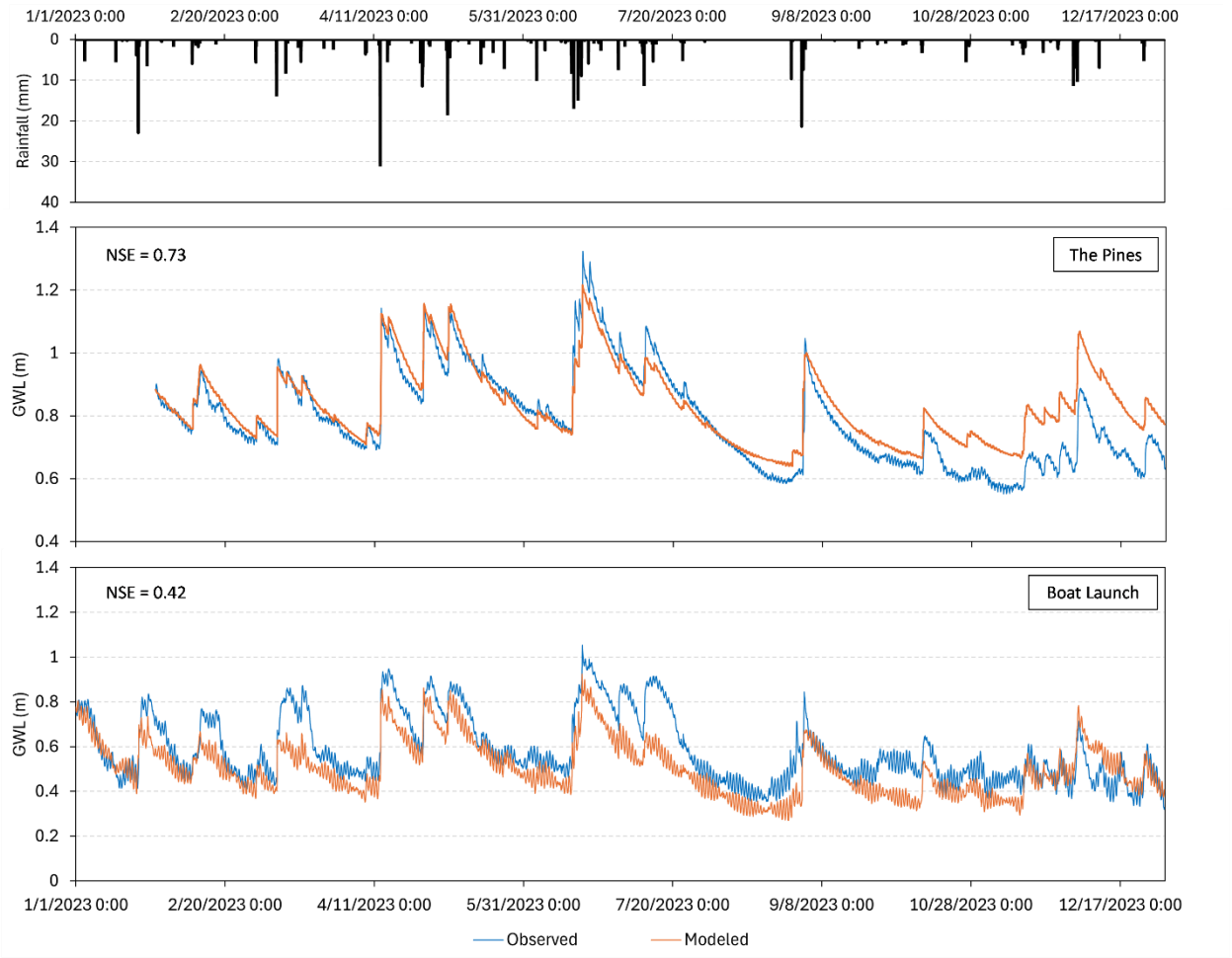

Figure 12 - Local Groundwater Level (GWL) measurements compared to Time-dependent Groundwater Level (GWLm) predictions for The Pines and Boat Launch sites between January and December 2023.

Starting in early October, a systematic discrepancy was noticed in the PN predictions. This discrepancy was particularly noticeable in the results for GWL_m using Eq. 8 to estimate recession. It is speculated that this difference stems from discrepancies between the rainfall observed at the PN site and what was measured in the MESONET station. These discrepancies could also be linked to measurement errors associated with temperature changes, as the water table is close to the surface. Changes in temperature and water composition can affect water density and, in turn, level measurements (Rau et al., 2019).At the PN site, a better fit was achieved PN had an NSE of 0.73, while the BL site had a smaller NSE of 0.42. RMSE values were also smaller at PN than at BL, 0.06 m against 0.11 m. These results align with *D*. Bowes et al. (2019) which used a Long-

Term Short Memory (LSTM) machine learning model to predict GW table level. The authors found RMSE values ranging from 0.06 m to 0.1 m, consistent with the present study.

GWL exceedance curves were derived for both observed data and predictions at the PN and BL sites and are presented in Figure 13. These curves help assess how long the subbase of AL-180 is affected by soil saturation over a hydrologic year without major coastal storms along Fort Morgan peninsula. At the PN site, GWL_m predictions showed a better fit for lower probabilities (i.e., higher GWLs), which is important to estimate the amount of time when the relatively shallow pavement layers might be saturated. The overestimation of GWL_m for higher probabilities (i.e., lower GWLs) may result from deviations in the modeled results towards the end of the simulation caused by differences in precipitation.

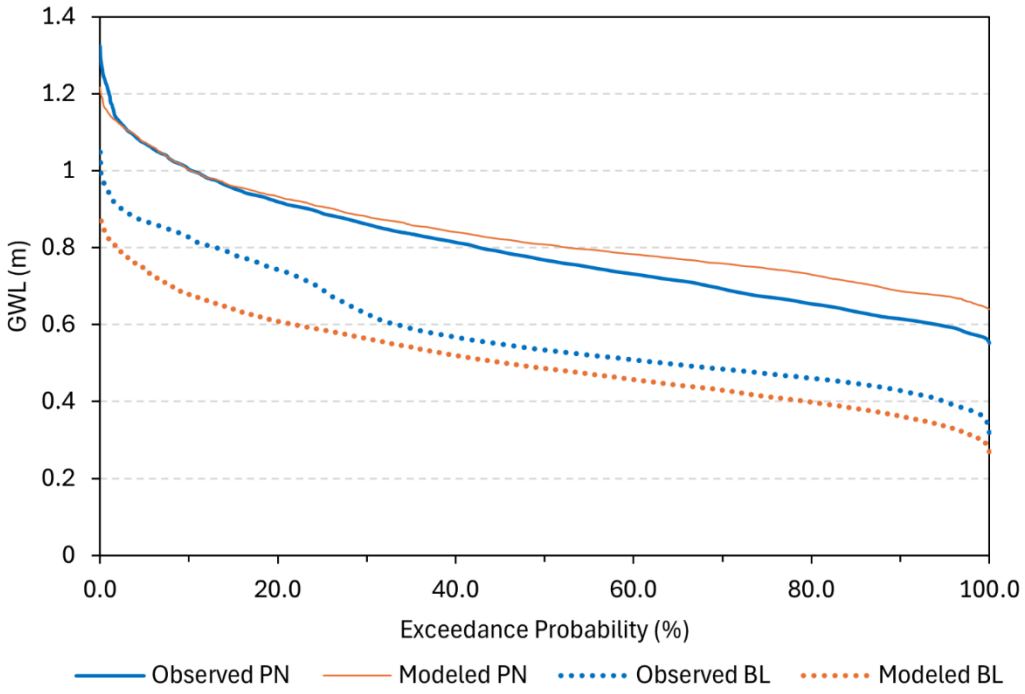

Figure 13 - GWL exceedance curves for The Pines and Boat Launch sites based on observed GWL and Time-dependent Groundwater Level (GWLm) predictions.

At BL, on the other hand, all GWL probabilities were underestimated by a relatively consistent amount, associated with the effect of the nearby drainage ditch that was not accounted for in Eq. 8. To verify this hypothesis, measured water levels from the drainage ditch near the well were added to the modeled results (Figure 14). After adding the ditch water levels to the predicted

GWL_m, the agreement improved. NSE values for the BL site with the ditch water level added increased from 0.42 to 0.65, and RMSE results dropped to 0.09 m. This refinement of the results may be associated with discharge from the channel to the groundwater when there is runoff on the ditch (Lambs, 2004). Furthermore, discharge on the ditch may consist of both surface and groundwater, with the remaining differences possibly stemming from groundwater flow to the channel.

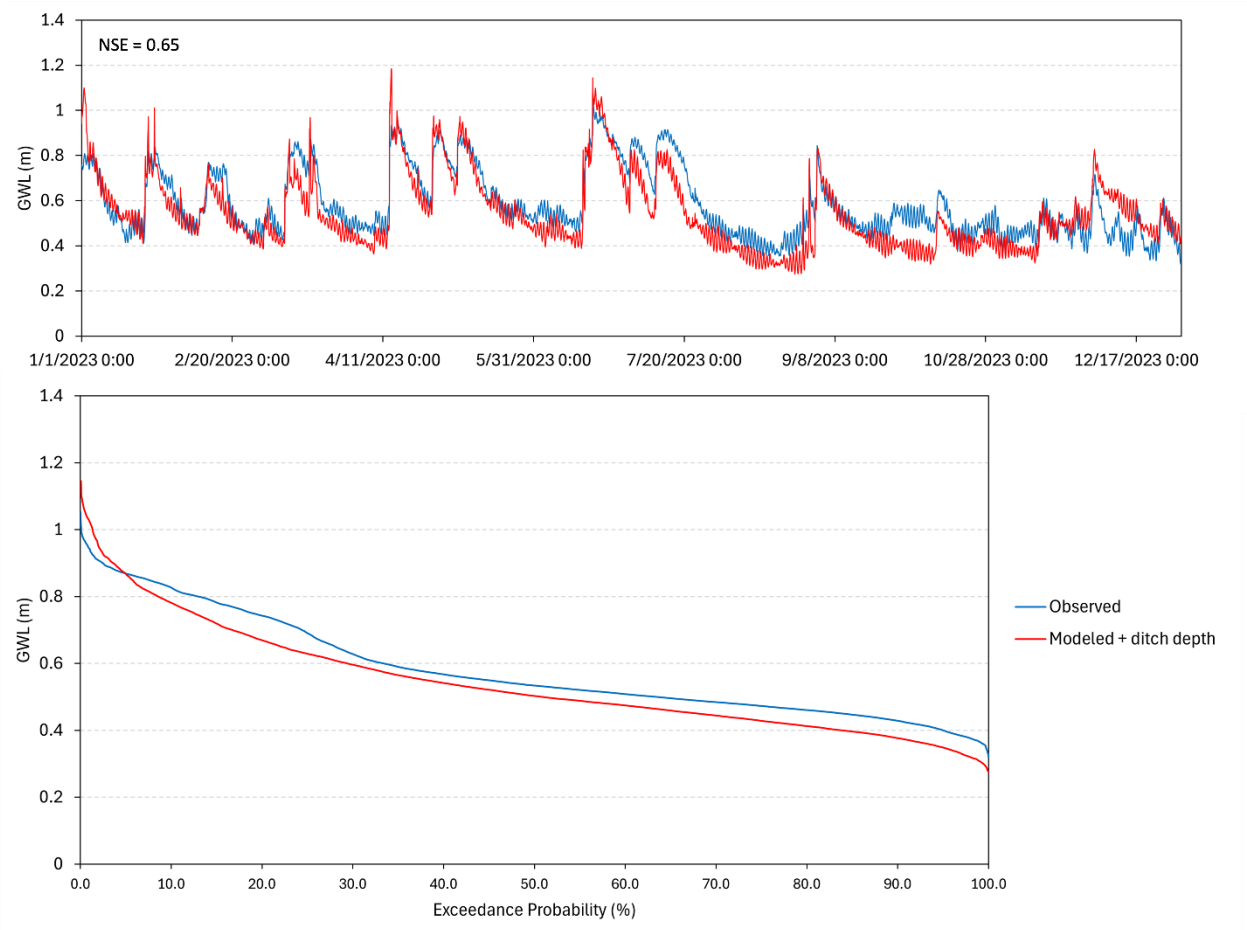

Figure 14 - Comparison between observed Groundwater Level (GWL) and Time-dependent Groundwater Level (GWLm) predictions for the Boat Launch site after considering the effect of the overlying drainage ditch on the GWL series and exceedance probability.

2.4.3. Model validation

As explained, the data collected at NC was not used in deriving the expressions for the groundwater recharge R (Eq. 5) or the recession estimates D (Eqs. 7 and 8). Figure 15 shows the

predicted and measured GWL values for the NC location. Overall, the results illustrate that the proposed method successfully captured the general behavior of the GWL variation, even though the site is several kilometers away from the rain gauges. Moreover, accurately captured most GWL peaks, which is crucial for predicting pavement exposure. Predictions had an NSE of 0.56, comparable to the results obtained for the BL site after correction using the ditch level.

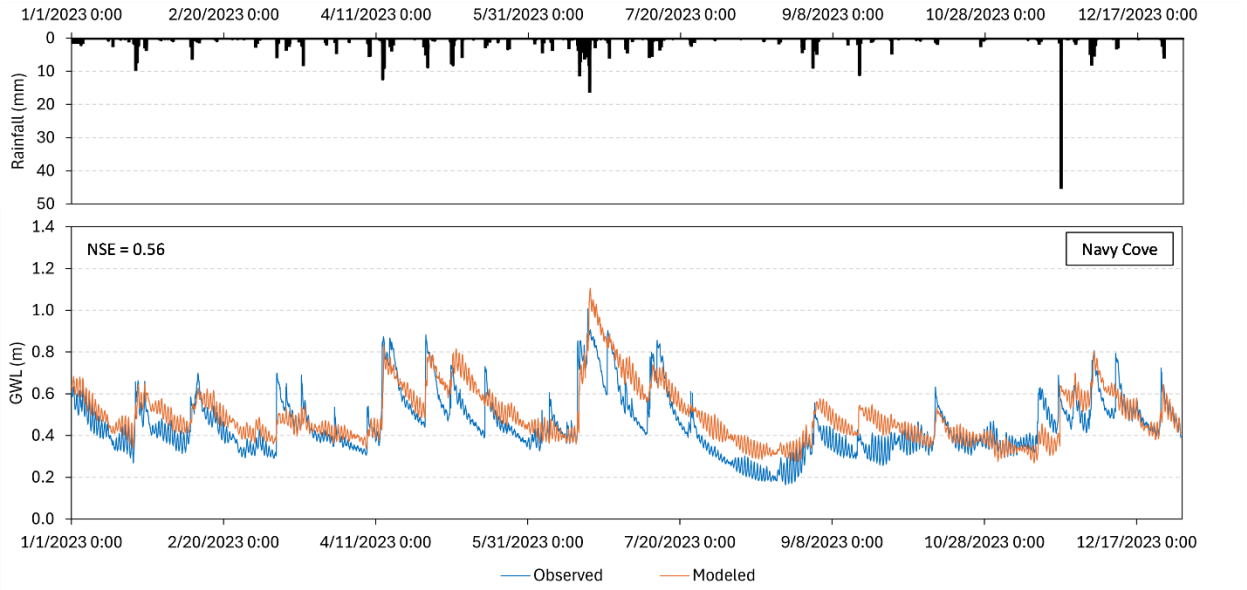

Figure 15 - Model run results for Navy Cove. 1st-order decay results are close to the observed GWL for most of the period.

GWL exceedance probability curves for NC had better results than those at BL and PN sites, as shown in Figure 16. Even though GWL values are slightly overestimated, the difference is minimal (less than 10 cm). The steepest variation occurs at a 10% exceedance probability for observed data, while the model predicts it starting around the 5% level. For the higher probabilities, on the other hand, the change in the slopes of the exceedance curves is similar between the observed and modeled. An important observation is that the exceedance probability curve reflects only one year of data collection. A longer observation record can potentially change these results, along with the occurrence of more intense rain events.

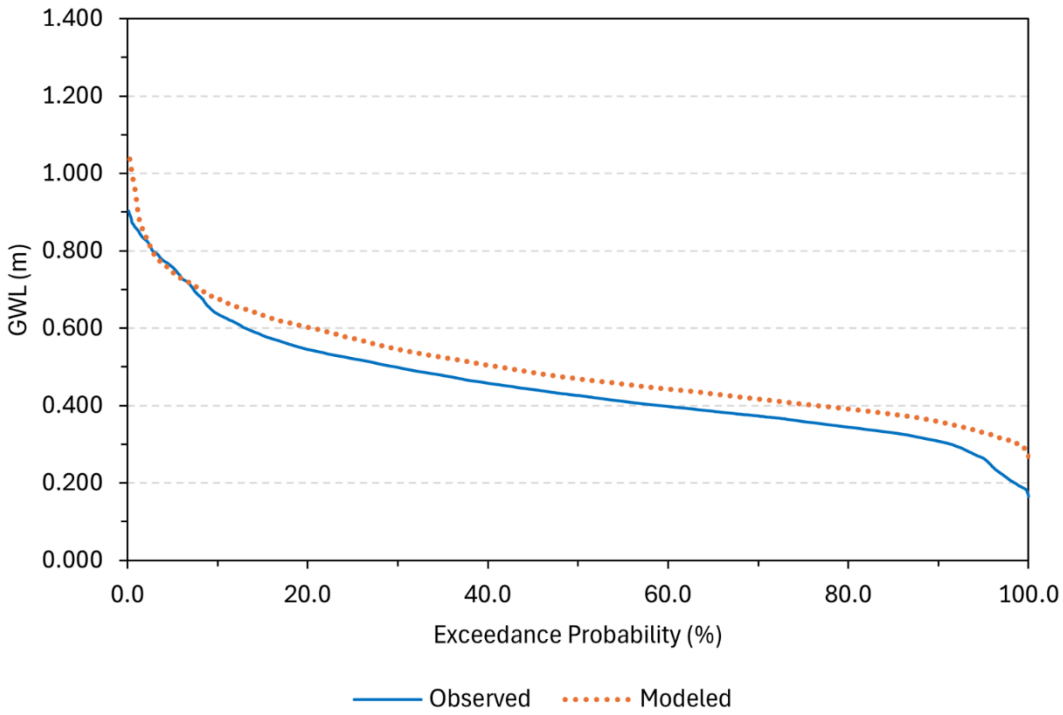

Figure 16 - GWL exceedance probability curves for the Navy Cove site based on observed GWL and Time-dependent Groundwater Level (GWLm) predictions.

Doglioni and Simeone (2017) found similar NSE values (0.49 to 0.65) modeling 52 years of monthly rainfall and groundwater response using evolutionary polynomial regression. However, few monitoring sites have long records that facilitate daily or sub-daily characterization. Using a three-dimensional GW model coupled with a surface water level model in a beach nourishment area in the Netherlands, Huizer et al. (2018) computed RMSE values varying from 0.08 m to 0.17 m for GWL predictions. However, their physical-based modeling required additional geologic characteristics and is more computationally demanding. Haaf et al. (2023) also found RMSE values close to 0.1 m using nonlinear regression to model daily groundwater series from neighboring locations, which is in the same range of this work. Therefore, the proposed model achieves the model accuracy found in related studies, but at sub-daily time scales and including tidal effects.

2.4.4. Estimating Effects of Sea Level Rise (SLR)

In the current scenario (Figure 17), pavement layers are exposed to saturation for less than 3% of the time. However, projections under climate change scenarios show a substantial increase in this risk. Based on SLR projections associated with SSP3-7.0 and SSP5-8.5, as illustrated in Figure 17, the frequency of subgrade saturation may increase dramatically. These scenarios were selected to represent a broad range of potential futures: SSP3-7.0 explores conditions under regionalized development pathways with varied adaptation and mitigation efforts. At the same time, SSP5-8.5 reflects rapid economic growth driven by fossil fuels. Under SSP5-8.5, for example, the subgrade may be saturated more than 90% of the time. Moreover, the base course and asphalt layers could be exposed more than 49% and 13% of the time. However, even under SSP3-7.0, a lower emissions scenario, the pavement may also be at risk because of high GW levels. Pavement subgrade saturation alone has been linked to service life reduction ranging from 5 to 20% (Inyim et al. 2016; Knott et al. 2017), and even more pronounced degradation can occur when the base course is affected. These results emphasize the vulnerability of infrastructure to rising groundwater levels under high-emissions scenarios. However, it is important to acknowledge persistent uncertainties related to local sea level trends, land subsidence, and storm surge interactions, which could further influence the magnitude and frequency of groundwater impacts.

The results and methodology presented in this study may help guide policy in terms of mitigation strategies. Among these strategies are roadway elevation, changes to drainage systems, incorporating permeable materials to the pavement to avoid upward pressures from GW, and nature and nature-based feature (NNBF) allocation (Picketts et al., 2016). As a planning tool, this model can be used for land use planning to identify infrastructure that is not at risk now but may be at risk in the future because of Sea Level Rise and increased rainfall intensity. In addition, such a tool could be used for real-time monitoring based on expected rainfall.

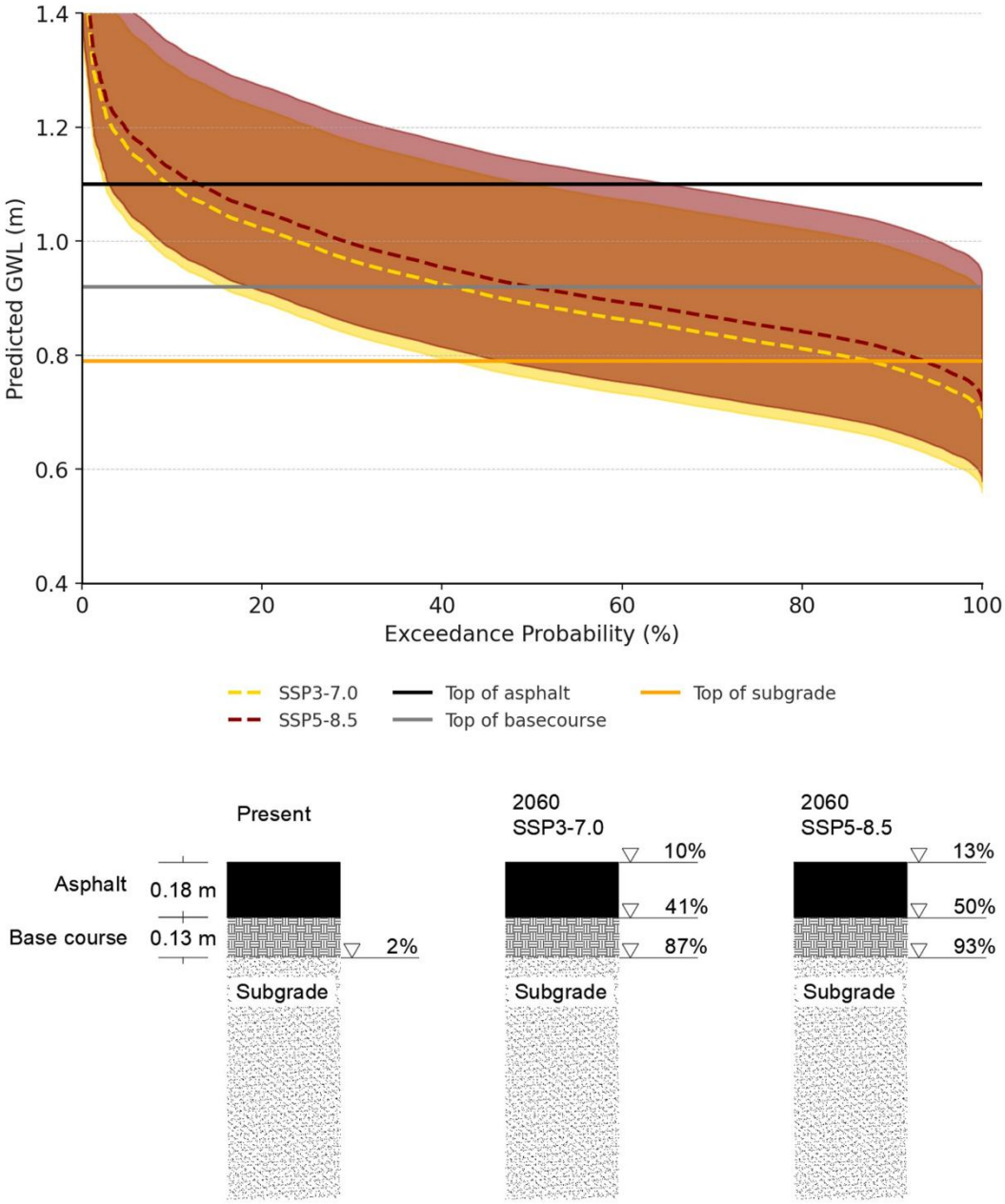

Figure 17 - GWLm exceedance curves for Navy Cove using equations (7) and (8), and its extrapolation considering SSP3-7.5 and SSP5-8.5, Shared Socioeconomic Pathways (SSPs) from the Intergovernmental Panel on Climate Change (IPCC) 6th Assessment Report (AR6) to assess pavement saturation in terms of Sea Level Rise (SLR). Shaded areas represent confidence intervals for GWL exceedance projections under each climate scenario, based on uncertainty in future sea level rise and rainfall patterns.

2.4.5. Model Limitations

While an NSE validation of 0.56 indicates moderate predictive performance, it also highlights the limitations of applying a simplified model to a highly dynamic coastal system. Key assumptions contributing to potential error include the representation of soil properties as spatially uniform across the peninsula and the exclusion of density differences between saline and freshwater. Although soil data indicate uniform sandy soils along AL-180, local-scale heterogeneities may influence GWL responses. Furthermore, limited data availability restricted model validation to a single site. This may restrict the model's transferability without further calibration. Despite these limitations, the model is designed to provide engineering-level estimates to support pavement maintenance decisions, which justifies the omission of lateral groundwater inflow. Moreover, Fort Morgan Peninsula's narrow geometry, ranging from 300 to 1000 meters in width, and the presence of constant head boundary conditions on both the Gulf of Mexico and Mobile Bay create a natural setting, allowing for the isolation of the effects of rainfall and boundary fluctuations on groundwater dynamics.

2.5. Conclusions

In this study, we developed a GWL modeling framework that is capable of predicting GWL time series based on available precipitation and tidal data. The approach offers a simple and intuitive methodology for assessing coastal infrastructure vulnerability to elevated GWLs. The model demonstrated a strong performance at calibration (NSE values as high as 0.73 and RMSE as low as 0.06m). Moreover, it had satisfactory prediction performance at the validation site (NSE = 0.56, RMSE = 0.09 m), even though the location was away from the rainfall data source location.

Beyond time series prediction, the model produced GWL exceedance probability curves, which can inform pavement deterioration and life span reduction assessments. This capability is critical for evaluating infrastructure risks, particularly for roads susceptible to high water tables. The GWLs generated using the proposed methodology may be improved with the use of longer-term monitoring data, especially when more intense hydrological events are included.

The study's findings have direct implications for coastal roadway management. Its transferability to other sites, however, relies on proper calibration of the proposed model equations

for coastal regions with appropriate physiographic characteristics. However, the successful application of this methodology depends on the following assumptions: the leading cause of groundwater rise is recharge from local rainfall, the site has high conductivity soils (facilitating rapid GWL response), and there are no other factors, such as nearby streams, lakes, or pumping wells, that can influence GWLs.

Despite its success, the model can be refined to improve the recession dynamics by including soil characteristics, which seemed to have a more substantial effect on the Navy Cove site. Moreover, evapotranspiration estimates could be improved using more sophisticated ET measurement approaches. Another means for improving the overall system dynamics is to consider seasonal climate effects in terms of the calibration parameters used for computing GWL recession. Finally, validating this framework in areas with different climatic and physiographic characteristics would also help enhance its applicability to other coastal roadways.

While this chapter introduced an empirical methodology to estimate groundwater level at the AL-180 corridor, the analysis was limited to three locations. The next chapter builds upon this framework by extending the methodology to the longer segments of this corridor, with particular emphasis on locations within 200 meters of Mobile Bay within the applicability reach of this methodology. This spatial expansion allows for a more comprehensive screening of vulnerable road segments using the same predictive approach.

2.6. Data Availability

The MS Excel VBA code and the observed groundwater data used in this study are available at https://github.com/bjs0091/data-driven-coastal-GW-model.

Chapter 3. Pavement Infrastructure Exposure to High Water Tables Along a Coastal Roadway

This chapter is a version of a paper that is under preparation for submission by Bruno J. de Oliveira Sousa, Luiz Menezes Morgado, and Jose G. Vasconcelos to Transportation Research Record.

De Oliveira Sousa, B. J., Morgado, L. M., Vasconcelos, J. G. (2025). "Pavement exposure to high water tables along AL-180 in coastal Alabama." [Manuscript under preparation]

3.1. Introduction

The combination of sea level rise with increasing frequency and intensity of extreme events contribute to pavement deterioration by increasing compressive strain, raising the likelihood of surface depressions and holes appearing, and causing pavement disintegration (Chen & Wang, 2023; Titus-Glover et al., 2019b). This occurs because soil saturation on and beneath the pavement subbase increases deformation under traffic loading, leading to premature failure. Studies have demonstrated that saturation of pavement layers may reduce their service life up to 90% (Knott et al., 2018). Moreover, recovery after flooding is a slow process because the subgrade's mechanical capacity may remain compromised for months after GWL recedes (King & Taylor, 2023). Understanding the temporal patterns of pavement saturation is crucial for informing effective management strategies. This is particularly relevant in coastal areas with shallow GWL and limited drainage due to their proximity to tidal water bodies. Therefore, understanding the spatial distribution of shallow groundwater conditions is crucial for maintenance prioritization, climate adaptation, and infrastructure resilience planning in coastal corridors.

Accurate hydrologic predictions are essential for understanding the risks posed by external drivers such as tidal variations and rainfall. Physics-based models are commonly used to represent surface runoff, infiltration, groundwater flow, and evapotranspiration processes under various meteorological conditions (Downer & Ogden, 2006; Keller et al., 2023). However, the applicability of physical models is often constrained in data-scarce or large-scale settings due to their high computational demand and calibration complexity, particularly when high-resolution temporal predictions are required (McAnally, 2025). Conversely, empirical models can offer a

data-driven alternative for estimating GWL fluctuations and saturation persistence. Tidal variations, surface elevation, and precipitation affect groundwater dynamics in coastal areas, making data-driven methods particularly effective in predicting GWL variations (De Oliveira Sousa et al., 2025). This enables the easy identification of periods when the GWL intersects with the pavement structure.

This study presents a geospatially distributed, empirical framework to predict groundwater-induced saturation along coastal roadways, using AL-180 as a case study. The framework expands the methodology (De Oliveira Sousa et al., 2025) but is evaluated at 100-meter intervals along Alabama State Route 180 (AL-180) in Fort Morgan Peninsula and Gulf Shores, AL. It encompasses the effects of Mobile Bay to the north, the Gulf of Mexico to the south, and a large water body known as Little Lagoon. Additionally, it incorporates surface elevation, rainfall, and tidal time series in its formulation. The goal is to perform a comparative evaluation of sections of AL-180 that are most susceptible to saturation of its layers and the implications for pavement resilience.

3.2. Methods

To demonstrate the usability of this methodology, a case study was conducted along AL-180 in Fort Morgan Peninsula, Alabama. The area was chosen because it is a barrier peninsula subject to constant groundwater fluctuations driven by tides and precipitation. For this study, the road was divided into 100-meter segments to allow for spatially explicit modeling along the corridor. This was done using the ArcGIS Pro "Generate Points Along Line" tool, which creates evenly spaced points along a polyline feature—in this case, the centerline of AL-180. The road shapefile was obtained from the TIGER/Line database (U.S. Census Bureau, 2024), which provides nationwide transportation data. To isolate the study area, the shapefile was clipped to the boundaries of the two relevant census tracts: Fort Morgan Peninsula (114.08) and Gulf Shores (114.07). However, the entire area was divided into two major subsections of AL-180 due to the influence of a large water body located on the east side of the peninsula, called Little Lagoon.

To quantify the distance from the tidal water body (d), only the “Estuarine and Marine Deepwater” features from the National Wetlands Inventory (NWI) (U.S. Fish & Wildlife Service, 2025) were used to represent the shoreline boundary. These features were extracted from the

original NWI shapefile and then used as input for the “Near” tool in ArcGIS Pro, where the distance from each road point to the nearest location on the shoreline shapefile was calculated. The "Near" tool in ArcGIS calculates the distance from each feature (wetland) in the input layer to the nearest feature in another layer (or within the same layer if no other is specified). This parameter was later saved as the “dist” column in the point input file. Selected points were used to illustrate groundwater level (GWL) trends in different locations along AL-180 using Exceedance probability curves.

3.2.1. Modeling framework

This model has two time-dependent input variables: rainfall depth (R) and tidal water level. The rainfall data was acquired from a station in the South Alabama Mesonet System (Lat: 30.2387°N; Long: 87.8540°W) (Kimball & Terwey, 2024), where precipitation is available at a one-minute temporal resolution. Therefore, it was resampled every 15 minutes to enhance calculation speed. Tidal water level, on the other hand, was obtained from the Dauphin Island monitoring station managed by the National Oceanic and Atmospheric Administration (NOAA) (NOAA, 2024). The water levels are available every 6 minutes, necessitating resampling to align both inputs at the same temporal resolution. To facilitate the calculation of time intervals between time steps, time was expressed in decimal days. Additionally, rainfall values were converted from millimeters to meters to match the scale of other model variables. Missing values in both series were addressed using either zero-filling or interpolation methods, depending on the context and data behavior.

The empirical groundwater model created by De Oliveira Sousa et al. (2025) (Chapter 2) estimated the groundwater table elevation (or modeled groundwater level, GWLm) at each location based on precipitation-driven recharge, recession, and tidal influence. It begins by computing a static GWL (GWLst), which depends on the distance from the point to the nearest shoreline and represents the minimum elevation that the GWL would reach. The next step involves calculating a tidal signal attenuation coefficient (GWL_T) that decreases exponentially with distance from the shoreline. Then, the model interactively computes the GWL above the GWLst in two scenarios: if there is rainfall, it adds the precipitation multiplied by a recharge factor (R); if there is no rainfall,

it follows a first-order decay to represent recession. GWL rise term $GWL_R(t)$, which is updated over time using Equation 9 presented below:

$$GWL_R(t + \Delta t) = GWL_R(t) + f(d, GWL_T(t), R, D) \quad (9)$$

where the terms of the function f are explained in the subsequent sections. $GWL_R(t)$ corresponds to the local GWL measured above the static value GWL_{st}. As shown in Figure 2, the predicted value for the local groundwater level is the summation of $GWL_R(t)$ and GWL_{st}:

$$GWL_R(t) = GWL_m(t) - GWL_{st} \quad (10)$$

The first dependent component, GWL_{st}, was obtained through curve fitting (Figure 3) in terms of the distance between the monitoring location and MB, defined as d (expressed in m):

$$GWL_{st} = 0.0041d + 0.0514 \quad (11)$$

Subsequently, an expression for the tide contribution to GWL, or $GWL_T(t)$, was identified, and in terms of the distance d:

$$GWL_T(t) = 0.260e^{-0.026 \cdot d} H_{tide}(t) \quad (12)$$

Where: $H_{tide}(t)$ = MB tide elevation with reference to NAVD88 vertical datum. Then, a linear trendline was adjusted between D and the observed GWL rise, shown in Equation 13:

$$R = 4.0 \cdot P \quad (13)$$

Where: R = GWL rise (m) and P = precipitation depth (m). In deriving Eq. 5, a few rain events recorded at the MESONET station were omitted, since they did not result in observable changes in GWL. These were assumed to be either incorrectly reported rainfall depths or that rain did not fall near the GW wells. Since rain events are episodic, GWL_R and GWL_m were updated after each rain event was over through equation 6, and the calculation time step Δt was set to the rainfall duration:

$$GWL_R(t + \Delta t) = GWL_R(t) + GWL_{tide}(t) + R$$

$$GWL_m(t + \Delta t) = GWL_{st} + GWL_R(t) + GWL_{tide}(t) + R \quad (14)$$

The method to compute the recession D, on the other hand, assumed that the GWL_R recession is first order (Petricci et al. 2023) and hence can be modeled using equation 15:

$$\frac{d}{dt} GWL_R = K_d \cdot GWL_R \tag{15}$$

Through equations 6 or 7, the effect of recession on GWL_R and GWL_m is expressed through equation 8:

$$GWL_R(t + \Delta t) = GWL_R(t) + GWL_T(t) + D$$

$$GWL_m(t + \Delta t) = GWL_{st} + GWL_R(t) + GWL_T(t) + D \tag{16}$$

The following step calculated the water depth based on land elevation along the road. To obtain the elevations along AL-180, the Coastal National Elevation Database (CoNED) Project Topobathymetric Digital Elevation Model (TBDEM) was used, which was collected in 2021 with a 1-meter cell resolution (OCM Partners, 2024). Groundwater depth was calculated as the surface elevation minus the GWL at each time step.

The results are stored in two formats: long, which has one record per location and timestamp, storing either the GWLm or the water depth, along with spatial coordinates; the second is the wide format, which has each step as a row and each point as a column, making it better for time series visualization. Both formats can be exported as .csv files to enable the transfer of results. The long format, for example, which also includes a datetime field, can be used for spatiotemporal analysis.

3.2.2. Spatiotemporal Analysis

The Space-Time Cube (STC) methodology in ArcGIS Pro (Esri, 2025) provides a framework for analyzing spatial and temporal patterns simultaneously by aggregating point-based observations into a three-dimensional cube structure, where each bin represents a specific location and time interval. This data structure enables the detection of localized temporal trends, the identification of statistically significant clusters, and the characterization of space-time dynamics across a study area (DeSousa et al., 2024). In this study, the cube was organized by specified locations based on the points along AL-180, where the distance from the tidal body (Mobile Bay) was less than 200 m. Additionally, the data must be structured in a specific manner, with a column containing an identifier, another column containing the date and time in a date format, and a third column containing the measurement. This analysis utilizes the long format; however, the date field

must be transformed into an ArcGIS Pro date field, and the depth column must be converted into a numeric field.

To assess the temporal direction of change at each spatial location, a Mann-Kendall trend test is applied to the attribute values within each bin series. The Mann-Kendall test is a non-parametric method suitable for detecting monotonic trends in environmental time series data without requiring assumptions about data distribution (Kendall, 1976; Yue et al., 2002). The output indicates whether a location exhibits a statistically significant increase, decrease, or no discernible trend over the study period. This permits the evaluation of the depth to saturated groundwater over time for each location. While this study analyzes a 15-year groundwater simulation, it is important to note that this time frame may not fully capture long-term climate variability.

Time series clustering was then applied to the STC to group locations based on the similarity of their temporal behavior. K-means clustering was used to partition locations into a predefined number of clusters, each representing a characteristic temporal pattern (e.g., increasing, oscillating, stable). This approach supports spatial interpretation of dominant temporal patterns across the study area (Esri, 2025; Macqueen, 1967). The optimal number of clusters is often determined using internal validation indices, such as the Calinski-Harabasz or Davies-Bouldin index (Warren Liao, 2005).

Lastly, Emerging Hot Spot Analysis applies the Getis-Ord Gi* statistic (Getis & Ord, 1992) across the space-time cube to identify statistically significant hot and cold spots over time. The Gi* statistic evaluates each bin in relation to its spatial and temporal neighbors to determine whether observed values are significantly higher (hot spots) or lower (cold spots) than expected. The analysis classifies each location based on the temporal evolution of these hot spots, such as new, consecutive, oscillating, or diminishing. New hotspots refer to locations that were not statistically significant but have become significant in recent time steps, which means the might be a new area of concern; Consecutive hotspots, on the other hand, have been statistically significant for an uninterrupted sequence of time; Oscillating hotspots refer to locations have changed between hot and cold spots over time, which means they may not be with w tables closer to the pavement for long periods of time; lastly, diminishing hotspots means a location is becoming less significant over time, which means the depth in relation to the pavement has not been increasing or decreasing significantly over time (Esri, 2025a). Hence, it provides insights into the

persistence or emergence of high-value clusters, which is particularly useful for understanding changes in groundwater level fluctuations (Esri, 2025b).

3.2.3. Exceedance

To quantify how often groundwater approaches the surface, the exceedance probability was calculated for each segment's points. The Weibull Plotting Position approach was utilized to derive these curves. This method involves ordering the GWL values in descending order and then calculating the probability of each water level using the Weibull Plotting Position formula shown below (Chow et al., 1988):

$$P = \frac{i}{N+1} \tag{17}$$

Where: P = probability that the value is equal to or higher than the current value; N = total number of data points/steps; i = rank of the data point from the largest to the smallest.

3.3. Results

The results were analyzed to characterize spatiotemporal patterns and the exceedance period of groundwater saturation along the road. Factors R and D were calibrated by Sousa et al. (2025) using data from wells along AL-180, yielding values of 4.0 and 0.06, respectively (the same as in the original study). Locations closer to the coastline exhibited more frequent and higher groundwater peaks, consistent with the influence of tidal forcing and reduced elevation. Conversely, inland locations demonstrated lower groundwater variability but higher water table depths, which makes them also vulnerable to pavement saturation.

Figure 18 illustrates the pavement elevation of AL-180 in comparison to simulated GWLs at the 10th, 50th, and 90th temporal percentiles along two segments in the western portion of the corridor. Between kilometers 2 and 7, the road is lower than the rest of its length, with elevations mostly ranging from 1.5 to 2.5 meters. At the same time, between kilometers 12 and 18, there is a greater topographic variability, and higher elevations in general. The simulated groundwater levels in both segments exhibit limited variation, with the 10% GWL often ranging from 1.2 to 1.4 meters in elevation. Between kilometers 5 and 6, for example, the separation between the pavement and

GWL is reduced, indicating locations where the water table may pose a greater risk of surface saturation or pavement subgrade vulnerability. However, most of the first segment's length may have been exposed to saturation for at least 10% of this 15-year period. The aerial images at the bottom provide spatial context, revealing the proximity of these segments to coastal and residential areas. Kilometers 14 to 18 may also be exposed to soil moisture, but with a different threshold. While the first segment is exposed to saturation at less than 0.3 m from the surface, the segment on the right is exposed to saturation only at approximately 1 m below the pavement surface.

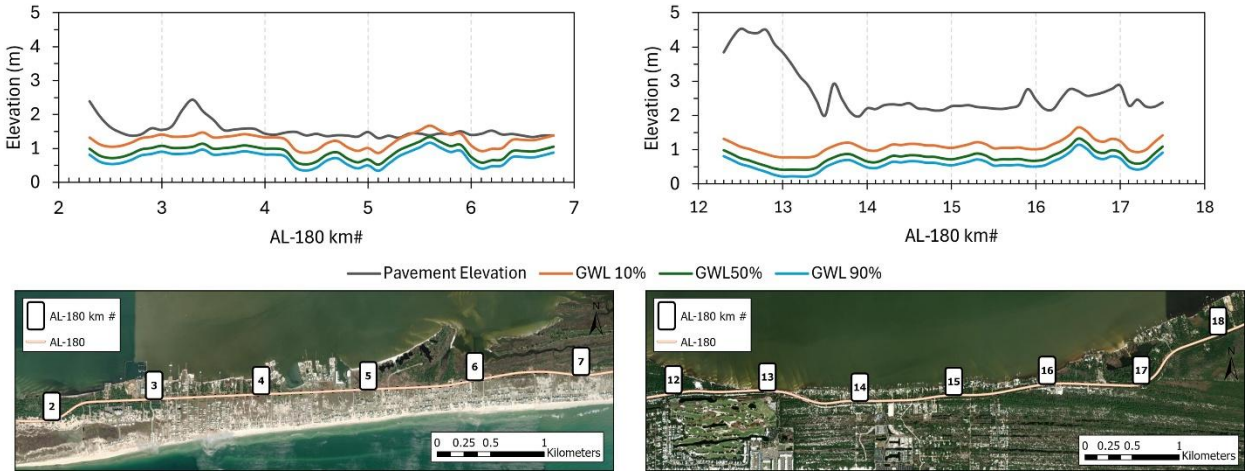

Figure 18 – Groundwater level exceedance at the western side of Fort Morgan Peninsula. The number legends represent the number of kilometers. GWL10%, 50%, and 90% represent the level that is exceeded 10%, 50%, and 90% of the time. Pavement Elevation refers to the surface elevation of the road according to the Digital Elevation Model.

Figure 19 presents the other two segments of the eastern portion of AL-180, covering kilometers 23 to 27 and 29 to 31. Pavement elevation in these segments is generally higher than in the western portion. Despite the higher road profile, simulated groundwater levels remain within a 1.3- to 1.5-meter range when considering the 10% GWL. In some locations, such as between kilometers 24 and 25, the elevation difference between the pavement and GWL10% is notably reduced, suggesting this area may be more vulnerable in the future if rainfall frequency and quantity increase. The same happens just before kilometer #30. The satellite images below show that these road segments traverse a mixture of residential developments, forested areas, and low-lying terrain adjacent to Mobile Bay. Moreover, the GWLs in these segments of AL-180 may be more influenced by the level of Little Lagoon, which appears to the south in the satellite images.

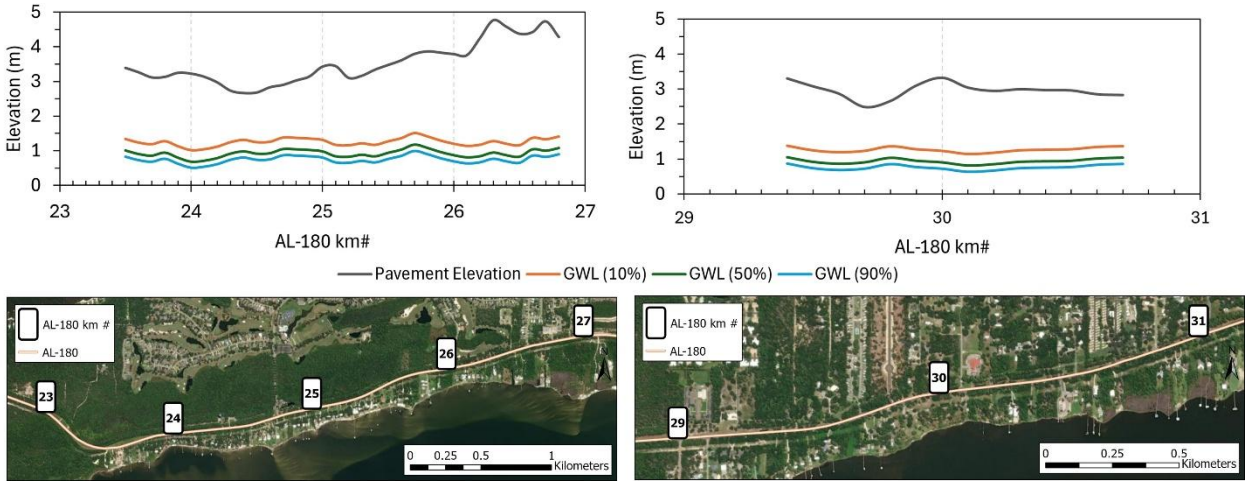

Figure 19 – Groundwater level exceedance at the eastern side of Fort Morgan Peninsula. The number legends represent the number of kilometers. GWL10%, 50%, and 90% represent the level that is exceeded 10%, 50%, and 90% of the time. Pavement Elevation refers to the surface elevation of the road according to the Digital Elevation Model.

The Mann-Kendall trend test showed an overall decreasing trend in water depths from the pavement surface, meaning the distance between the pavement surface and the saturated lens has been decreasing over the last 15 years. The time series clustering (Figure 20, top panel) reveals a gradual intensification of temporal patterns on the left, and from the center toward the eastern parts of the segment, with clusters 6 through 10 dominating this stretch. These clusters likely correspond to locations experiencing increasingly frequent or persistent high groundwater levels. The emerging hot spot analysis (bottom panel) supports this interpretation: a band of decreasing hot spots in the western portion suggests a declining distance from the saturated groundwater lens to the pavement surface. The presence of oscillating hot spots in the mid-section indicates fluctuations in significance over time. Therefore, it cannot be concluded that the water depth is decreasing at these locations. Part of the eastern portion exhibits no detectable spatial-temporal pattern, possibly due to either low variability or insufficient significance. The low variability can be attributed to the increase in distance from Mobile Bay, which reduces the influence of tidal variations. However, there are some new hotspots in the central part of the segment, as well as one kilometer of new hotspots on the extreme right of this segment. This means that while groundwater levels may not be increasing as much in the west, they remain dynamic in the center (at kilometers

4 and 5), and the increase is more pronounced in the east of this segment (between kilometers 6 and 7).

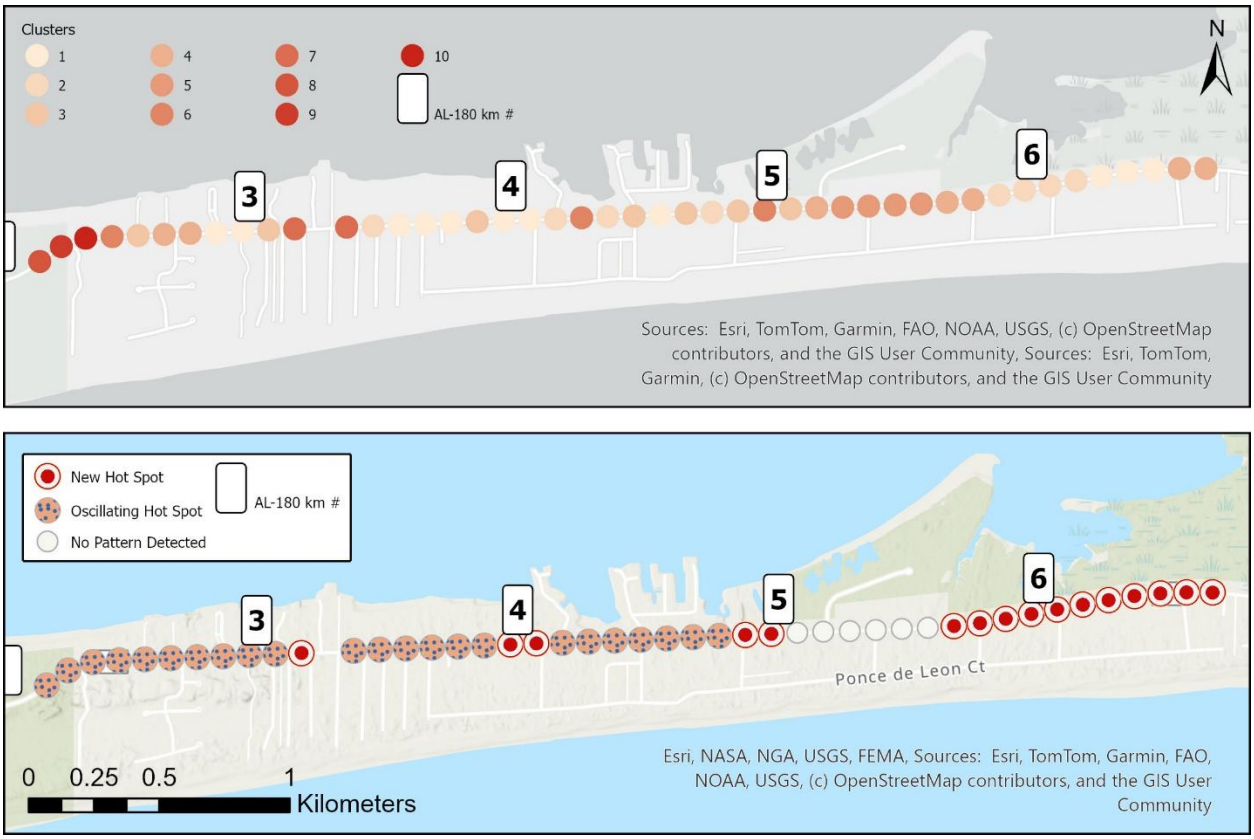

Figure 20 - Clusters and Emerging Hotspot Analysis results for kilometers 2 to 7.

The top panel of Figure 21 shows a concentration of clusters (8 to 10) in the western portion of the segment, which transitions into lower-numbered clusters toward the east. This may indicate a west-to-east gradient in groundwater behavior or hydrological response, which is consistent with the increase in distance from Mobile Bay and higher elevations towards the east of the peninsula. This trend also happens in the emerging hotspot analysis (bottom panel), where the western section is dominated by oscillating hotspots. This means that these areas have experienced alternating magnitudes of groundwater depth over time, and these changes in groundwater depths may be significant at some points in time, but not in others. Of particular concern are the decreasing hotspots to the west of this section, which confirms that the groundwater depth has been approximating the pavement over the last 15 years. Therefore, these findings highlight the need

for enhanced monitoring and adaptation strategies, as kilometers 12 to 14 have the highest probability of presenting smaller groundwater depths (closer to the pavement) over time.

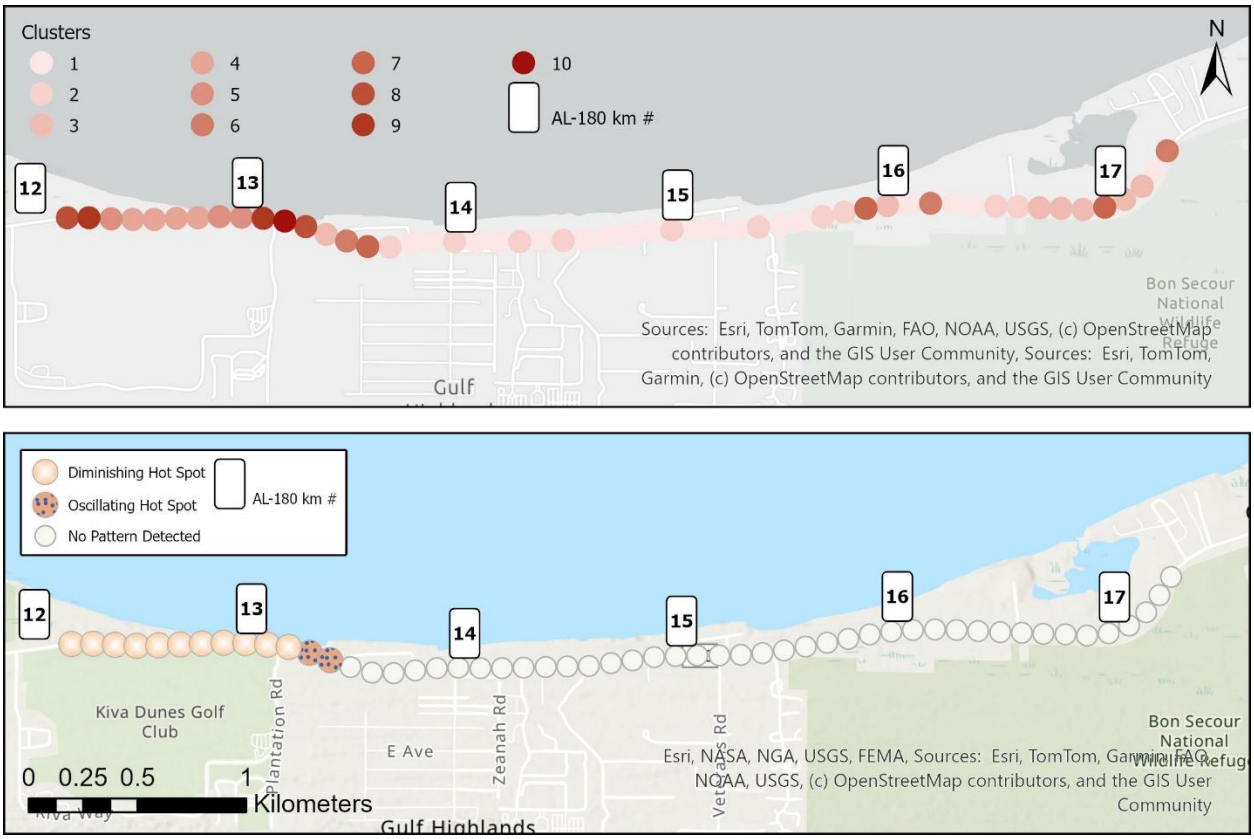

Figure 21 - Clusters and Emerging Hotspot Analysis results for kilometers 12 to 18.

3.4. Discussion

The results along the AL-180 corridor demonstrate that the empirical methodology applied was effective in capturing spatial and temporal patterns of pavement exposure to shallow groundwater in coastal areas. The simulations indicated that segments located at lower elevations and closer to water bodies exhibited higher frequencies of groundwater level (GWL) peaks and smaller gaps between the water table and the pavement surface, especially for the 10th percentile GWL. This is consistent with the literature describing groundwater dynamics in zones under simultaneous influence of tides and intense rainfall, particularly in barrier islands and transition zones between shallow aquifers and coastal water bodies (Habel et al., 2024; Werner et al., 2013). However, if the distance from the tidal body increases without an accompanying elevation

increase, the GWL may continue to rise inland, following the Boussinesq formulation (Hayek, 2019; Tang et al., 2016), and impact the pavement integrity. This is what may happen at kilometers 14, and 16 to 17.

Because the model simulates continuously over a 15-year period, percentiles such as the 10% exceedance level represent the condition in which groundwater was within 0.3 meters of the pavement for 10% of the total simulation time. This corresponds to a substantial duration (e.g., more than 500 days) and should be considered a severe condition. Therefore, even a 1% exceedance threshold, equivalent to 55 days, may indicate concerning levels of pavement vulnerability in these segments.

The application of the Space-Time Cube methodology revealed the presence of temporal trends, clusters with similar hydrological behavior, and the emergence of statistically significant hotspots. The occurrence of decreasing hot spots in the western segment suggests a progressive reduction in groundwater depth over the last 15 years, while oscillating hot spots in the central segment indicate fluctuations that may be associated with interannual climate variability and tidal seasonality. New hotspots observed in the eastern segment indicate a recent intensification of GWL dynamics, possibly driven by changes in rainfall. Previous studies have shown that areas near water bodies tend to experience more frequent surface saturation due to intensified recharge events and shorter recession periods (Chegini et al., 2025; Hunt et al., 2006).

Although the model used only three main inputs (distance from a tidal water body, tidal levels, and rainfall depths), the results indicated a strong capacity to represent the spatiotemporal variability of GWL along the corridor. This approach provides an alternative for studies in areas with limited data availability and a need for rapid assessments, particularly across long coastal road segments. When compared to more complex physics-based models, which require extensive calibration, soil parameters, and a more elaborate monitoring infrastructure (Cherubini et al., 2023). The presented framework allows scalable and low-cost screening for prioritizing monitoring and adaptation of road infrastructure.

However, certain limitations must be acknowledged. The model assumes a uniform exponential attenuation of the tidal signal based only on distance to the shoreline, without accounting for hydrogeological factors such as hydraulic conductivity, soil heterogeneity, or aquifer conditions. Additionally, the use of historical precipitation and tide time series to simulate

past behavior may not accurately represent future responses under sea level rise and intensifying extreme events (Ferguson & Gleeson, 2012). Future improvements may include the incorporation of soil parameters, climate scenarios, and seasonal effects on groundwater abstractions, as well as continuous calibration with field data from wells and sensors distributed along other corridors.

3.5. Conclusions

This study presented a groundwater-level modeling framework based on empirical equations to estimate the depth to groundwater along a coastal highway corridor subjected to tidal variation and intense precipitation events. Applied to Alabama State Route 180 in the Fort Morgan Peninsula, the approach enabled the identification of potentially vulnerable road segments with prolonged exposure to shallow water levels. The 15-year simulation revealed that segments between kilometers 5 to 6 and 14 to 18 were particularly at risk, especially in areas where pavement elevation was lower than 2 meters.

The integration of model results with spatiotemporal tools, such as the Space-Time Cube, enabled a deeper understanding not only of the geographical distribution of vulnerability but also of its temporal evolution. These findings underscore the importance of accounting for groundwater fluctuations as a key variable in assessing the vulnerability of transportation infrastructure in low-lying coastal zones, particularly in the context of climate variability.

Future applications should focus on comparing these findings with maintenance records and pavement health metrics, extending the methodology to other coastal road corridors, and evaluating the model's sensitivity to varying soil and land cover conditions. Additionally, normalizing the parameters may help reduce uncertainty and create a resilience index for coastal pavement infrastructure based on shallow groundwater levels. This framework can support decision-making processes by helping identify priority areas for adaptation, maintenance, and resilient infrastructure planning.

The empirical method presented in this chapter enabled the vulnerability evaluation of segments of AL-180 in terms of groundwater saturation based on tide, proximity to tidal waters, and rainfall. However, to support design-level decisions and evaluate complex interactions at short time scales, a more detailed, physically based hydrologic model is required. Chapter 4 addresses

this need by applying the Gridded Surface Subsurface Hydrologic Analysis (GSSHA) model to a representative domain at the Boat Launch location, offering insight into hydrologic behavior at the sub-daily scale and providing a higher-resolution understanding of groundwater-surface water interactions and flood dynamics.

Chapter 4. Evaluating Distributed Hydrologic Modeling to Assess Coastal Highway Vulnerability to High Water Tables

This chapter is a revised version of a paper submitted by Bruno J. de Oliveira Sousa, Luiz Menezes Morgado, and Jose G. Vasconcelos to MDPI Water.

De Oliveira Sousa, B. J., Morgado, L. M., Vasconcelos, J. G. (2025). "Evaluating Distributed Hydrologic Modeling to Assess Coastal Highway Vulnerability to High Water Tables." [Manuscript accepted for publication]

4.1. Introduction

Hydrological modeling tools are widely applied in the inland context of infrastructure planning and design (Lee et al., 2020; Palanisamy et al., 2024; Yuan et al., 2023). Due to increased water-related stressors, their role in highway and transportation infrastructure design and assessment is becoming more significant. These tools can assist in predicting and managing impacts such as flooding, bridge scour, and stormwater runoff on roads and bridges. As detailed in (Vasconcelos et al., 2023), these models have been applied to assess infrastructure vulnerability and resiliency to flooding (Ahmari et al., 2021; Giacomoni et al., 2019; Thomas et al., 2020), evaluate bridge and streambed processes (Schwartz, 2018; Vasconcelos et al., 2018), and manage stormwater runoff from roadways to improve water quality and quantity (Herb et al., 2017; Hoogestraat, 2017; Zhang et al., 2018).

Yet, such modeling tools encounter specific challenges when applied in coastal settings, where perennial streams are often absent and tidal effects are present. To date, semi- or fully distributed hydrological modeling tools have not been extensively tested in local-scale coastal areas, particularly considering varying shallow groundwater dynamics. While popular, lumped models are also not applicable since these are designed to estimate peak flows (Vasconcelos et al., 2023), helping in conveyance design, such as culverts. Even widely used distributed models like the Hydrologic Modeling System (HEC-HMS) (Scharffenberg, 2016) and Stormwater Management System (EPA-SWMM) (Rossman, 2015), when applied in coastal regions, often average sub-catchment parameters, relying on channelized flows and overlooking localized land cover impacts. This limitation is particularly critical in coastal environments, where factors such

as rising water tables and pavement saturation are known to significantly compromise roadway integrity by weakening the underlying structural support of the pavement as moisture levels increase in the subgrade and base layers (Knott et al., 2018). Most hydrological tools average soil saturation results, thus losing spatial discretization. Surface water-groundwater interactions, frequently neglected in surface-focused hydrological models, can significantly skew water balance and soil moisture computations (Bragg et al., 2025). Therefore, the capacity of distributed models such as Gridded Surface Subsurface Hydrologic Analysis (GSSHA) (Kampf & Burges, 2007) to accurately track groundwater levels becomes essential for robust coastal hydrological assessment.

GSSHA is a physics-based, distributed hydrologic model that allows for detailed assessment of flood and high water table vulnerability on roads. It enables 2D overland flow simulation, 1D channel routing, infiltration, surface and groundwater interaction, a 2D groundwater surface, and simulation of evapotranspiration and surface retention (Downer & Ogden, 2003; Weston et al., 2015). In addition, GSSHA has been applied in various contexts, such as urban stormwater planning, rural and forested areas, watershed management, and urban coastal areas. Regarding urban stormwater planning, there is a good agreement between observed streamflow and the location of best management practices (BMPs), which is more significant in distributed models than in lumped models (Brendel et al., 2021; Fry & Maxwell, 2018). It provides more insights into water movements using the Penman-Monteith method, surface water and groundwater interactions, and the simulation of tile drains in forested and rural areas (Hamedi & Fuentes, 2015; Sith & Nadaoka, 2017).

GSSHA has also been used to predict water tables for roadway infrastructure planning and the allocation of BMPs, highlighting a key contrast with SWMM. Semi-distributed models typically average the groundwater elevation for multiple subcatchments and do not account for lateral flow (Moore et al., 2017). The work by Karamouz et al. (2017) predicted that a rise in sea level and an increase in rainfall intensity would lead to an increase in the number of areas impacted by flooding in lower Manhattan, NY. However, natural physical processes such as surface runoff generation and infiltration are significantly altered in such an urbanized area compared to a low-urbanization peninsula. Therefore, there is a need to assess the extent to which hydrologic models capture subsurface interactions at high spatial and temporal resolutions so that roadway saturation can be accounted for in coastal areas.

Therefore, this study evaluates whether GSSHA can represent key hydrologic processes in a coastal environment where the tool is not typically used. The model application focuses on quantifying the vulnerability of coastal transportation infrastructure due to saturated water tables, including extreme coastal events. Two model scales were used: the large-scale model, covering the entire peninsula at a 30-meter grid cell resolution, was used to provide a general assessment of surface flooding along the corridor; the small-scale model focused on a 2 km segment of AL-180 using a 3-meter resolution. It incorporated field-collected groundwater level data for calibration, high-resolution land cover classification, and detailed boundary conditions to evaluate groundwater table responses to rainfall. By doing so, we aim to provide insights that will inform technical and policy decisions, ultimately enhancing the long-term resilience of coastal infrastructure.

4.2. Local-Scale Model

4.2.1. Study Area

The study area is situated in Baldwin County, Alabama, along Alabama State Route 180 (AL-180) in Fort Morgan Peninsula (Figure 23). According to NLCD land cover data, the land cover classes in the area are Developed, Low, Medium, High intensity, and Sand Barren land. Also, the predominant soil in the study area is sand. To the north, there is Mobile Bay, and to the south, there is the Gulf of America. The mean annual rainfall in the region is 1580.7 mm (Kimball & Terwey, 2024). Its climate is classified as Temperate, with no dry season, and a hot summer (Beck et al., 2018). However, the area is susceptible to floods, sea level rise, and storm surges due to its low elevations, which range from 2.13 to 2.74 m (7 to 9 feet). Furthermore, the proximity to water makes the area directly exposed if it is on the trajectory of a hurricane.

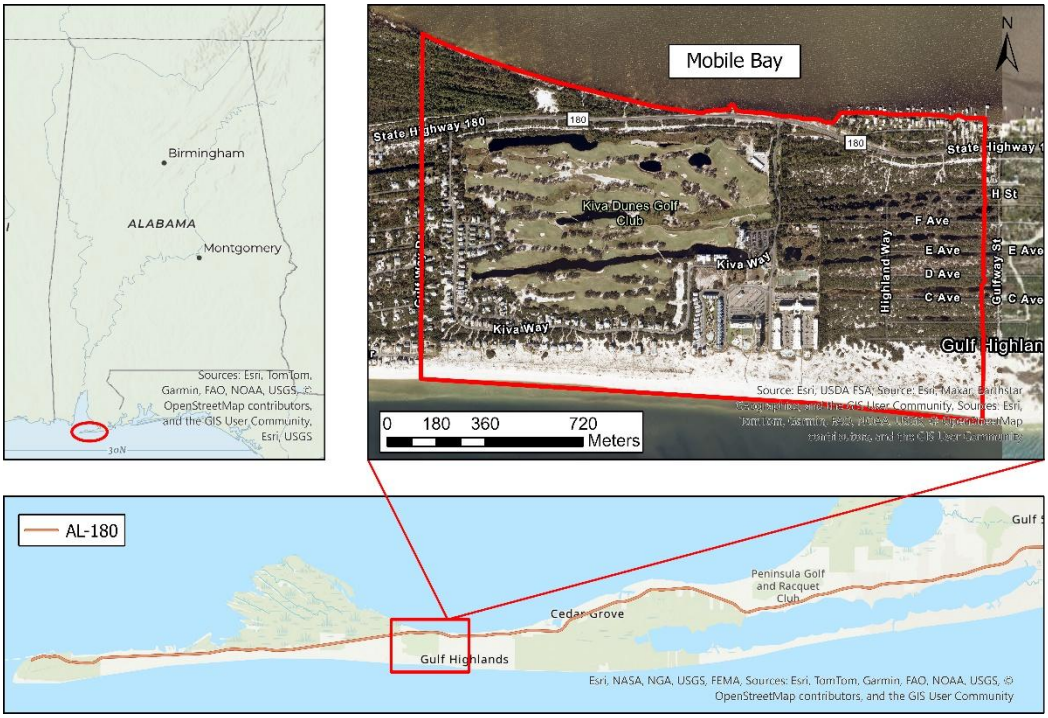

Figure 22 - Study area for the small-scale GSSHA modeling. The water body to the north is Mobile Bay, and the one to the south is the Gulf of America.

4.2.2. Data

Several datasets were used to configure the GSSHA models, including Soil Data from the Soil Survey Geographic (SSURGO) database for Baldwin County (Soil Survey Staff, 2022); Land Cover Data from the National Land Cover Database (NLCD); Im-agery from the National Agriculture Imagery Program (NAIP) (OCM Partners, 2022) was used to improve the resolution of the land cover classification using GeOBIA for the local-scale simulation (Dewitz, 2024); Elevation Data: Based on our analysis, we utilized the one-meter Digital Elevation Model (DEM) from the U.S. Geological Survey (USGS) Coastal National Elevation Database (CoNED) Applications Project as it is more recent and aligns with field investigations. Rainfall and tide data were also col-lected from the South Alabama Mesonet (Kimball & Terwey, 2024)and from NOAA Tides and Currents' Dauphin Island station (NOAA, 2024). The Alabama Department of Transportation (DOT) supported the installation of one HOBO level logger, model U20L, to capture shallow groundwater elevation (Figure 24, blue pin). In addition, the authors installed another level logger of the same model to measure atmospheric pressure close to the groundwater well (Figure 2, yellow pin).

Figure 23 - Monitoring locations used in the distributed hydrologic model.

4.2.3. Land Cover Classification using GeOBIA

This study employed Geographic Object-Based Image Analysis (GeOBIA) on NAIP imagery to improve land cover classification. The eCognition Developer software was used, with Band 1 designated as the red band, Band 2 as the green band, Band 3 as the blue band, and the last as the Near Infrared band (NIR). Then, segmentation was processed using the Spectral Difference Segmentation algorithm, which identified the following classes: barren land, trees (forest), grass, shrub/scrub, buildings, paved areas, and water. Height classification was executed to enhance classification accuracy based on specific thresholds: buildings and trees exceeding 2 meters (approximately 6 feet) in height, shrub/scrub ranging from 1 to 2 meters (approximately 3 to 6 feet), and grass measuring less than 1 meter (approximately 3 feet) in height (Gilman, 2023; UC Santa Barbara, 2023). This improved the identification of surface characteristics, yielding more realistic infiltration estimates and Manning's roughness values (Figure 25). Elevation was obtained from a point cloud (lidar dataset), which was obtained from the U.S. Geological Survey (USGS) using the National Map download application. This dataset was collected in 2018 and is available in .laz format. The study area required four separate tiles for full coverage. Therefore, it was necessary to convert it into a .las dataset before incorporating it into our analysis. This dataset was chosen because it includes the first return points that allow the software to identify buildings and trees.

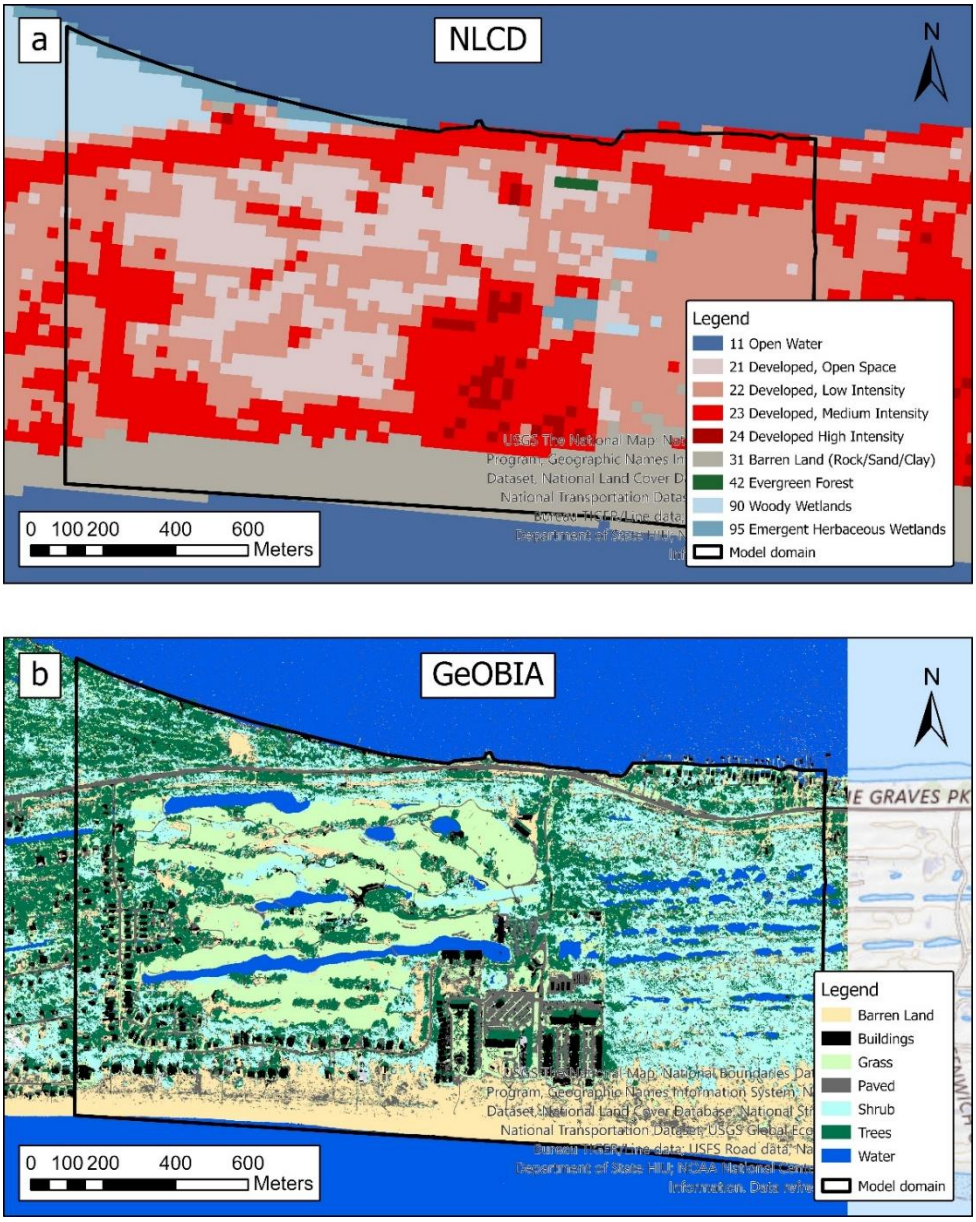

Figure 24 - Comparison between NLCD and GeOBIA land use classifications.

4.2.4. Modeling

GSSHA modeling of the Boat Launch site was created with high spatial accuracy (i.e., 3-m calculation cells) aimed to represent infiltration, groundwater (GW) level fluctuation and saturation in a coastal setting. Key model configurations included:

- The Green-Ampt infiltration method was used, adjusting hydraulic conductivity to reflect local land cover. Paved surfaces were assigned lower infiltration rates to

replicate urban runoff behavior. Infiltration was modeled using the Green-Ampt equation with redistribution, a method recognized as a close approximation to the numerical solution of Richards' Equation (Downer & Ogden, 2006). Table 1 illustrates the remaining infiltration parameters used in this study. Hydraulic conductivities were reduced following the indices found by (Robinson et al., 2022) for the different land cover classes.

- Surface roughness parameters were assigned based on the resultant land cover classifications shown in Figure 25. The authors converted the land use classification to a 3-m cell resolution raster to improve software performance. Then, it was uploaded to the project and converted into a land use grid, which allowed Manning's n values to be set for each land cover classification.
- Groundwater-surface water interactions were also included, accounting for additional parameters such as aquifer depth, initial water table elevations, hydraulic conductivity, and soil porosity.
- Initial water table elevation is spatially variable, with the levels matching Mobile Bay and the Gulf of America to the north and south boundaries, respectively. Higher water table elevations are assumed with increased distance from the coast, reaching 1 m above the current sea level at the start of the simulation. Furthermore, due to the same land use and elevation, GW flows are assumed not to occur through the east and west borders of the subcatchment. As a result, GW discharges occur only through the northern and southern borders of the model.

4.2.5. Model Setup

GSSHA enables the dynamic simulation of hydrologic processes, including pre-cipitation, overland flow, infiltration, and groundwater flow, which are modeled in this study. First, overland flow is solved using the 2D diffusive wave approximation of the shallow water equations (Downer & Ogden, 2006). The fluxes in the x and y direc-tions are denoted as p (Eq. 18) and q (Eq. 19), respectively. The depth is updated as follows in Equation 20, which allows for lateral water movement between cells.

$$p_{i,j}^{n} = \frac{1}{n}\left(d_{i,j}^{n}\right)^{5/3}\left(S_{fx}\right)^{1/2} \quad (18)$$

$$q_{i,j}^{n} = \frac{1}{n}\left(d_{i,j}^{n}\right)^{5/3}\left(S_{fy}\right)^{1/2} \quad (19)$$

$$d_{i,j}^{n+1} = d_{i,j}^{n} + \frac{\Delta t}{\Delta x}\left(p_{i-1,j}^{n} + q_{i,j-1}^{n} - p_{i,j}^{n} - q_{i,j}^{n}\right) \quad (20)$$

Where $d_{i,j}$ = water depth in the grid cell (i, j); n = Manning's roughness coefficient; Δt = time step; S_{fx} and S_{fy} = slopes in the x and y directions; Δx = cell size. Second, infiltration is calculated using the Green-Ampt method for each grid cell, as shown in equations 21 and 22. This permits spatial variation in infiltration due to differences in soil type and land cover.

$$f_p = K_s\left(1 + \frac{\varphi_f \theta_d}{F}\right) \quad (21)$$

$$F_{t+\Delta t} = K_s \Delta t + F_t + \varphi_f \theta_d \ln\left(\frac{F_{t+\Delta t} + \varphi_f \theta_d}{F_t + \varphi_f \theta_d}\right) \quad (22)$$

Where f_p = infiltration rate; Ks = saturated hydraulic conductivity (referred to in this study as infiltration hydraulic conductivity (K_{inf})); φ_f = capillary suction at the wetting front; θ_d = moisture deficit; F = cumulative infiltration (Mein & Larson, 1973). Lastly, groundwater flow simulation uses an adapted version of the two-dimensional free surface groundwater problem (Trescott et al., 1976), but diagonal terms are ignored, and transmissivity is assumed to be the product of saturated hydraulic conductivity and saturated depth (saturated surface to aquifer bottom) (Downer & Ogden, 2006). Equation 23 illustrates the calculation of groundwater flow.

$$\frac{\partial}{\partial x}\left(K_{xx} B \frac{\partial E_{ws}}{\partial x}\right) + \frac{\partial}{\partial y}\left(K_{yy} B \frac{\partial E_{ws}}{\partial y}\right) = S \frac{\partial E_{ws}}{\partial t} + W_s(x, y, t) \quad (23)$$

Where E_{ws} = groundwater table elevation, which is referred to in this study as groundwater level (GWL); K_{xx} and K_{yy} = saturated hydraulic conductivities on the x and y directions, referred to in the next sections as groundwater hydraulic conductivity (K_{GW}) and are assumed to be the same by the model; B = depth of saturated soil, which is related to the aquifer bottom depth (Aq. Bot.); S = specific yield; Ws = fluxes from infiltration and stream, if present.

The starting hydraulic conductivity of 17 cm/h was extracted from NRCS soil data (Soil Survey Staff, 2022). The porosity for this study area was calculated in three different locations by de Oliveira Sousa et al. (2025), with the best approximation being 25%, which was then used in all the simulations. For groundwater boundary conditions, the average tidal water level for the

simulated periods was 0.25 m, which was applied as a fixed boundary condition on the north and south boundaries of the model domain.

Three key structures were incorporated into the model: an embankment and two culverts, representing a double culvert at the model's outlet. The embankment, located along AL-180 but constrained within the model domain, has a top elevation of 2.1 m and slopes of 0.13 toward the north and south. The culverts, each 0.61 m in diameter and 25 m in length, were placed at the intersection of the channel and the embankment. Overbank flow and backwater effects were removed from the channel setting to avoid instabilities, if the drainage area's land cover and infiltration characteristics prevent significant overbank flow conveyance. Figure 26 illustrates the remaining parameters used for model calibration, which will be presented in the following sections.

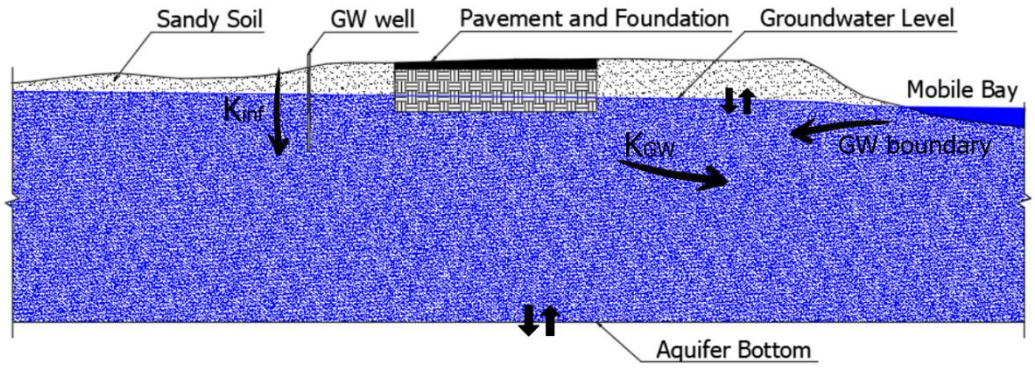

Figure 25 - Diagram of the parameters used for calibration, including the aquifer bottom level, infiltration hydraulic conductivity (Kinf), and groundwater hydraulic conductivity (KGW).

4.2.6. Boundary Conditions

GSSHA does not allow tidal, time-varying water level boundary conditions for groundwater flow calculation. Such time-varying GW boundary conditions exist only for interactions between channels and shallow groundwater, as well as water withdrawal from wells. Therefore, the north and south boundaries were assumed to have a fixed groundwater level above the NAVD88 vertical datum corresponding to the tide elevation at the start of the simulation. This is consistent with the stable water level methodology presented by De Oliveira Sousa et al. (2025),

where the distance from the tidal body determines the water table elevation. Surface water level boundary conditions, on the other hand, can be represented as a fixed or variable level condition.

4.2.7. Calibration

The calibration process for infiltration hydraulic conductivity (K_{inf}) and groundwater flow hydraulic conductivity (K_{GW}) was guided by literature values and sensitivity analysis using the GSSHA model. The process began with the adjustment of the model's initial soil moisture, which was set at 0.07 (7%), to better reflect the antecedent moisture conditions. This parameter was held constant after preliminary testing, and calibration then focused on the conductivities governing infiltration and subsurface flow.

A range of 15 to 45 cm/h was selected for both K_{inf} and K_{GW}, based on values reported by Nimmo & Akstin (1988) for sandy soils. To account for the spatial variability in surface conditions, K_{inf} was scaled by land cover type using the approach described by Robinson et al. (2022), which allows infiltration capacity to vary according to vegetation and imperviousness. These adjustments influenced the model's representation of the baseline groundwater level but did not sufficiently capture the tidal fluctuations, which in GSSHA are imposed only at the surface boundary condition.

Final calibration was achieved by refining three key physical parameters:

- The depth of the aquifer bottom, which was varied to control the available saturated storage.
- K_{GW} influences the rate of lateral subsurface flow and recession.
- K_{inf} is related to the vertical infiltration from the surface to the saturated zone.

4.3. Results

4.3.1. Calibration results

The model calibration was finalized by adjusting the physical parameters. The configuration with the best performance was the one with the aquifer bottom set at -12 m and infiltration and groundwater conductivities of 15 cm/h and 20 cm/h, respectively, accurately

representing the observed peaks and recessions in the groundwater level (Figure 27f). This setup achieved a Nash-Sutcliffe Efficiency (NSE) of 0.9 and a Root Mean Square Error (RMSE) of 0.05 m for the calibration event. This occurred because increasing KGW by more than 20 cm/h caused the model to respond too quickly to precipitation and recession, resulting in sharper recessions after precipitation stopped (Figures 27a and 27c). On the other hand, lowering KGW and Kinf caused the model to overestimate GWLs (Figures 27d and 27e). In addition, increasing KGW while maintaining the aquifer bottom at -12 m (Figures 27b and 27c) resulted in a more rapid recession, which deviated from observed data. Lowering the aquifer bottom without adjusting KGW and Kinf may artificially elevate groundwater levels by increasing initial storage (Figures 27d and 27e).

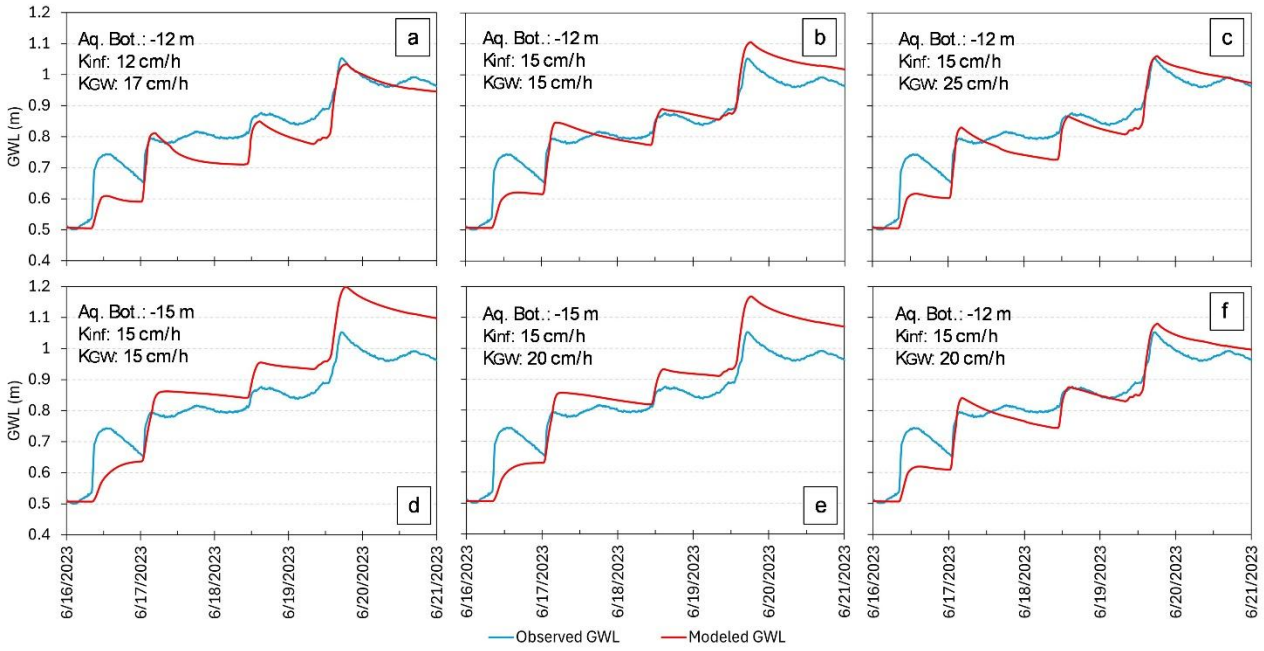

Figure 26 - Exploratory variation of groundwater saturated soil hydraulic conductivity (KGW), surface infiltration K values (Kinf), and the elevation of the aquifer bottom.

Figures 27b and 27f presented better agreement with the observed peaks and recession trends, but the configuration in Figure 27f had a better NSE. Furthermore, a "warm-up" period was implemented before the first precipitation event to ensure realistic initial conditions for the validation scenarios, allowing the initial soil moisture in the model to stabilize. The warm-up period consisted of at least 24 hours before the event started. The final parameter values used in this study are shown in Table 2.

Table 2 - Soil parameters initially extracted from Robinson et al. (2022) and Nimmo & Akstin (1988). Values were adjusted during calibration to match observed GWL responses.

Land Cover	Manning's n	Hydraulic Conductivity (cm/h)
Trees	0.12	15
Water	0.025	0.001
Paved	0.016	1.5
Shrub	0.1	15
Barren Land	0.025	15
Buildings	0.15	1.5
Grass	0.035	1.5

Calibration was performed using a 10-day period in October 2023 that included multiple rainfall events and allowed for sub-daily analysis of groundwater level response and recession. Figure 28a shows the time series generated by the model and the observed time series at a well at the Boat Launch location. The model produced a very good representation of the GWL variation, with only the recession being overestimated. The possible cause for this is the fact that evapotranspiration was not simulated, which made the recession only dependent on the calibration of K_{GW}. However, because the simulations were implemented for short periods, the effect of not simulating evapotranspiration did not considerably impact the results. In addition to the temporal calibration, the model was used to evaluate the spatial distribution of pavement saturation. Figures 28b and 28c display the results of this analysis, mapping the saturation along the 2 km stretch of AL-180. Figure 28b shows the most critical Hydraulic Grade Lines (HGL) at two points in time during the simulation. In Figure 28c, saturation is defined as periods when the groundwater table is 1 meter or less from the pavement surface. This spatial analysis identifies the highway segments that are most vulnerable to long-duration saturation, which poses a greater risk to pavement integrity, especially where the segments are located at lower elevations.

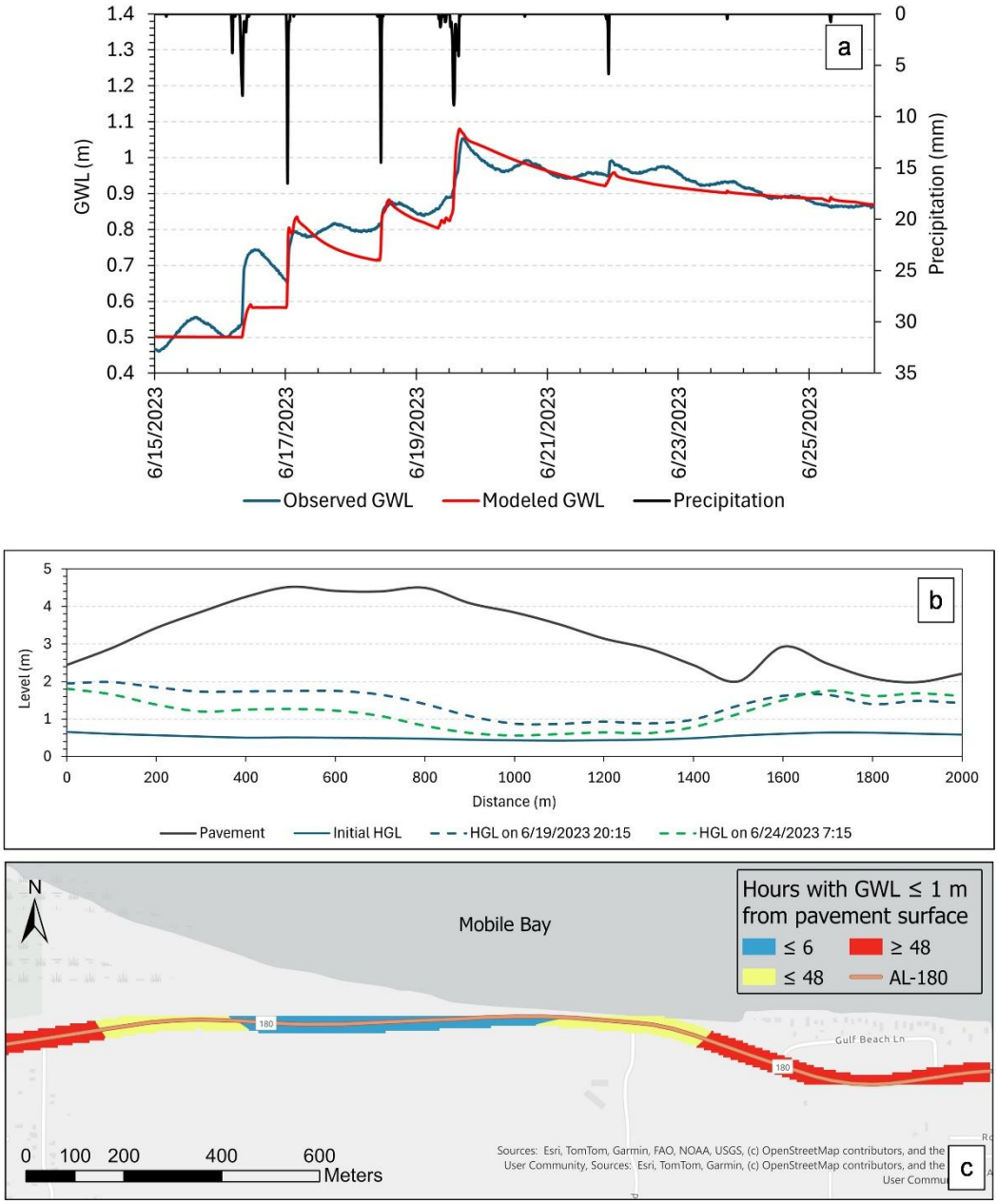

Figure 27 - Calibration results for a 10-day event. This simulation yielded an RMSE of 0.9. a: GWL time series at the location where the monitoring was performed; b: groundwater level along AL-180 during peak times; c: saturation along this 2km section of AL-180.

4.3.2. Validation results

Two other field-observed datasets were used to validate the GSSHA model. A 14-day period (April 8th to 22nd, 2023) and a 5-day period (September 3rd to 8th, 2024) were simulated, including rainfall events that totaled 135 mm and 74 mm, respectively. In the first case (Figure

29a), the model closely follows the observed GWL, including the start of the groundwater rise of April 13th, but overestimates the magnitude of the peak GWL. In addition, the tidal sign shown in the observed time series is smoothed in the modeled GWL as its influence on the variation of shallow groundwater cannot be represented. However, following the precipitation event, the model successfully represents the recession trend with a slight overestimation (approximately 0.1 m) after April 16th. The NSE for the first validation simulation was 0.83, indicating very good agreement between the observed and modeled GWL, with an RMSE of 0.06 m.

Figure 29b shows the HGL along this section of AL-180. Interestingly, there were two moments of concern: the first represented the highest average peak GWL on April 13th, immediately after the first rainfall event; the second happened on April 17th, following a small precipitation event. The GWL approaches the pavement (0.9 to 0.3 m) between 1,400 and 2,000 meters, similar to what is shown in Figure 28c for the calibration run. This coincides with the location of the drainage channel and a depression zone visible in the elevation profile.

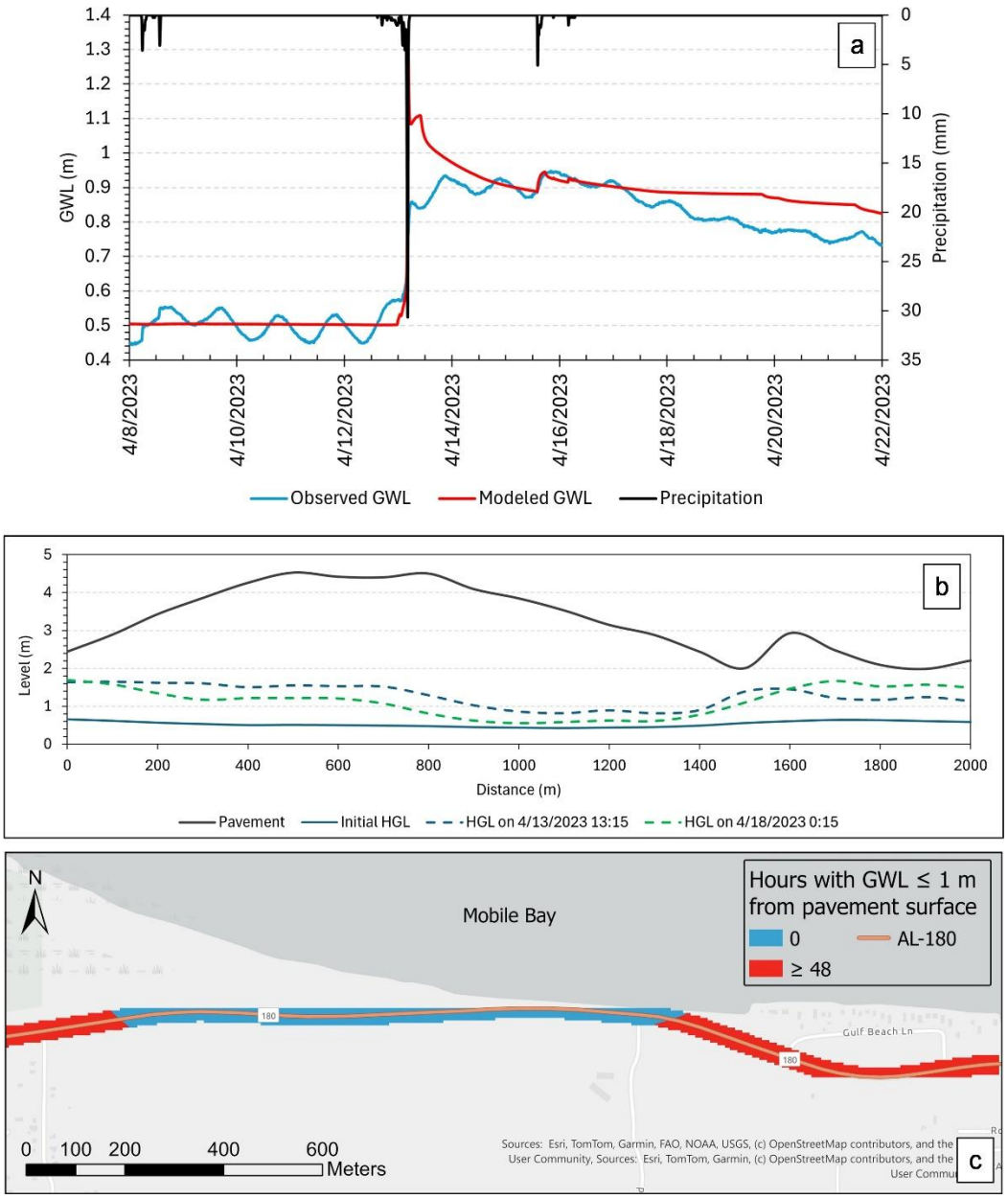

Figure 28 - Validation results for a 14-day event. This simulation yielded an RMSE of 0.9. a: GWL time series at the location where the monitoring was performed; b: groundwater level along AL-180 during peak times.

For the second validation event (Figure 30a), the model accurately captured the groundwater response to multiple events that occurred between September 5 and 7, 2024, following a warm-up period. The model underpredicted the GWL rise until September 6 and overpredicted it after that date, as it began to rise gradually due to subsequent precipitation events.

However, the error in both periods is approximately 0.05 m. The NSE for this simulation was 0.58, indicating an acceptable agreement with the observed data, while the RMSE was 0.05 m. Figure 28b displays the GWL profile along the same segment of AL-180. In this instance, the GWL remains 1 to 1.5 meters away from the pavement between 1400 and 2000 meters. However, the exposure times at the 1 m threshold were reduced to less than 4 hours.

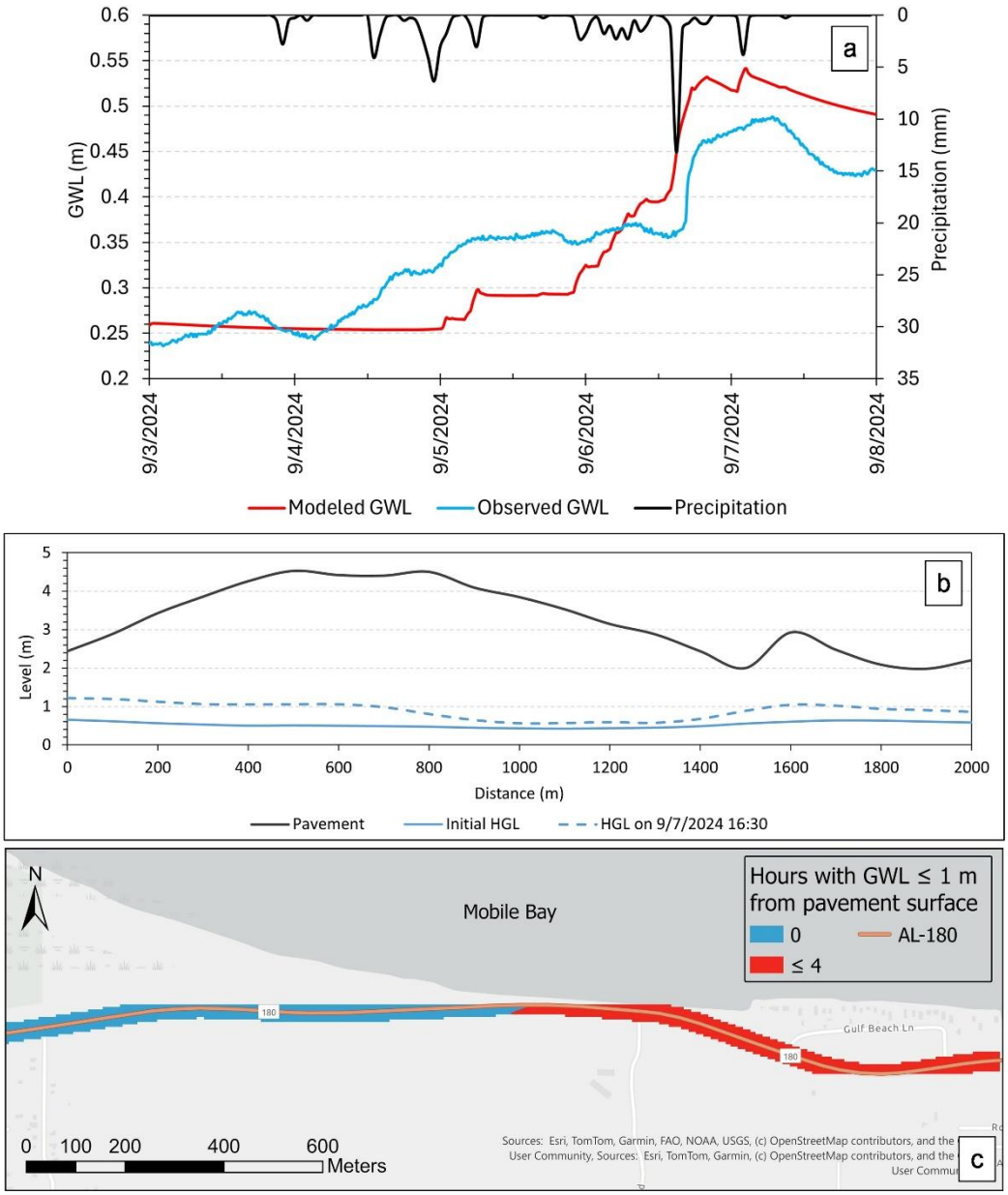

Figure 29 - Validation results for a 5-day event. This simulation yielded an RMSE of 0.58. a: GWL time series at the location where the monitoring was performed; b: groundwater level along AL-180 during peak times.

Decreasing the magnitude of rainfall also resulted in lower groundwater levels. This demonstrates the model's ability to reflect variations in rainfall intensity and antecedent conditions across events. The saturation exposure is evident on the eastern side of this segment, indicating that it is the most sensitive section, where saturation occurs even for small rainfall events. However, prolonged high water table conditions only occurred for the calibration and first

validation event, indicating a precipitation threshold that impacts the pavement. Also, when comparing the calibration and the first validation run, which have almost the same precipitation volume, the results suggest that pavement exposure is influenced not only by total rainfall but also by rainfall distribution over time.

4.3.3. Extreme Event Modeling

Figure 31 illustrates the spatial distribution of pavement surface saturation following Hurricane Sally in September 2020. The storm recorded a total precipitation of 555 mm and made landfall at Fort Morgan Peninsula before moving inland. Figure 31a depicts the rainfall/groundwater head relationship at our monitoring location. Figure 31b illustrates saturation along the entire segment during the most critical moments in terms of groundwater. Conversely, Figure 31c presents a detailed view of a 2 km segment of AL-180, focusing on the duration during which sections were saturated at a depth of less than 0.3 m from the pavement surface. Regarding pavement saturation, the results indicate an inland gradient, with longer saturation times observed as the road extends further from the coast. Over two-thirds of this section of the road remains saturated for more than 6 hours, with a significant portion of the analyzed segment experiencing saturation for over 12 to 24 hours, and in some areas exceeding 48 hours, as illustrated by the red and orange segments. Finally, Figure 31c shows the variation in groundwater level (GWL) from the simulation's start to the most critical GWL during the event along this road segment. According to the model results, the groundwater lens varied up to 4 m depending on the location, reaching pavement surface level.

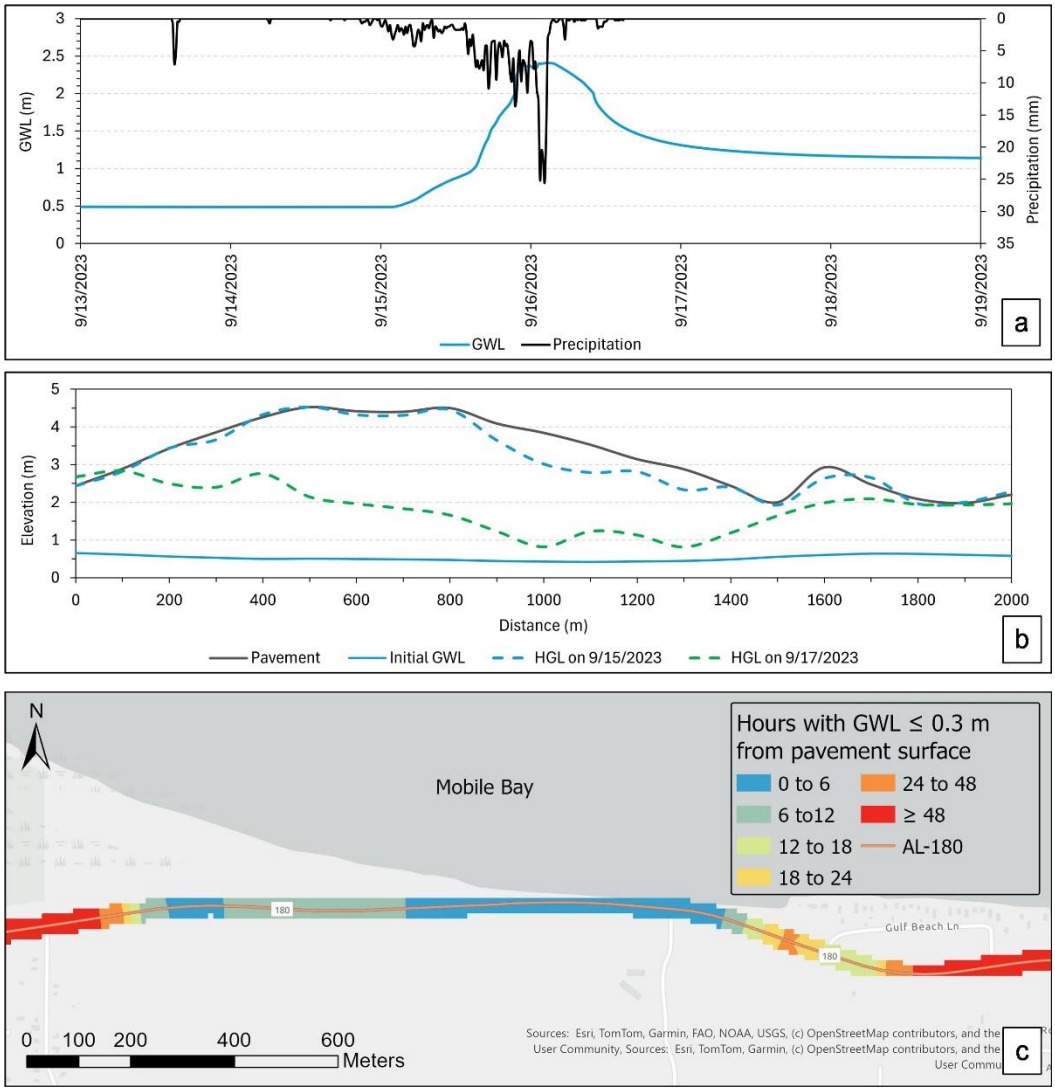

Figure 30 - GWL results from the simulation of the same area for Hurricane Sally, which happened in September 2020, with 555 mm of rainfall. a: rainfall/groundwater head relationship at our monitoring location; b: saturation along the whole segment. c: detailed view of the segment with the duration during which sections were saturated at less than 0.3 m from the pavement surface.

Some areas near the pavement also showed signs of flooding, mainly where the road shifted farther from Mobile Bay, similar to where prolonged saturation occurred (Figure 32a). According to the model results, flooding can vary from 0.3 to 1.0 m near the pavement in these two areas. In addition to the flooding, the groundwater level (GWL) took a long time to recede after the event. Therefore, the GWL may remain close to the pavement for extended periods, as observed between September 15th and 18th in Figure 32b. In the 100 m section, the GWL reaches the surface, which may lead to flooding and pressure from below. Conversely, the 1800 m section shows near

pavement saturation without flooding from below, and the surface flooding depicted in the figure is adjacent to the pavement.

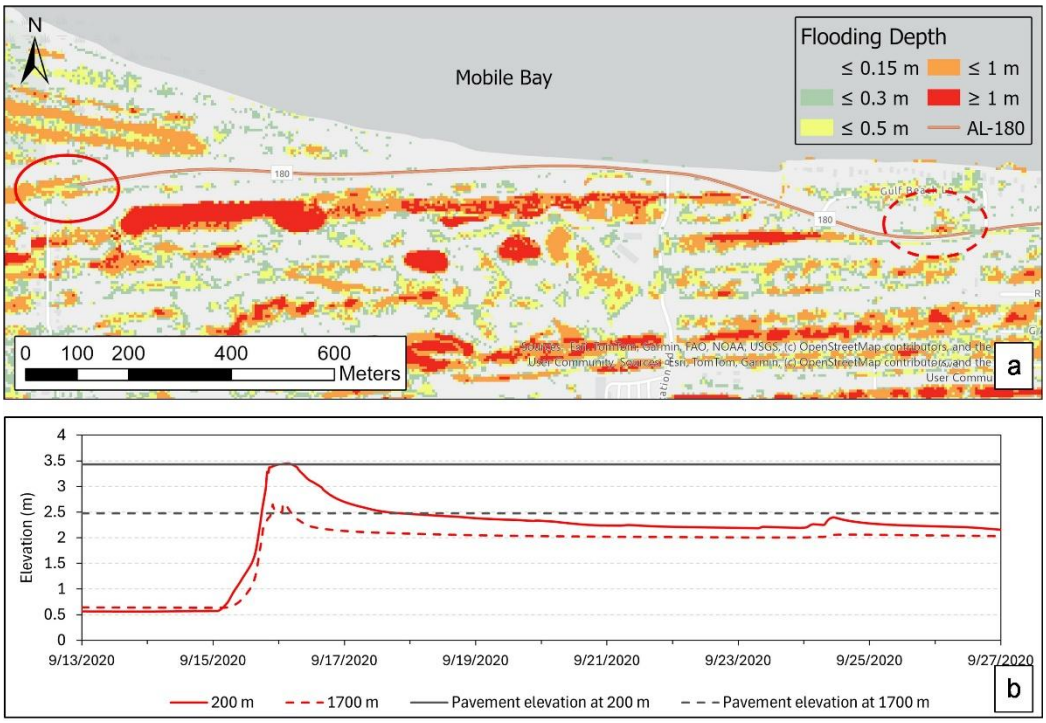

Figure 31 - Flooding and GWL results from the simulation of the same area for Hurricane Sally, which happened in September 2020, with 555 mm of rainfall.

4.4. Large Scale Model

The large-scale GSSHA model was developed with topographic preprocessing performed using the Topographic Parameterization (TOPAZ) algorithm (Garbrecht & Martz, 1997) to calculate flow directions and accumulations. To optimize computational performance, the Digital Elevation Model (DEM) was trimmed to the combined extent of the two census tracts comprising the study area, with an added 100-meter buffer toward Mobile Bay (MB) and the Gulf of Mexico (GM). Soil and land cover data were converted into model coverages within WMS, allowing the creation of lookup tables to assign infiltration and roughness parameters across the watershed. Then, a 30-meter grid resolution was used, and flood depths were referenced to the NAVD88 vertical datum, consistent with the elevation dataset. Given the scale and topography of the peninsula, no well-defined channels were present, so channel routing was disabled. Instead, the model focused on simulating surface runoff, infiltration, and groundwater interactions. In addition,

Surface roughness was assigned based on land cover classifications from the National Land Cover Database (NLCD), with Manning's n values selected from the HEC-RAS 2D User's Manual (Brunner, 2021). Infiltration was computed using the Green-Ampt method with redistribution, which is a reliable approximation of Richards' Equation for variably saturated flow (Ogden & Saghafian, 1997).

To represent subsurface processes, groundwater-surface water interactions were incorporated into the model. This required additional inputs such as aquifer bottom elevation, initial groundwater table, saturated hydraulic conductivity, and soil porosity. The simulation time step was set to 10 seconds to prevent numerical instability and to ensure smooth representation of rapid hydrologic responses. Lastly, the study area was subjected to a 2-year, 24-hour storm event totaling 152 mm of rainfall, which followed a Type III temporal distribution curve, as specified for coastal areas in Technical Release 55 (TR-55) by the Soil Conservation Service (SCS, 1986).

4.4.1. Results

Regarding the Peninsula model, a detailed analysis of both the western and eastern sections of the study area revealed localized flooding patterns consistent with field observations (Figure 22). On the west, standing water observed during field visits matched model predictions, validating the accuracy of the flood simulations. The eastern side displayed increased flooding close to and over the roadway, posing potential risks for evacuation routes and emergency access. These insights emphasize the importance of considering localized hydrological behavior in infrastructure planning for flood-prone areas.

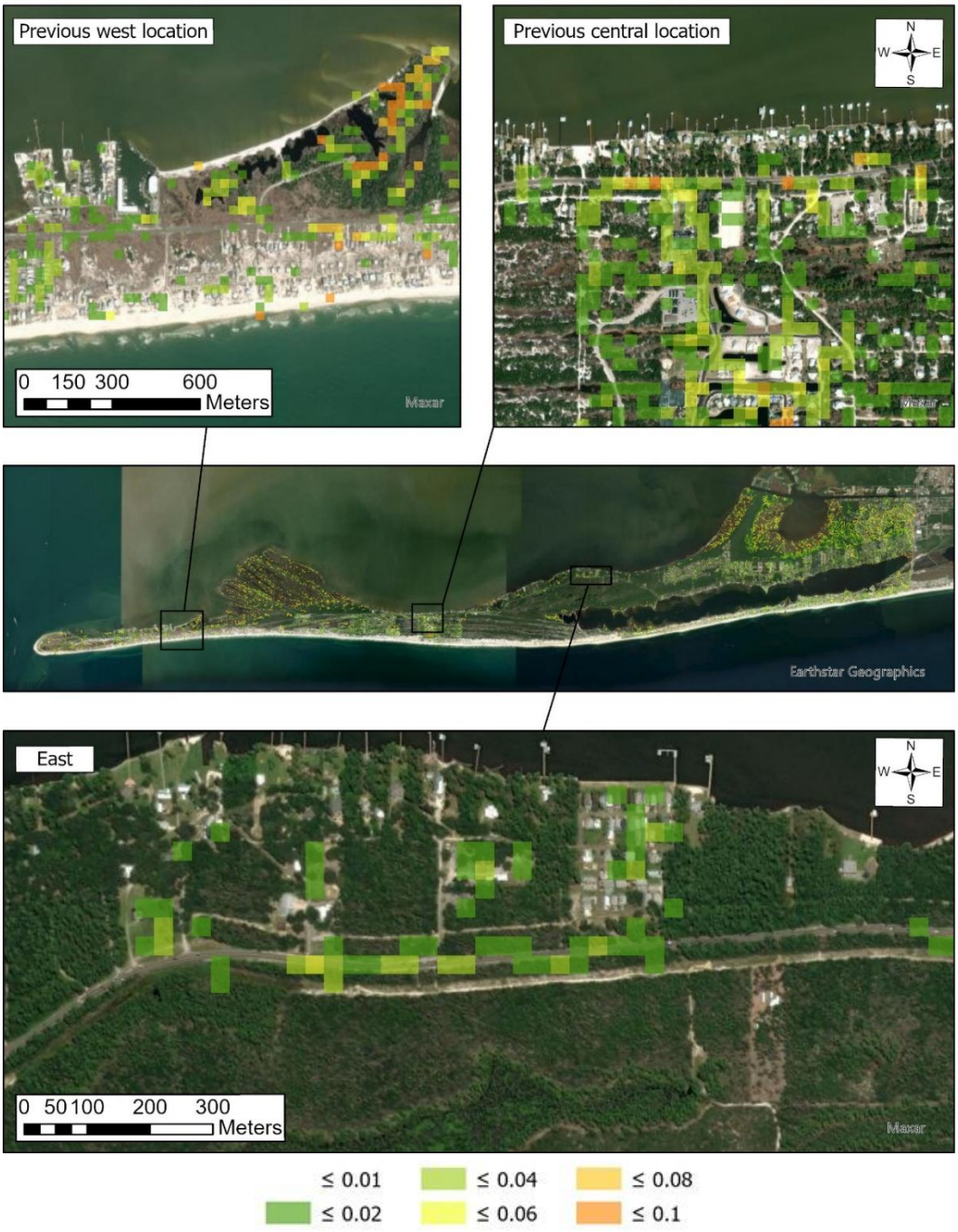

Figure 32 - Flood depths in meters found by the peninsula model.

Including groundwater interactions resulted in a reduced flood extent compared to simpler models that considered only surface runoff and infiltration (Sousa & Vasconcelos, 2024). The inclusion of subsurface flow processes contributed to this decrease, as water was allowed to percolate and distribute below the surface. Additionally, the model exhibited a lower mass

conservation error, confirming its enhanced capacity to replicate complex hydrological conditions along the roadway, which is crucial for improving flood resilience and informing targeted mitigation strategies.

4.5. Discussion

Hydrologic modeling in coastal environments presents unique challenges due to interactions between precipitation, infiltration, and tidal variations. While the GSSHA model provides robust capabilities for simulating surface and shallow groundwater processes, its performance has proven variable depending on the model configuration. Studies have indicated difficulty in calibrating GSSHA for sandy soils or in situations with limited hydrologic data. Because of its 2D formulation, GSSHA may better replicate groundwater dynamics than SWMM; however, replicating hydrographs remains challenging when groundwater contributions are dominant (Moore et al., 2017). Additionally, their study lacked external forcing such as tidal variation. Other research has demonstrated that GSSHA model calibration can be effective, but is highly sensitive to parameters, including roughness, storage depth, and rainfall depth distribution (Chin-talapudi et al., 2014; Weston et al., 2015).

In earlier studies at AL-180, simulations used synthetic storms and assumed a dry initial moisture condition (Sousa & Vasconcelos, 2024). Despite the high volumes of rainfall (152-228 mm in 24 hours), significant infiltration occurred, with limited overland flow and no flooding in some areas where flooding had previously been observed. This may be attributed to the area's sandy soils and the lack of groundwater representation in the model, which limits infiltration. In addition, our study illustrates how significantly the initial water table and groundwater boundary conditions may influence GWL model predictions and need to be calibrated as much as other parameters.

In this study, the model shows a satisfactory agreement with the observed GWL in both validation periods, capturing the general sub-daily trends and magnitudes of the response to precipitation and subsequent recession. This confirms GSSHA's capabilities to represent the responses to high-intensity rainfall. The lower NSE for our second validation suggests limitations in representing smaller rainfall events. The pavement saturation analysis revealed that less intense events do not pose a threat. In addition, a sequence of rainfall events in the calibration

demonstrated that antecedent moisture is critical in determining how long the pavement remains saturated. Lower elevations, on the other hand, may define where the pavement is vulnerable during less intense precipitation events.

Tidal interactions with groundwater are also critical in coastal hydrological simulations but are not easily applied. Our GSSHA model represented sea level as a fixed boundary along Mobile Bay and the Gulf of Mexico. This approach aligns with (Karamouz et al., 2017), which coupled GSSHA with coastal inundation models to simulate storm surge dynamics. However, similar to what was shown in our study, other authors recognize GSSHA's limitation in terms of representing dynamic tidal boundaries linked to astronomical cycles or storm surges (Fattahi et al., 2023; Wijayarathne & Gomezdelcampo, 2019). This constraint may limit the simulation of real compound events, including extreme storm surges combined with higher initial water tables and precipitation. GSSHA response is highly influenced by grid resolution and Green-Ampt parameters (Fattahi et al., 2023). In their case, they also reduced cell size and increased stream network, which affected predictions up to 57%. In our case, on the other hand, the saturated hydraulic conductivities for both infiltration and groundwater flows were calibrated, in addition to the aquifer bottom, which greatly influenced the magnitude of the GWL values.

The extreme event simulation indicated that the pavement in the study area may remain saturated for several days. Prolonged saturation may increase pavement susceptibility to rutting, shear deformation, and premature failure under loading (Chen & Wang, 2023a; Titus-Glover et al., 2019). Additionally, flooding in locations adjacent to the pavement may result from poor drainage, leading to shoulder erosion and moisture accumulation in the pavement's structural layers. Therefore, making it available for traffic before the GWL drains after an event such as Hurricane Sally could compromise the pavement's structural reliability. There may be a need to delay the reopening of this segment of AL-180 after extreme events. The short saturation duration as AL-180 approaches Mobile Bay may be related to faster drainage conditions, indicating that the segment closer to the bay may be more vulnerable to storm surges than to higher water tables.

These results suggest that surface runoff alone underrepresents the risks posed by flooding and high water tables at AL-180. However, validation demonstrated that the GSSHA model, as presented here, is suitable for detecting high groundwater levels near roadways, especially after intense precipitation events. Simulations predicting future rainfall, storms, and sea level

conditions, including groundwater dynamics, are crucial for assessing elevated water table-induced saturation, particularly for low-lying infrastructure. While this study captured the dynamics of GWL changes and surface flooding, it does not explicitly address the potential impact of storm surges on infiltration processes because tidal variation cannot be represented in the groundwater simulation in GSSHA. Therefore, storm surge should be included in future studies to enhance coastal vulnerability assessment, as it can increase water table elevations.

To support application in other settings, the following generalized steps are recommended:

- Characterize soil and land cover using soil data or site-specific information; scale K_{inf} values by land cover following empirical methods (e.g., Robinson et al., 2022).
- Set initial soil moisture based on typical values for the soil type, adjusting only if supported by local data.
- Use observed groundwater level (GWL) data to calibrate both response to precipitation and recession trends after rainfall and tidal events.
- Perform sensitivity analysis on K_{inf} and K_{GW} within a realistic range, adjusting in small increments (e.g., 5 cm/h).
- Test aquifer bottom depth to control the saturated soil column size.
- Evaluate model performance using metrics like Nash-Sutcliffe Efficiency (NSE), Root Mean Square Error (RMSE), and Percent Bias (PBIAS) to evaluate model accuracy.
- Document all assumptions.

4.6. Conclusions

This study utilized GSSHA hydrologic modeling to evaluate groundwater level dynamics along a vulnerable section of AL-180 in Fort Morgan Peninsula, Alabama. The results indicated that GSSHA, when accurately calibrated, can depict the interactions between precipitation and shallow groundwater in sandy, low-lying coastal environments. The model effectively captured the timing and magnitude of groundwater peaks during validation and revealed extended periods of saturation following extreme events, such as Hurricane Sally. These findings emphasize that surface runoff alone fails to adequately capture the full complexity of hydrologic risks for coastal roads.

By incorporating groundwater processes, the simulations identified critical segments of the road that may remain saturated for hours or days, potentially compromising the pavement's structural integrity if it is open to traffic immediately after the event ends. These results suggest that transportation agencies should consider delaying the reopening of roads such as AL-180 until groundwater levels have receded to prevent long-term damage. Additionally, locations closer to the bay may require special attention for storm surge vulnerability, while inland segments are more sensitive to groundwater-induced saturation.

The modeling framework is replicable for similar coastal corridors characterized by sandy soils, high water tables, and proximity to tidal bodies. Other DOTs can adopt this method to prioritize infrastructure investments and establish road closure thresholds by accessing basic elevation, land cover, rainfall, and tide data. Although the modeling approach addressed significant challenges such as high infiltration rates and shallow aquifers, limitations persist in representing tidal fluctuations within the groundwater component. Future studies should investigate coupling GSSHA with models that enable dynamic tidal boundary conditions or integrating manual tide-based corrections.

By shifting from an empirical analysis to a physically based, local-scale model, this chapter closes the methodological loop initiated in Chapter 2. Together, the two approaches offer a scalable framework for evaluating coastal road vulnerability—from road segment vulnerability screening to localized design. The concluding section synthesizes these results and proposes how both methods can be adapted into practical guidelines for federal and regional agencies involved in coastal infrastructure planning and design.

4.7. Data Availability

The original models used to generate the results presented in the study are openly available at https://github.com/bjs0091/GSSHA-coastal-model.

Chapter 5. Summary and Conclusions

5.1. Summary of the study

The importance of representing the interactions between coastal groundwater levels (GWL) and infrastructure is highlighted by rapid population growth, aging infrastructure, and increased hydrological stressors created by climate change and sea level rise. The dynamics of GWL are very complex due to the wide range of physical processes and the time/spatial scale at which these occur, which thus necessitate research efforts. In particular, this dissertation focused on how GWL could be represented in assessing the potential impacts of saturation on coastal roadways.

Groundwater evaluations in coastal settings have traditionally relied on numerical models like MODFLOW (Langevin et al., 2017). These approaches, while effective in certain contexts, are limited in low-elevation, tidally influenced regions due to their coarser time scales, which do not capture rapid fluctuations. This dissertation addresses this gap by creating a simplified, data-driven groundwater predictor and by establishing a framework for using distributed hydrologic modeling in this context. The models were calibrated and validated using field observations from Fort Morgan Peninsula in Alabama. The study captured spatial and temporal dynamics at event and long-term time scales to investigate groundwater level interaction with the pavement. Each modeling approach addressed specific limitations in current methodologies and, together, contributed to increasing the understanding of the hydrologic stressors affecting coastal infrastructure.

5.2. General Conclusions

The empirical component introduced a simplified GWL predictor that can represent sub-daily groundwater fluctuations using precipitation, tidal levels, and spatial variables such as elevation and distance to large water bodies. Validated with field data collected in collaboration with the Alabama DOT, the model achieved satisfactory performance (NSE = 0.56–0.73; RMSE $\leq$ 0.09 m) and was extended to longer segments of AL-180 with 100-meter resolution. This spatial implementation enabled the detection of segments which most exposed to shallow GWL,

supporting prioritization for maintenance and adaptation. Additionally, the application of spatiotemporal analyses, including exceedance curves and emerging hotspot detection, revealed areas with persistent or increasing exposure, particularly between kilometers 5 and 6 and 14 and 18. The proposed GWL predictor offers a simplified yet effective approach to estimate shallow water table behavior in coastal areas. It allows for sub-daily time resolution assessment using only tidal data, rainfall, and distance from the major water body, making it a viable tool for planners and engineers with limited resources. However, the model is currently applicable for sandy soils with conductivities ranging from 15 to 35 cm/h and may require recalibration in different physiographic contexts. This happens because it may change depending on soil characteristics, such as saturated hydraulic conductivity, porosity, and land cover, which include water detention or wetlands, which may influence local water levels.

The GSSHA-based simulations provided detailed insight into surface and subsurface interactions under varying rainfall conditions and an extreme event (Hurricane Sally). When properly calibrated, the model successfully reproduced observed groundwater responses (NSE = 0.58–0.90; RMSE $\leq$ 0.06 m), allowing for the identification of vulnerable segments prone to prolonged saturation. The results indicated that both the magnitude and timing of rainfall may influence the duration of saturation, and that pavement exposure often extends to after the end of storm events. Furthermore, the model findings indicate that groundwater representation is crucial for explaining observed flooding and road degradation, particularly in areas with high water tables. These results demonstrate how sub-surface parameters in GSSHA can be modified to simulate near-surface saturation to offer actionable insights for transportation departments and infrastructure managers. Nevertheless, GSSHA has high data and computational demands, and the calibration and validation process remain time-consuming.

Together, the models demonstrated that coastal pavement vulnerability is susceptible to hydrologic conditions such as soil hydraulic conductivity and depth of the low-permeability layer, with compounded risks arising from the interaction of rainfall, tides, and sea level rise (SLR). Nevertheless, more tests would be needed to apply the methodology for different soil types as this finding may not be true for clay or silt soils, for example. Projections using IPCC scenarios indicate that, under high-emissions pathways (SSP5-8.5), the subgrade may experience saturation more than 90% of the time in the future, compromising long-term performance and serviceability of infrastructure assets.

This work contributes to ongoing efforts in infrastructure resilience by:

- Proposing a transferable modeling framework that offers sub-daily groundwater level predictions for coastal corridors with limited monitoring capacity.
- Highlighting the importance of shallow groundwater as a critical driver of pavement degradation.
- Creating a framework to apply distributed hydrologic models to low-lying coastal areas.
- Demonstrating the value of integrating spatial tools (e.g., GIS, GeOBIA, and Space-Time Cube) into hydrologic modeling result analysis and infrastructure risk assessment.

The two methodologies developed in this dissertation offer complementary tools for agencies such as the Federal Highway Administration (FHWA) and the National Oceanic and Atmospheric Administration (NOAA) to assess and manage coastal road vulnerability. The empirical framework described in Chapters 2 and 3 is well suited for preliminary assessments, helping planners identify high-risk segments where strategic decisions, such as road relocation, elevation, or project prioritization, must be made. In contrast, the physically based modeling approach in Chapter 4 supports detailed design and engineering applications at smaller spatial scales, enabling simulation of hydrologic conditions over days to weeks. Together, these methods can guide a tiered decision-making process, from early planning to final design, for coastal resilience in transportation infrastructure.

5.3. Limitations and Future Studies

In addressing these challenges, this dissertation also raises new research questions. First, how does the empirical predictor perform under different climatic regimes, coastal morphologies, or levels of urbanization? Second, what would the impact of Nature and Nature-based Features on shallow groundwater responses be? Future research should focus on (1) validating the model in other coastal corridors; (2) integrating evapotranspiration, soil characteristics, and NNBFs into the empirical predictors. These are crucial to support robust planning under increasing climate variability and sea-level rise.

Chapter 6. References

Ahmari, H., Hummel, M., Chao, S.-H., Md Imran Kabir, S., Pervaiz, F., Acharya, B. R., Dean, M., & Mowla, Q. A. E. (2021). Identify and Analyze Inundated Bridge Superstructures in High Velocity Flood Events.

Ali, A. S. A., Jazaei, F., Clement, T. P., & Waldron, B. (2024). Physics-informed neural networks in groundwater flow modeling: Advantages and future directions. Groundwater for Sustainable Development, 25, 101172. https://doi.org/10.1016/j.gsd.2024.101172.

Althoff, D., and L. N. Rodrigues. 2021. "Goodness-of-fit criteria for hydrological models: Model calibration and performance assessment." J Hydrol (Amst), 600 (July): 126674. Elsevier B.V. https://doi.org/10.1016/j.jhydrol.2021.126674.

Bartlett, M. S., and A. Porporato. 2018. "A Class of Exact Solutions of the Boussinesq Equation for Horizontal and Sloping Aquifers." Water Resour Res, 54 (2): 767–778. https://doi.org/10.1002/2017WR022056.

Beck, H. E., Zimmermann, N. E., Mcvicar, T. R., Vergopolan, N., Berg, A., & Wood, E. F. (2018). Data Descriptor : Present and future Köppen-Geiger climate classification maps at 1 -km resolution. Nature Publishing Group, 1–12. https://doi.org/10.1038/sdata.2018.214.

Bosserelle, A. L., L. K. Morgan, D. E. Dempsey, and I. Setiawan. 2023. "Shallow groundwater characterisation and hydrograph classification in the coastal city of Ōtautahi/Christchurch, New Zealand." Hydrogeol J, (0123456789). Springer Berlin Heidelberg. https://doi.org/10.1007/s10040-023-02745-z.

Bowes, B. D., J. M. Sadler, M. M. Morsy, M. Behl, and J. L. Goodall. 2019. "Forecasting groundwater table in a flood prone coastal city with long short-term memory and recurrent neural networks." Water (Switzerland), 11 (5). https://doi.org/10.3390/w11051098.

Bragg, M. A., Poudel, A., & Vasconcelos, J. G. (2025). Comparing SWMM and HEC-RAS Hydrological Modeling Performance in Semi-Urbanized Watershed. Water, 17(9), 1331. https://doi.org/10.3390/w17091331.

Brendel, C. E., Dymond, R. L., & Aguilar, M. F. (2021). Modeling Storm Sewer Networks and Urban Flooding in Ro-anoke, Virginia, with SWMM and GSSHA. Journal of Hydrologic Engineering, 26(1), 5020044. https://doi.org/10.1061/(ASCE)HE.1943-5584.0002021.

Burek, P., Satoh, Y., Kahil, T., Tang, T., Greve, P., Smilovic, M., Guillaumot, L., Zhao, F., & Wada, Y. (2020). Development of the Community Water Model (CWatM v1.04) – a high-resolution hydrological model for global and regional assessment of integrated water resources management. Geoscientific Model Development, 13(7), 3267–3298. https://doi.org/10.5194/gmd-13-3267-2020.

Casasso, A., Molfetta, A. D., & Sethi, R. (2015). Groundwater monitoring at a building site of the tidal flood protection system "MOSE" in the Lagoon of Venice, Italy. Environmental Earth Sciences, 73(5), 2397–2408. https://doi.org/10.1007/s12665-014-3588-8.

Chang, S. W., K. Nemec, L. Kalin, and T. P. Clement. 2016. "Impacts of Climate Change and Urbanization on Groundwater Resources in a Barrier Island." Journal of Environmental Engineering, 142 (12). https://doi.org/10.1061/(ASCE)EE.1943-7870.0001123.

Chegini, T., Li, H., Yang, Y. C. E., Blöschl, G., & Leung, L. R. (2025). A Scale-Adaptive Urban Hydrologic Framework: Incorporating Network-Level Storm Drainage Pipes Representation. Water Resources Research, 61(3). https://doi.org/10.1029/2024WR037268.

Chen, X., & Wang, H. (2023a). Impact of sea level rise on asphalt pavement responses considering seasonal ground-water and moisture gradient in subgrade. Transportation Geotechnics, 40, 100992. https://doi.org/10.1016/j.trgeo.2023.100992.

Chen, X., & Wang, H. (2023b). Transportation Geotechnics Impact of sea level rise on asphalt pavement responses considering seasonal groundwater and moisture gradient in subgrade. Transportation Geotechnics, 40(April), 100992. https://doi.org/10.1016/j.trgeo.2023.100992.

Cherubini, C., Sathish, S., & Pastore, N. (2023). Dynamics of Coastal Aquifers: Conceptualization and Steady-State Calibration of Multilayer Aquifer System-Southern Coast of Emilia Romagna. Water (Switzerland), 15(13). https://doi.org/10.3390/w15132384.

Chintalapudi, S., Sharif, H., & Xie, H. (2014). Sensitivity of Distributed Hydrologic Simulations to Ground and Satellite Based Rainfall Products. Water, 6(5), 1221–1245. https://doi.org/10.3390/w6051221.

Chow, V. Te, Maidment, D. R., Mays, L. W., & Ven Te Chow, David R. Maidment, L. W. M. (1988). Applied Hydrology Chow 1988.pdf (pp. 1–294). http://ponce.sdsu.edu/Applied_Hydrology_Chow_1988.pdf.

Cox, A. H., Loomis, G. W., & Amador, J. A. (2019). Preliminary Evidence That Rising Groundwater Tables Threaten Coastal Septic Systems. Journal of Sustainable Water in the Built Environment, 5(4), 1–12. https://doi.org/10.1061/jswbay.0000887.

Curtis, Z. K., Li, S., Liao, H., & Lusch, D. (2018). Data-Driven Approach for Analyzing Hydrogeology and Groundwater Quality Across Multiple Scales. Groundwater, 56(3), 377–398. https://doi.org/10.1111/gwat.12584.

Das, K., S. Sarkar, A. Mukherjee, P. Das, and A. Pathak. 2021. "Observing tidal and storm generated wave height impact on groundwater levels in a tropical delta (the Sundarbans)." J Hydrol (Amst), 603 (PA): 126813. Elsevier B.V. https://doi.org/10.1016/j.jhydrol.2021.126813.

De Oliveira Sousa, B. J., Webb, B. M., Wright, D. B., Clement, T. P., & Vasconcelos, J. G. (2025). Conceptual data-driven approach for analyzing the vulnerability of coastal roadways to groundwater level changes. Journal of Environmental Management, 390, 1–12. https://doi.org/10.1016/j.jenvman.2025.126295.

DeSousa, S., Bhaskar, A. S., Kelleher, C., & Livneh, B. (2024). Understanding Spatiotemporal Patterns and Drivers of Urban Flooding Using Municipal Reports. Hydrological Processes, 38(12). https://doi.org/10.1002/hyp.70028.

Dewitz, J. (2024). National Land Cover Database (NLCD) 2019 Products (ver. 3.0, February 2024). U.S. Geological Survey. https://doi.org/10.5066/P9KZCM54.

DHI. (2025). MIKE 2025: User Guide and Reference Manual (p. 810) [User Guide and Reference Manual].

Doglioni, A., and V. Simeone. 2017. "Evolutionary Modeling of Response of Water Table to Precipitations." J Hydrol Eng, 22 (2). https://doi.org/10.1061/(ASCE)HE.1943-5584.0001465.

Downer, C. W., & Ogden, F. L. (2003). Prediction of runoff and soil moistures at the watershed scale: Effects of mod-el complexity and parameter assignment. Water Resources Research, 39(3). https://doi.org/10.1029/2002WR001439.

Downer, C. W., & Ogden, F. L. (2006). Gridded Surface Subsurface Hydrologic Analysis (GSSHA) User's Manual, Version 1.43 for Watershed Modeling System 6.1. In US Army Corps of Engineers, Engineer Research and Devel-opment Center (Issue September). http://oai.dtic.mil/oai/oai?verb=getRecord&metadataPrefix=html&identifier=ADA455335.

Easterling, D. R., Kunkel, K. E., Arnold, J. R., Knutson, T. R., LeGrande, A. N., Leung, L. R., Vose, R. S., Waliser, D. E., & Wehner, M. (2017). Precipitation change in the United States. In: Climate Science Special Report: Fourth National Climate Assessment. Fourth National Climate Assessment, Volume I, I, 207–230. https://doi.org/10.7930/J0H993CC.U.S.

Esri. (2025a). Emerging Hot Spot Analysis (Space Time Pattern Mining). Retrieved July 17, 2025, from https://pro.arcgis.com/en/pro-app/latest/tool-reference/space-time-pattern-mining/emerginghotspots.htm

Esri. (2025b). An overview of the Space Time Pattern Mining toolbox. Esri. Retrieved May 13, 2025, from https://pro.arcgis.com/en/pro-app/latest/tool-reference/space-time-pattern-mining/an-overview-of-the-space-time-pattern-mining-toolbox.htm

Fattahi, A. M., Hosseini, K., Farzin, S., & Mousavi, S.-F. (2023). An innovative approach of GSSHA model in flood analysis of large watersheds based on accuracy of DEM, size of grids, and stream density. Applied Water Science, 13(2), 33. https://doi.org/10.1007/s13201-022-01838-6.

Ferguson, G., & Gleeson, T. (2012). Vulnerability of coastal aquifers to groundwater use and climate change. In Nature Climate Change (Vol. 2, Issue 5, pp. 342–345). https://doi.org/10.1038/nclimate1413.

Fry, T. J., & Maxwell, R. M. (2018). Using a Distributed Hydrologic Model to Improve the Green Infrastructure Pa-rameterization Used in a Lumped Model. Water, 10(12), 1756. https://doi.org/10.3390/w10121756.

Gao, Y., Zhang, Z., & Liu, Y. (2019). Sensitivity Analysis of Parameters of a HEC-HMS Model with Polders. Journal of Coastal Research, 93(sp1), 163. https://doi.org/10.2112/SI93-023.1.

Garner, G. G., Hermans, T., Kopp, R. E., Slangen, A. B. A., Edwards, T. L., Levermann, A., Nowicki, S., Palmer, M. D., Smith, C., Fox-Kemper, B., Hewitt, H. T., Xiao, C., Aðalgeirsdóttir, G., Drijfhout, S. S., Golledge, N. R., Hemer, M., Krinner, G., Mix, A., Notz, D., … Pearson, B. (2021). IPCC AR6 Sea Level Projections (Version 20210809) [Dataset]. Zenodo. https://doi.org/10.5281/zenodo.6382554.

Getis, A., & Ord, J. K. (1992). The Analysis of Spatial Association by Use of Distance Statistics. Geographical Analysis, 24(3), 189–206. https://doi.org/10.1111/j.1538-4632.1992.tb00261.x.

Giacomoni, M. H., Olivera, F., & do Lago, C. (2019). Assessing the Impacts of Super Storm Flooding in the Transportation Infrastructure – Case Study: San Antonio, Texas (Issue 18HSTSA02).

Gilman, E. F. (2023). Spartina bakeri Marsh Grass, Sand Cordgrass.

Gleeson, T., Moosdorf, N., Hartmann, J., & Van Beek, L. P. H. (2014). A glimpse beneath earth's surface: GLobal HYdrogeology MaPS (GLHYMPS) of permeability and porosity. Geophysical Research Letters, 41(11), 3891–3898. https://doi.org/10.1002/2014GL059856.

Haaf, E., M. Giese, T. Reimann, and R. Barthel. 2023. "Data-Driven Estimation of Groundwater Level Time-Series at Unmonitored Sites Using Comparative Regional Analysis." Water Resour Res, 59 (7). John Wiley and Sons Inc. https://doi.org/10.1029/2022WR033470.

Habel, S., C. H. Fletcher, K. Rotzoll, A. I. El-Kadi, and D. S. Oki. 2019. "Comparison of a simple hydrostatic and a data-intensive 3d numerical modeling method of simulating sea-level rise induced groundwater inundation for Honolulu, Hawai'i, USA." Environ Res Commun, 1 (4). IOP Publishing. https://doi.org/10.1088/2515-7620/ab21fe.

Habel, S., Fletcher, C. H., Barbee, M. M., & Fornace, K. L. (2024). Hidden Threat: The Influence of Sea-Level Rise on Coastal Groundwater and the Convergence of Impacts on Municipal Infrastructure SLR: sea-level rise. Annual Review of Marine Science, 16, 81–103. https://doi.org/10.1146/annurev-marine-020923.

Habel, S., Fletcher, C. H., Rotzoll, K., & El-kadi, A. I. (2017). Development of a model to simulate groundwater inundation induced by sea-level rise and high tides in Honolulu , Hawaii. Water Research, 114, 122–134. https://doi.org/10.1016/j.watres.2017.02.035.

Hamedi, A., & Fuentes, H. R. (2015). Comparative Effectiveness and Reliability of NEXRAD Data to Predict Outlet Hy-drographs Using the GSSHA and HEC-HMS Hydrologic Models. 1444–1453. https://doi.org/10.1061/9780784479162.142.

Hayek, M. (2019). Accurate approximate semi-analytical solutions to the Boussinesq groundwater flow equation for recharging and discharging of horizontal unconfined aquifers. Journal of Hydrology, 570(December 2018), 411–422. https://doi.org/10.1016/j.jhydrol.2018.12.057.

Herb, W., Janke, B., & Stefan, H. (2017). Study of De-icing Salt Accumulation and Transport Through a Watershed (Issue MN/RC 2017-50).

Hoogestraat, G. (2017). Rainfall-Runoff Modeling for Improved Peak Flow Estimates in the Black Hills Area of South Dakota (Issues SD2013-03-F).

Housego, R., B. Raubenheimer, S. Elgar, S. Cross, C. Legner, and D. Ryan. 2021. "Coastal flooding generated by ocean wave- and surge-driven groundwater fluctuations on a sandy barrier island." J Hydrol (Amst), 603 (PB): 126920. Elsevier B.V. https://doi.org/10.1016/j.jhydrol.2021.126920.

Huff, F. A. 1967. "Time distribution of rainfall in heavy storms." Water Resour Res, 3 (4): 1007–1019. https://doi.org/10.1029/WR003i004p01007.

Huizer, S., M. Radermacher, S. De Vries, G. H. P. Oude Essink, and M. F. P. Bierkens. 2018. "Impact of coastal forcing and groundwater recharge on the growth of a fresh groundwater lens in a mega-scale beach nourishment." Hydrol Earth Syst Sci, 22 (2): 1065–1080. https://doi.org/10.5194/hess-22-1065-2018.

Hunt, W. F., Jarrett, ; A R, Smith, ; J T, & Sharkey, L. J. (2006). Evaluating Bioretention Hydrology and Nutrient Removal at Three Field Sites in North Carolina. Journal of Irrigation and Drainage Engineering, 132(6), 600–608. https://doi.org/10.1061/ASCE0733-94372006132:6600.

Hussain, F., Wu, R. S., & Shih, D. S. (2022). Water table response to rainfall and groundwater simulation using physics-based numerical model: WASH123D. Journal of Hydrology:

Regional Studies, 39(November 2021), 100988. https://doi.org/10.1016/j.ejrh.2022.100988.

Intergovernmental Panel on Climate Change (IPCC) (Ed.). (2023). Ocean, Cryosphere and Sea Level Change. In Climate Change 2021 – The Physical Science Basis: Working Group I Contribution to the Sixth Assessment Report of the Intergovernmental Panel on Climate Change (pp. 1211–1362). Cambridge University Press. https://doi.org/10.1017/9781009157896.011.

Inyim, P., Pereyra, J., Bienvenu, M., & Mostafavi, A. (2016, July). Environmental assessment of pavement infrastructure: A systematic review. In Journal of Environmental Management (Vol. 176, pp. 128–138). Academic Press. https://doi.org/10.1016/j.jenvman.2016.03.042.

Jafarzadegan, K., Moradkhani, H., Pappenberger, F., Moftakhari, H., Bates, P., Abbaszadeh, P., Marsooli, R., Ferreira, C., Cloke, H. L., Ogden, F., & Duan, Q. (2023). Recent Advances and New Frontiers in Riverine and Coastal Flood Modeling. Reviews of Geophysics, 61(2). https://doi.org/10.1029/2022rg000788.

Jon Dewitz. (2024). National Land Cover Database (NLCD) 2019 Products (ver. 3.0, February 2024) [Dataset]. U.S. Geological Survey. https://doi.org/10.5066/P9KZCM54.

Kampf, S. K., & Burges, S. J. (2007). A framework for classifying and comparing distributed hillslope and catchment hydrologic models. Water Resources Research, 43(5). https://doi.org/10.1029/2006WR005370.

Karamouz, M., Ahmadvand, F., & Zahmatkesh, Z. (2017). Distributed Hydrologic Modeling of Coastal Flood Inundation and Damage: Nonstationary Approach. Journal of Irrigation and Drainage Engineering, 143(8), 1–14. https://doi.org/10.1061/(asce)ir.1943-4774.0001173.

Keller, A. A., Garner, K., Rao, N., Knipping, E., & Thomas, J. (2023). Hydrological models for climate-based assessments at the watershed scale: A critical review of existing hydrologic and water quality models. Science of the Total Environment, 867(December 2022), 161209. https://doi.org/10.1016/j.scitotenv.2022.161209.

Kendall, M. G. (1976). Rank Correlation Methods. In Time-Series (pp. 146–163). Springer US.

Khan, J., Lee, E., Balobaid, A. S., & Kim, K. (2023). A Comprehensive Review of Conventional, Machine Learning, and Deep Learning Models for Groundwater Level

(GWL) Forecasting. Applied Sciences, 13(4), 2743. https://doi.org/10.3390/app13042743.

Kimball, S. K., & Terwey, W. (2024). South Alabama Mesonet. http://chiliweb.southalabama.edu/archived_data.php.

Knott, J. F., Daniel, J. S., Jacobs, J. M., & Kirshen, P. (2018). Adaptation planning to mitigate coastal-road pavement damage from groundwater rise caused by sea-level rise. Transportation Research Record, 2672(2), 11–22. https://doi.org/10.1177/0361198118757441.

Knott, J. F., Elshaer, M., Daniel, J. S., Jacobs, J. M., & Kirshen, P. (2017). Assessing the Effects of Rising Groundwater from Sea Level Rise on the Service Life of Pavements in Coastal Road Infrastructure. Transportation Research Record: Journal of the Transportation Research Board, 2639(1), 1–10. https://doi.org/10.3141/2639-01.

Koley, S. (2023). Arsenic calamity in India's West Bengal: A critical review of mitigation scenarios. Engineering Sustainability, 176(4). https://doi.org/10.1680/jensu.21.00066.

Kopp, R. E., Garner, G. G., Hermans, T. H. J., Jha, S., Kumar, P., Reedy, A., Slangen, A. B. A., Turilli, M., Edwards, T. L., Gregory, J. M., Koubbe, G., Levermann, A., Merzky, A., Nowicki, S., Palmer, M. D., & Smith, C. (2023). The Framework for Assessing Changes To Sea-level (FACTS) v1.0: A platform for characterizing parametric and structural uncertainty in future global, relative, and extreme sea-level change. Geoscientific Model Development, 16(24), 7461–7489. https://doi.org/10.5194/gmd-16-7461-2023.

Lambs, L. (2004). Interactions between groundwater and surface water at river banks and the confluence of rivers. Journal of Hydrology, 288(3–4), 312–326. https://doi.org/10.1016/j.jhydrol.2003.10.013.

Langevin, C. D., Hughes, J. D., Banta, E. R., Niswonger, R. G., Panday, S., & Provost, A. M. (2017). Documentation for the MODFLOW 6 Groundwater Flow Model (Techniques and Methods). U.S. Geological Survey. https://doi.org/10.3133/tm6A55.

Lee, S., Kang, T., Sun, D., & Park, J.-J. (2020). Enhancing an Analysis Method of Compound Flooding in Coastal Areas by Linking Flow Simulation Models of Coasts and Watershed. Sustainability, 12(16), 6572. https://doi.org/10.3390/su12166572.

Lee, S., Yen, H., Yeo, I. Y., Moglen, G. E., Rabenhorst, M. C., & McCarty, G. W. (2020). Use of multiple modules and Bayesian Model Averaging to assess structural uncertainty of

catchment-scale wetland modeling in a Coastal Plain landscape. Journal of Hydrology, 582(January), 124544. https://doi.org/10.1016/j.jhydrol.2020.124544.

Li, H., Jiao, J. J., Luk, M., & Cheung, K. (2002). Tide-induced groundwater level fluctuation in coastal aquifers bounded by L-shaped coastlines. Water Resources Research, 38(3). https://doi.org/10.1029/2001WR000556.

Macqueen, J. (1967). Some Methods for Classification and Analysis of Multivariate Observations. 281–297.

Mein, R. G., & Larson, C. L. (1973). Modeling infiltration during a steady rain. Water Resources Research, 9(2), 384–394. https://doi.org/10.1029/WR009i002p00384.

Moore, M. F., Vasconcelos, J. G., & Zech, W. C. (2017). Modeling Highway Stormwater Runoff and Groundwater Table Variations with SWMM and GSSHA. Journal of Hydrologic Engineering, 22(8), 1–15. https://doi.org/10.1061/(asce)he.1943-5584.0001537.

Motovilov, Y. G., Gottschalk, L., Engeland, K., & Rodhe, A. (1999). Validation of a distributed hydrological model against spatial observations. Agricultural and Forest Meteorology, 98–99, 257–277. https://doi.org/10.1016/S0168-1923(99)00102-1.

Moynihan, K., & Vasconcelos, J. (2014). SWMM Modeling of a Rural Watershed in the Lower Coastal Plains of the United States. Journal of Water Management Modeling, January. https://doi.org/10.14796/jwmm.c372.

Navarro-Farfán, M. D. M., García-Romero, L., Martínez-Cinco, M. A., Hernández-Hernández, M. A., & Sánchez-Quispe, S. T. (2024). Comparison between MODFLOW Groundwater Modeling with Traditional and Distributed Recharge. Hydrology, 11(1), 9. https://doi.org/10.3390/hydrology11010009.

Nimmo, J. R., & Akstin, K. C. (1988). Hydraulic Conductivity of a Sandy Soil at Low Water Content After Compaction by Various Methods. Soil Science Society of America Journal, 52(2), 303–310. https://doi.org/10.2136/sssaj1988.03615995005200020001x

NOAA. (2024). NOAA Dauphin Island, AL - Station Home Page. In NOAA Tides and Currents. https://tidesandcurrents.noaa.gov/stationhome.html?id=8735180&units=metric.

OCM Partners. (2022). AIP Digital Orthophoto (DOQQ - quarter-quadrangle) m_3008749_nw_16_030_20211113.

OCM Partners. (2024). 1885 - 2021 USGS CoNED Topobathy DEM (Compiled 2022): Northern Gulf of Mexico.

Palanisamy, B., Borkar, R., Sangeetha, K., & Narasimhan, B. (2024). Evaluation of augmented infiltration based LIDs for low lying urbanizing coastal catchments: a case study of Chennai city, India. Urban Water Journal, 21(5), 638–655. https://doi.org/10.1080/1573062X.2024.2331187.

Park, E., and J. C. Parker. 2008. "A simple model for water table fluctuations in response to precipitation." J Hydrol (Amst), 356 (3–4): 344–349. https://doi.org/10.1016/j.jhydrol.2008.04.022.

Petricci, R. H., F. G. Herring, J. D. Madura, and C. Bissonnette. 2023. General Chemistry: principles and modern applications. Pearson Education Limited.

Peña, F., F. Nardi, A. Melesse, J. Obeysekera, F. Castelli, R. M. Price, T. Crowl, and N. Gonzalez-Ramirez. 2022. "Compound flood modeling framework for surface-subsurface water interactions." Natural Hazards and Earth System Sciences, 22 (3): 775–793. https://doi.org/10.5194/nhess-22-775-2022.

Peña, F., Obeysekera, J., Jane, R., Nardi, F., Maran, C., Cadogan, A., Groen, F. de, & Melesse, A. (2023). Investigating compound flooding in a low elevation coastal karst environment using multivariate statistical and 2D hydrodynamic modeling. Weather and Climate Extremes, 39(November 2022). https://doi.org/10.1016/j.wace.2022.100534.

Picketts, I. M., Andrey, J., Matthews, L., Déry, S. J., & Tighe, S. (2016). Climate change adaptation strategies for transportation infrastructure in Prince George, Canada. Regional Environmental Change, 16(4), 1109–1120. https://doi.org/10.1007/s10113-015-0828-8.

Rahimi, R., H. Tavakol-Davani, C. Graves, A. Gomez, and M. F. Valipour. 2020. "Compound inundation impacts of coastal climate change: Sea-level rise, groundwater rise, and coastal precipitation." Water (Switzerland), 12 (10): 1–16. https://doi.org/10.3390/w12102776.

Rau, G. C., Post, V. E. A., Shanafield, M., Krekeler, T., Banks, E. W., & Blum, P. (2019). Error in hydraulic head and gradient time-series measurements: A quantitative appraisal. Hydrology and Earth System Sciences, 23(9), 3603–3629. https://doi.org/10.5194/hess-23-3603-2019.

Rawls, W. J., Brakensiek, D. L., & Saxton, K. E. (1984). Estimation of Soil Water Properties. Transactions of the ASAE. https://doi.org/10.13031/2013.33720.

Robinson, D. A., Nemes, A., Reinsch, S., Radbourne, A., Bentley, L., & Keith, A. M. (2022). Global meta-analysis of soil hydraulic properties on the same soils with differing land use. Science of The Total Environment, 852, 158506. https://doi.org/10.1016/j.scitotenv.2022.158506.

Rossman, L. A. (2015). Storm Water Management Model User's Manual Version 5.1 (Manual No. EPA/600/R-14/413b). U.S. Environmental Protection Agency.

Rotzoll, K., & Fletcher, C. H. (2013). Assessment of groundwater inundation as a consequence of sea-level rise. Nature Climate Change, 3(5), 477–481. https://doi.org/10.1038/nclimate1725

Saha, G. C., & Quinn, M. (2020). Integrated Surface Water and Groundwater Analysis under the Effects of Climate Change, Hydraulic Fracturing and its Associated Activities: A Case Study from Northwestern Alberta, Canada. Hydrology, 7(4), 70. https://doi.org/10.3390/hydrology7040070.

Scharffenberg, W. (2016). Hydrologic Modeling System HEC-HMS User's Manual (Issue CPD-74A).

Schwartz, J. S. (2018). Evaluation and Prediction of Bridge Pier and Contraction Scour of Cohesive River Sediments in Tennessee (Issue RES#2013-36).

Shaikh, B. Y., and T. I. Eldho. 2021. "Analytical Solution for Tide-Influenced Groundwater Variation along Sloping Complex Coastal Aquifer in Presence of Rainfall Infiltration." J Hydrol Eng, 26 (12). American Society of Civil Engineers (ASCE). https://doi.org/10.1061/(asce)he.1943-5584.0002131.

Sith, R., & Nadaoka, K. (2017). Comparison of SWAT and GSSHA for High Time Resolution Prediction of Stream Flow and Sediment Concentration in a Small Agricultural Watershed. Hydrology, 4(2), 27. https://doi.org/10.3390/hydrology4020027.

Soil Conservatio Service (SCS). (1986). Urban Hydrology for Small Watersheds. In U.S. Department of Agriculture (Vol. 1, p. 163).

Soil Survey Staff. (2022). Web Soil Survey. Natural Resources Conservation Service, United States Department of Agriculture. http://websoilsurvey.sc.egov.usda.gov/.

Solomatine, D., See, L. M., & Abrahart, R. J. (2008). Data-Driven Modelling: Concepts, Approaches and Experiences. In R. J. Abrahart, L. M. See, & D. P. Solomatine (Eds.), Practical Hydroinformatics: Computational Intelligence and Technological Developments

in Water Applications (pp. 17–30). Springer. https://doi.org/10.1007/978-3-540-79881-1_2.

Sousa, B. J. O., & Vasconcelos, J. G. (2024). GSSHA Modeling Applied to a Coastal Roadway in Alabama. World En-vironmental and Water Resources Congress 2024, 716–723. https://doi.org/10.1061/9780784485477.063.

Sousa, B. J. O., & Vasconcelos, J. G. (2024). GSSHA Modeling Applied to a Coastal Roadway in Alabama. World Environmental and Water Resources Congress 2024, 716–723. https://doi.org/10.1061/9780784485477.063.

Sukop, M. C., M. Rogers, G. Guannel, J. M. Infanti, and K. Hagemann. 2018. "High temporal resolution modeling of the impact of rain, tides, and sea level rise on water table flooding in the Arch Creek basin, Miami-Dade County Florida USA." Science of the Total Environment, 616–617: 1668–1688. Elsevier B.V. https://doi.org/10.1016/j.scitotenv.2017.10.170.

Sun, J., Hu, L., Li, D., Sun, K., & Yang, Z. (2022). Data-driven models for accurate groundwater level prediction and their practical significance in groundwater management. Journal of Hydrology, 608, 127630. https://doi.org/10.1016/j.jhydrol.2022.127630.

Sun, Q., Zhang, X., Zwiers, F., Westra, S., & Alexander, L. V. (2021). A global, continental, and regional analysis of changes in extreme precipitation. Journal of Climate, 34(1), 243–258. https://doi.org/10.1175/JCLI-D-19-0892.1.

Sweet, W. V., Kopp, R. E., Weaver, C. P., Obeysekera, J., Horton, R. M., Thieler, E. R., & Zervas, C. (2017). Global and Regional Sea Level Rise Scenarios for the United States. NOAA Technical Report NOS CO-OPS 083, September, 1–56. https://tidesandcurrents.noaa.gov/publications/techrpt83_Global_and_Regional_SLR_Scenarios_for_the_US_final.pdf.

Sweet, W.V., B.D. Hamlington, R.E. Kopp, C.P. Weaver, P.L. Barnard, D. Bekaert, W. Brooks, M. Craghan, G. Dusek, G. Garner, T. Frederikse, A.S. Genz, J.P. Krasting, D. Marcy, E. Larour, J.J. Marra, J. Obeysekera, M. Osler, M. Pendleton, … C. Zuzak. (2022). Global and Regional Sea Level Rise Scenarios for the United States: Updated Mean Projections and Extreme Water Level Probabilities Along U.S. Coastlines (No. NOAA Technical Report NOS 01; p. 111). National Oceanic and Atmospheric Administration, National Ocean Service.

Tang, Y., Jiang, Q., & Zhou, C. (2016). Approximate analytical solution to the Boussinesq equation with a sloping water-land boundary. Water Resources Research, 52(4), 2529–2550. https://doi.org/10.1002/2015WR017794.

Thomas, W., Newell, D., Bernzott, E., Szekeres, D., Harris, J., Tabb, C., & Siddiquee, F. (2020). Development of Site-Specific Hydrologic and Hydraulic Analyses for Assessing Transportation Infrastructure Vulnerability & Risks to Climate Change (Issue FHWA-HEP-21-025).

Titus-Glover, L., Darter, M. I., & Von Quintus, H. (2019). Impact of Environmental Factors on Pavement Performance in the Absence of Heavy Loads (Issue March).

Trescott, P. C., Pinder, G. F., & Larson, S. P. (1976). Finite difference model for aquifer simulation in two dimensions with results of numerical experiments.

U.S. Census Bureau, "TIGER/Line Shapefile, 2024, State, Alabama, AL, Census Tract", TIGER/Line Shapefiles, 2024, https://www2.census.gov/geo/tiger/TIGER2023/STATE/, accessed July 16, 2024.

U.S. Fish & Wildlife Service. (2025, May 13). National Wetlands Inventory.

UC Santa Barbara. (2023). Coastal Sage Scrub. UC Santa Barbara. https://www.ncos.ccber.ucsb.edu/native-plant-habitats/coastal-sage-scrub.

University of South Alabama. (n.d.). Archived data. CHILI Web. Retrieved November 13, 2024, from http://chiliweb.southalabama.edu/archived_data.php.

USDA-FSA Aerial Photography Field Office (AFPO) (2022). AIP Digital Orthophoto (DOQQ - quarter-quadrangle) m_3008749_nw_16_030_20211113.

Vasconcelos, J. G., Fang, X., Anderson, J. B., Tamang, S., & Song, W. (2018). Analysis and Potential Solutions to Sediment Deposition in Dean Road Bridge Watershed, Midland City, AL (Issue ALDOT 930-925-1).

Vasconcelos, J. G., Fang, X., Geller, V. G., Nicolaico, G. G., & Reyes, E. M. (2023). Resilient Design with Distributed Rainfall-Runoff Modeling. In Resilient Design with Distributed Rainfall-Runoff Modeling. Transportation Re-search Board. https://doi.org/10.17226/27051.

Warren Liao, T. (2005). Clustering of time series data - A survey. Pattern Recognition, 38(11), 1857–1874. https://doi.org/10.1016/j.patcog.2005.01.025.

Werner, A. D., Bakker, M., Post, V. E. A., Vandenbohede, A., Lu, C., Ataie-Ashtiani, B., Simmons, C. T., & Barry, D. A. (2013). Seawater intrusion processes, investigation and management: Recent advances and future challenges. Advances in Water Resources, 51, 3–26. https://doi.org/10.1016/j.advwatres.2012.03.004.

Weston, D. M., Skahill, B. E., Downer, C. W., Graulau-Santiago, J. A., Pradhan, N., & Byrd, A. R. (2015). Gridded Sur-face Subsurface Hydrologic Analysis Modeling for Analysis of Flood Design Features at the Picayune Strand Restoration Project.

Wijayarathne, D. B., & Gomezdelcampo, E. (2019). Using shallow groundwater modeling to frame the restoration of a wet prairie in the Oak Openings Region, Ohio, USA: GSSHA model implementation. Environmental Earth Sciences, 78(6), 1–13. https://doi.org/10.1007/s12665-019-8208-1.

Xiao, X., Y. Fang, J. Qian, T. Zheng, L. Ma, X. Zheng, S. Gao, and H. Wang. 2024. Temporal and spatial evolution of residual saltwater contamination in coastal subterranean reservoirs. J Environ Manage, 370: 122913. https://doi.org/10.1016/j.jenvman.2024.122913.

Xie, X., and X. Zhang. 2024. Development of a deep surrogate model with spatiotemporal characteristics mining capabilities for the prediction of groundwater level in coastal areas. J Environ Manage, 370. Academic Press. https://doi.org/10.1016/j.jenvman.2024.122724.

Xu, K., Han, Z., Bin, L., Shen, R., & Long, Y. (2024). Rapid forecasting of compound flooding for a coastal area based on data-driven approach. Natural Hazards. https://doi.org/10.1007/s11069-024-06846-0.

Yu, X., L. Luo, P. Hu, X. Tu, X. Chen, and J. Wei. 2022. “Impacts of sea-level rise on groundwater inundation and river floods under changing climate.” J Hydrol (Amst), 614 (PB): 128554. Elsevier B.V. https://doi.org/10.1016/j.jhydrol.2022.128554.

Yuan, L., Mikelonis, A. M., & Yan, E. (2023). Using SWMM for emergency response planning: A case study evaluating biological agent transport under various rainfall scenarios and urban surfaces. Journal of Hazardous Materials, 458, 131747. https://doi.org/10.1016/j.jhazmat.2023.131747.

Yue, S., Pilon, P., Phinney, B., & Cavadias, G. (2002). The influence of autocorrelation on the ability to detect trend in hydrological series. Hydrological Processes, 16(9), 1807–1829. https://doi.org/10.1002/hyp.1095.

Zhang, Q., Lu, Q., Kwon, C., Xu, X., & Schreiber, D. (2018). Spatial Sustainability Assessment of Green Stormwater In-frastructure for Surface Transportation Planning, Phase I.